HIGHWAY RESEARCH
RECORD

Number 52

Mechanical and Physico-Chemical Properties of Soils
5 Reports

Department of Soils, Geology and Foundations

Eldon J. Yoder, Chairman
Joint Highway Research Project, Purdue University
Lafayette, Indiana

COMMITTEE ON COMPACTION OF EMBANKMENTS, SUBGRADES AND BASES
(As of December 31, 1963)

L. D. Hicks, Chairman
Chief Soils Engineer
North Carolina State Highway Commission, Raleigh

W. F. Abercrombie, State Highway Materials Engineer, State Highway Department of Georgia, Atlanta
W. H. Campen, Manager, Omaha Testing Laboratories, Omaha, Nebraska
Miles D. Catton, Consultant, Park Ridge, Illinois
Lawrence A. DuBose, Testing Service Corporation, Lombard, Illinois
J. D. Geesaman, Highway Engineer, Portland Cement Association, Chicago, Illinois
C. A. Hogentogler, Jr., Hogentogler and Company, Chevy Chase, Maryland
James M. Hoover, Assistant Professor, Civil Engineering Department, Iowa State University, Engineering Experiment Station Laboratory, Ames
Delbert L. Lacey, Assistant Engineer of Materials, Kansas State Highway Commission, Topeka
William H. Mills, Consulting Engineer, Atlanta, Georgia
O. J. Porter, Managing Partner, Porter, O'Brien and Armstrong, Newark, New Jersey
C. K. Preus, Materials and Research Engineer, Minnesota Department of Highways, St. Paul
Thomas B. Pringle, Chief, Civil Engineering Branch, Engineering Division, Military Construction, Office, Chief of Engineers, Department of the Army, Washington, D. C.
Leo J. Ritter, Jr., Senior Editor, Engineering News-Record, New York, New York
John R. Sallberg, Highway Research Engineer, Soils, Foundations and Flexible Pavement Branch, U. S. Bureau of Public Roads, Washington, D. C.
W. T. Spencer, Soils Engineer, Materials and Tests, Indiana State Highway Commission, Indianapolis

COMMITTEE ON SOILS-CALCIUM CHLORIDE ROADS
(As of December 31, 1963)

Charles R. McCullough, Chairman
Department of Civil Engineering
North Carolina State College, Raleigh

W. B. Drake, Director of Research, Kentucky Department of Highways, Lexington
Kenneth E. Ellison, State Materials Engineer, Virginia Department of Highways, Richmond
J. E. Gray, Engineering Director, National Crushed Stone Association, Washington, D. C.

William B. Greene, Chief, Soils & Foundations Section, Bureau of Materials and
    Research, Maryland State Roads Commission, Baltimore
L. D. Hicks, Chief Soils Engineer, North Carolina State Highway Commission, Raleigh
Roger Lachance, Allied Chemical—Canada, Montreal, Quebec, Canada
C. K. Preus, Materials and Research Engineer, Minnesota Department of Highways,
    St. Paul
George B. Schoolcraft, Chief, Engineering Services Branch, Engineering Research
    and Development Laboratories, Fort Belvoir, Virginia
Floyd O. Slate, Department of Engineering Materials, Cornell University, Ithaca,
    New York
Harry A. Smith, Senior Regional Engineer, Calcium Chloride Institute, Washington,
    D. C.
William F. Staley, Manager, Public Business Sales, P. P. G., Columbia-Southern
    Chemical Corporation, Pittsburgh, Pennsylvania
Lewis A. Tomes, Calcium Chloride Institute, Washington, D. C.
J. F. Tribble, Research and Development Engineer, Alabama State Highway Depart-
    ment, Montgomery
Eldridge J. Wood, Assistant to Chief, Bureau of Materials and Research, Maryland
    State Roads Commission, Baltimore

COMMITTEE ON PHYSICO-CHEMICAL PHENOMENA IN SOILS
(As of December 31, 1963)

Hans F. Winterkorn, Chairman
Head, Soil Physics Laboratory
Princeton University, Princeton, New Jersey

Gail C. Blomquist, School of Civil Engineering, Michigan State University, East
    Lansing
James H. Havens, Assistant Director of Research, Kentucky Department of Highways,
    Lexington
J. B. Hemwall, The Dow Chemical Company, Chemicals Laboratory, Midland,
    Michigan
Earl B. Kinter, U. S. Bureau of Public Roads, Washington, D. C.
Philip F. Low, Department of Agronomy, Purdue University, Lafayette, Indiana
R. C. Mainfort, Michigan State Highway Department, Lansing
Edward Penner, Division of Building Research, National Research Council of Canada,
    Ottawa
Ralph L. Rollins, Associate Professor of Civil Engineering, Brigham Young
    University, Provo, Utah
Elmer A. Rosauer, Engineering Experiment Station, Iowa State University, Ames
J. B. Sheeler, Associate Professor of Civil Engineering, Engineering Experiment
    Station, Iowa State University, Ames
F. L. D. Wooltorton, c/o Lloyd's Bank, London, England

Contents

Comparison of Soil-Aggregate Mixture Strength by Two Methods

EUGENE Y. HUANG and DARRELL G. LOHMEIER
Respectively, Professor of Transportation Engineering, Michigan Technological University, and Graduate Research Assistant, Department of Civil Engineering, University of Illinois

This investigation compares strength values of soil-aggregate road materials as determined in-place by the Burggraf Shear Apparatus and by the triaxial compression test in the laboratory. A large number of soil-aggregate surface course materials, including both pit-run gravel and crushed stone materials, were tested.

The in-place strength of these materials was determined essentially according to ASTM Designation D-916-47T. The triaxial compression tests were performed on samples taken directly from the field test points and remolded to the same moisture content and density as existed during the field test.

The results of these tests indicated that, within the scope of the types and conditions of the materials studied, a definite relationship exists between the strength values determined by the two different methods.

•THE RESISTANCE of soil-aggregate road materials to deformation by traffic loads is largely governed by their shear strength. The measurement of this property is necessary, not only in the understanding of the service behavior of these materials but also in the formulation of working principles for mixture design.

There are several strength tests that may be applied to soil-aggregate materials. In the laboratory, the triaxial compression test is probably the most useful. In this well-known test, a cylindrical specimen is subjected to a confining pressure on all sides, and a vertical axial stress is applied to the end until the specimen fails in shear. The stresses may be applied under conditions closely parallel with actual field conditions; hence, the results may have a more direct application to practical problems than those from other laboratory tests. However, the test has to be performed on laboratory molded specimens, as it is impossible to obtain soil-aggregate specimens from the road without appreciable disturbance. The test is of particular value in the laboratory evaluation of the relative importance and quantitative effect of the various material factors on the strength characteristics of soil-aggregate materials, which is an important procedure in mixture design.

For the evaluation of the in-place strength of soil-aggregate road materials, the Burggraf Shear Apparatus can be most effectively used. In this procedure, a horizontal thrust is applied, by means of a screw-propelled plunger-type pump, through a compression plate, to an exposed vertical section of a soil-aggregate layer until the material ahead of the plate fails in shear. The method was developed by Fred Burggraf and has been adopted by ASTM as Designation D-916-47T [1]. By means of this apparatus, various road surface materials can be tested under actual environmental conditions, and the criteria for their strength and performance can be deter-

mined (2, 3, 4). Although the portable mechanical device may be adapted to laboratory testing, its use thus far has been confined to the field evaluation of road materials.

Whereas the methods of procedure for these two tests are different, both are concerned with the resistance of soil-aggregate materials to shearing. From the point of view of mechanics a main difference between the two tests appears to be the manner in which the materials are loaded to failure. As shown in Figure 1, the major principal stress in the triaxial compression test is the applied vertical stress, and the lateral stress applied all around is the minor principal stress. In the in-place shear test by the Burggraf Shear Apparatus, the applied horizontal stress is the major principal stress and the minor principal stress is that due to the weight of the wedge of soil-aggregate material or any vertical loads applied as a surcharge to the surface of the wedge adjacent to the compression plate (5). Because of the differences in the general setup of these tests, the behavior of soil-aggregate materials under the loading conditions in each of these tests at the time of failing also becomes separately distinct. In the triaxial compression test, a soil-aggregate material is failed under the condition of triaxial loading. In the Burggraf shear test, however, it is failed in a plane strain condition. Consequently, the strength values as obtained from these two tests may be expected to be characteristically different.

OBJECTIVE AND SCOPE OF INVESTIGATION

The investigation described here was made to provide data for comparing the strength values of soil-aggregate road materials as determined in-place by the Burggraf Shear Apparatus and those as determined by the triaxial compression test in the laboratory. It was hoped that a correlation between these values might be established by
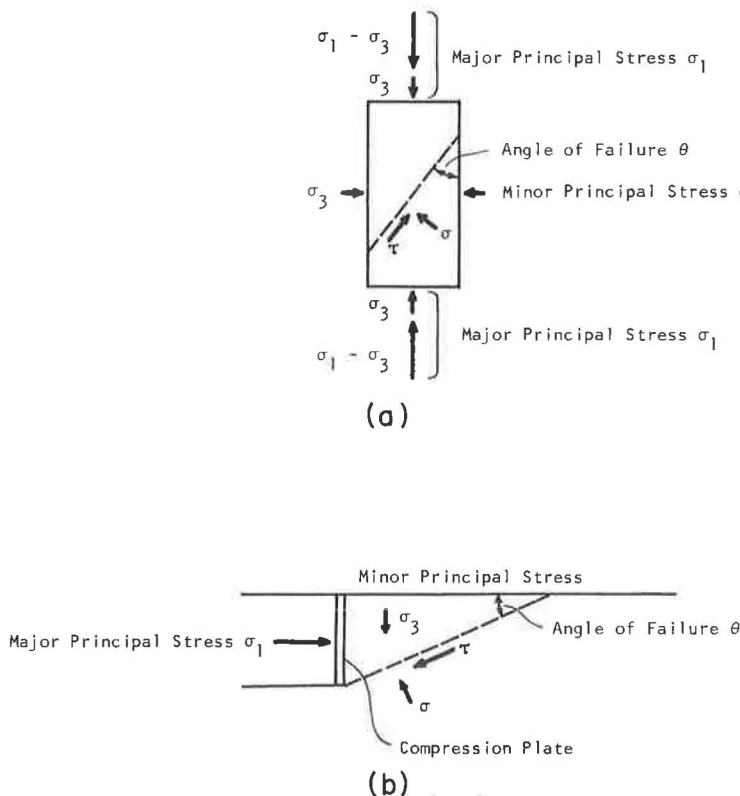

Figure 1. Stress conditions in (a) triaxial compression test and (b) Burggraf shear test.

which the laboratory test results might be used for estimating the possible in-place strength of soil-aggregate materials and, in turn, for predicting those behavior characteristics associated with their in-place strength. For instance, field investigations on the service conditions of soil-aggregate road surfaces conducted at the University of Illinois have shown that potholes and washboard formations seldom occur in materials with high Burggraf shear values.

Included in the study was a total of 65 soil-aggregate surface course materials from secondary and local roads in all parts of Illinois. The in-place strength of these materials was determined essentially according to ASTM Designation D-916-47T. The triaxial compression tests were performed on specimens prepared in the laboratory from materials taken directly from the field test points. These specimens were remolded to the same moisture content and density as existed during the field test. The relationship between the strength values determined by the two tests is indicated by a correlation-regression analysis.

TESTING PROGRAM

All materials involved in this study had been placed for at least 2 yr, and a few for as many as 5 or 6 yr, before the field tests were performed. Both pit-run gravel and crushed stone, typical surfacing materials for soil-aggregate roads, were represented in this investigation. In the selection of test sites, those materials with a history of high stability were included as well as those exhibiting poor service. The tests were conducted during various seasons of the year, but most were performed in summer and fall. The moisture content of these materials was, in general, quite low, ranging from 1.0 to 5.4 percent with an average value of 2.5 percent.

With the Burggraf Shear Apparatus a hole about 10 by 10 in. is dug in the layer to be tested to a sufficient depth, and a vertical face against which the test is to be made is carefully cut to receive a standard compression plate connected to the thrust cylinder. The horizontal thrust is then applied by turning a hand wheel operating the screw-propelled plunger-type pump at a uniform rate to force the compression plate against the soil-aggregate layer until the material ahead of the plate fails. The area of the surface on which the failure occurs is measured, and the strength value is determined by dividing the maximum horizontal thrust by the sheared area. The angle of failure, θ (Fig. 1 (b)), is determined by measuring its tangent, which consists of one measurement from the top of the compression plate to the bottom of the cavity divided by the distance from the face of the compression plate to the most remote edge of the sheared surface.

In the present investigation, the parabolic compression plate, having a height of $2\,^{15}/_{32}$ in., a width of $7\,^{1}/_{2}$ in., and an area of 12.2 sq in., was used to adapt to the limited thickness of the surface courses. To provide a uniform bearing area, a fast setting plaster, Hydrocal White, approximately $^{1}/_{4}$ in. in thickness, was applied between the compression plate and the vertical face to be tested. The horizontal thrust was applied at a uniform rate of 10 lb/sec, until the point of maximum pressure was noted. A typical failure at the end of the test is shown in Figure 2.

The triaxial compression test was performed on the soil-aggregate materials taken directly from each field test point. The cylindrical specimens were 4 in. in diameter and 8 in. in height. The materials were compacted to in-place density with the field moisture content. The in-place density and

Figure 2. Typical failure of soil-aggregate surface course in Burggraf shear test.
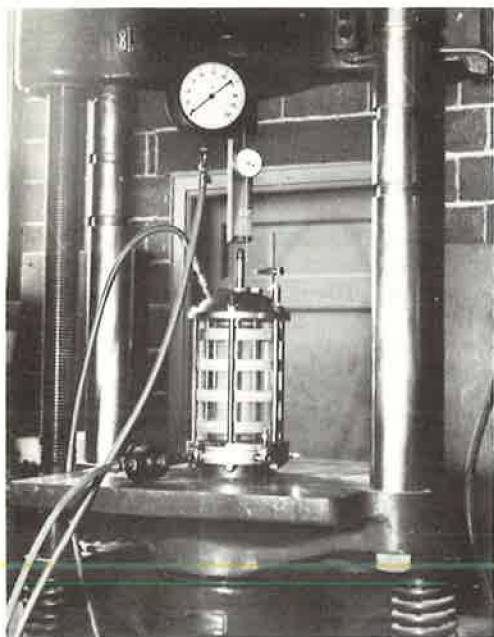
Figure 3. Apparatus setup for triaxial compression test.

moisture content of the surface course materials were determined according to AASHO Designation T-147-54; the volume of the density hole was measured by means of the sand-density cone using standard Ottawa sand. Confining pressures of 5, 15 and 30 psi were applied by compressed air and maintained constant throughout the test. The axial load was applied to produce a constant rate of vertical deflection of 0.1 ipm until the specimen failed. The apparatus for this test is shown in Figure 3.

RESULTS AND DISCUSSIONS

The results of the in-place and laboratory strength tests conducted on the soil-aggregate surface course materials are summarized in Table 1. The in-place shear strength was calculated by dividing the maximum horizontal thrust by the sheared area. The sheared area was determined, after the sheared-out material had been removed, by placing a piece of paper in the cavity and outlining the edge of the sheared surface. The numerical value was found by means of a planimeter. The laboratory strength value for the comparable loading condition was taken from the Mohr diagram plotted from the data of triaxial compression tests for the three different confining pressures. Because only the weight of the wedge of soil-aggregate material acted as a confining load during the in-place strength test, which was negligible in magnitude, the laboratory strength value was determined in the Mohr diagram from a failure circle representing zero confining pressure. The ordinate of the point of tangency of the circle with the failure envelope was taken as the shear strength of the material.

Also given in Table 1 are the major principal stresses, σ_1, at failure and the angles of failure, θ, of various materials as determined by the two strength tests. The major principal stress at failure in the in-place strength test was determined by dividing the maximum horizontal thrust by the area of the parabolic compression plate. For the triaxial compression test, this value was obtained in the Mohr diagram from the failure circle for zero confining pressure. For the triaxial compression test, the angle θ was computed from the angle of shearing resistance, ϕ, as indicated in the Mohr diagram, according to the expression

$$\theta = 45° - \phi/2 \tag{1}$$

The three sets of data in Table 1 are also plotted in Figures 4, 5, and 6, with the in-place test value as ordinate and the corresponding laboratory value as abscissa.

In studying the data, it may be immediately noted that, regardless of the type of surface material, the shear strength from the in-place test is consistently of higher value than that obtained from the triaxial compression test. Because the shearing stress in the soil-aggregate materials at zero confining pressure is a function of the major principal stress, this trend is also indicated between the major principal stresses at failure for the two tests. On the other hand, the angle of failure is, as a rule, smaller in the in-place test than in the triaxial compression test under comparable conditions.

TABLE 1

SUMMARY OF TEST DATA

Sample	Shearing Value, τ (psi)		Major Principal Stress, σ_1 (psi)		Angle of Failure, θ (deg)	
	Burggraf	Triaxial	Burggraf	Triaxial	Burggraf	Triaxial
			(a) Gravel			
1	30.4	17.5	123	46	20.7	25.5
2	24.3	12.5	121	36	18.4	23.5
3	40.6	21.0	162	56	23.3	24.0
4	69.3	27.5	328	86	19.6	20.0
5	23.9	12.5	127	32	20.7	24.5
6	10.6	10.5	44	22	22.6	24.7
7	24.8	10.5	153	28	19.6	24.5
8	14.3	11.0	39	30	28.0	24.0
9	38.2	20.0	213	52	18.4	25.2
10	38.6	17.0	141	46	25.7	23.2
11	18.1	12.0	121	31	17.4	24.5
12	56.1	26.0	242	72	22.6	22.5
13	26.0	17.0	114	46	18.4	24.2
14	34.4	18.0	197	48	19.2	25.0
15	9.2	9.5	58	26	16.8	24.2
16	29.6	13.2	213	36	22.0	24.0
17	15.8	16.0	96	46	16.4	22.5
18	31.6	20.0	140	60	20.5	21.2
19	35.5	20.7	202	54	19.0	25.0
20	32.7	14.0	139	38	21.7	23.5
21	22.8	16.5	148	48	16.4	25.5
22	23.5	12.2	184	32	14.0	25.0
23	38.3	19.0	187	50	19.6	24.5
24	32.8	14.5	130	40	22.6	24.0
25	38.6	23.0	126	70	24.4	21.0
26	36.4	19.0	142	60	22.0	20.0
27	30.8	13.5	117	44	23.3	19.5
28	36.3	17.0	148	50	21.2	21.2
29	26.8	17.0	148	46	19.4	23.2
30	32.1	9.5	170	24	19.6	25.5
31	47.4	21.3	265	59	18.0	23.0
32	58.7	19.0	221	52	24.0	23.5
33	58.4	20.0	185	53	25.7	24.7
34	40.0	18.5	201	54	18.9	21.7
			(b) Crushed Stone			
1	44.3	17.5	224	50	20.7	21.7
2	34.4	13.0	188	35	18.4	24.0
3	21.5	19.0	120	53	21.7	23.5
4	58.8	30.5	316	82	21.1	23.7
5	34.4	16.5	208	46	16.4	23.7
6	36.9	14.0	184	40	20.2	24.0
7	40.8	20.0	239	58	18.9	22.5
8	44.4	28.7	260	78	17.8	24.5
9	42.4	21.0	258	66	16.4	20.0
10	24.3	19.3	156	58	16.6	20.5
11	28.4	14.0	111	38	24.5	23.7
12	37.5	24.0	135	66	23.3	22.7
13	35.5	19.3	272	54	16.4	20.7
14	50.7	17.3	312	46	16.4	24.7
15	49.1	22.0	275	62	19.9	22.7
16	53.0	20.0	348	58	16.6	22.0
17	46.7	17.0	224	50	21.1	22.0
18	62.8	26.5	242	74	22.3	23.5
19	52.1	20.5	219	60	21.1	21.7
20	47.5	22.5	238	60	19.4	24.5
21	64.5	25.0	279	70	21.4	24.5
22	78.3	28.5	284	84	23.3	23.5
23	64.3	27.5	344	84	18.2	19.5
24	63.9	24.5	277	70	21.6	22.2
25	54.0	20.5	234	54	18.2	25.2
26	41.6	13.5	133	38	23.7	22.7
27	37.6	12.5	165	34	21.4	24.5
28	38.6	25.5	221	70	17.4	24.0
29	32.8	17.5	201	46	16.4	25.0
30	48.3	22.5	254	66	19.6	21.5
31	16.0	8.7	78	24	17.4	23.2

8

with a standard error of estimate of 8.2, and a correlation coefficient of 0.80 For the crushed stone materials, the equation is

$$B = 1.82\,T + 7.8 \tag{4}$$

with a standard error of estimate of 10.1, and a correlation coefficient of 0.70.

To test the hypothesis that the correlation coefficients for the pit-run gravel and the crushed stone materials were drawn at random from the same population, a z-value of -0.95 was calculated from the correlation coefficients for both materials. Because this value is less than that indicated in the standard table for z values at the 5 percent level of significance, the hypothesis is not rejected, and it is concluded that the two coefficient values were drawn at random essentially from the same population.

The two-tailed F-test was also performed using the variance ratio, calculated by dividing the deviation mean square from regression for each of the two materials by that for the combined materials. The calculated ratio for the pit-run gravel is 0.87, and that for the crushed stone is 1.26. Both values are insignificant at the 5 percent level, indicating that there are fewer than 5 chances in 100 that the disparity between the calculated values is due to chance.

On the basis of the preceding tests, it is concluded that the relationship between the two strength values is not separately distinct for the two different soil-aggregate materials, and that the regression equation (Eq. 2) is applicable to both materials in this investigation.

CONCLUSIONS

From the results of the testing, the following conclusions have been drawn:

1. The shear strength of a soil-aggregate surface material as determined in-place by the Burggraf Shear Apparatus is consistently of higher value than that determined in the laboratory by the triaxial compression test. This trend is also indicated between the major principal stresses at failure for the two tests. The angle of failure is consistently smaller in the in-place test than in the triaxial compression test under comparable conditions. It is believed that the above differences are due in part to the different strength characteristics between the field conditioned material and the laboratory remolded material and, particularly, to the different state of stress at failure in these two tests.

2. Within the scope of the types and conditions of the materials studied, there is a definite relationship between the in-place strength value of a soil-aggregate material as determined by the Burggraf Shear Apparatus and that as determined by triaxial compression tests in the laboratory. The correlation between the two strength values appears to be not separately distinct for the two types of materials involved in this investigation. A regression equation has been established for estimating the in-place strength of soil-aggregate materials on the basis of the results of their triaxial compression tests.

ACKNOWLEDGMENTS

Burggraf Shear Apparatus for the field testing. The authors are indebted to Robert D. Seif, Assistant Professor of Biometry, and Alfred J. Hendron, Research Associate in Civil Engineering, for review of parts of the paper and many helpful suggestions.

Special acknowledgment is due to Ellis Danner, Director of the Illinois Cooperative Highway Research Program and Professor of Highway Engineering, University of Illinois, for his interest and general advice.

REFERENCES

1. "Tentative Methods of Test for Shear Strength of Flexible Road Surfaces, Subgrades, and Fills by the Burggraf Shear Apparatus." 1961 Book of ASTM Standards, Part 4, pp. 1368-1372 (1961).
2. Burggraf, F., "Use of Calcium Chloride in Road Stabilization." Proc. HRB, 18, Part II, pp. 249-253 (1938).
3. Burggraf, F., "Field Test on Shearing Resistance." Proc. HRB, 19: 484-489 (1939).
4. Burggraf, F., "Field Tests and Their Application to the Design of Stabilized Soil Roads." Proc. Amer. Road Builders' Assoc., pp. 324-335 (1940).
5. Burmister, D. M., "General Discussion on Triaxial Testing of Soils and Bituminous Mixtures." ASTM Spec. Tech. Publ. 106, p. 301.
6. Burmister, D. M., "Discussion on Road Tests, Field Studies, and Performance Criteria." Internat. Conf. on the Structural Design of Asphalt Pavements Proc., Univ. of Michigan, p. 108 (1963).
7. Hendron, A. J., "The Behavior of Sand in One-Dimensional Compression." Ph.D. Diss., Univ. of Illinois, Dept. of Civil Eng., p. 34 (1963).
8. Wittke, W., "Über die Scherfestigkeit rollinger Erdstaffe, Rechnerische und Experimentelle Untersuchung von Kugelschüttunger." Veröffent. des Inst. für Bodenmechanik und Grundbau der T. H. Fridericiana in Karlsruhe, 11 (1962).
9. Leussink, H., and Wittke, W., "Difference in Triaxial and Plane Strain Shear Strength Theoretical and Experimental Investigations." Presented at ASTM Sym. on Lab. Shear Testing of Soils (1963).

Some important properties of these packings are given in Table 1.

The coordination number is the number of contacts that a typical sphere makes with its neighbors. The unit cell may be defined as that smallest portion of the system which gives a complete representation of the manner of packing. Graton and Frazer (32) discuss this for each type of packing. Reference is also made to other properties of these systems, such as the interfacial angles of the unit cells.

TABLE 1

PROPERTIES OF REGULAR
PACKINGS OF UNIFORM SPHERES

Type	Void Ratio	Porosity (%)	Coordination No.	Layer Spacing
Cubic	0.91	47.64	6	$R\sqrt{4}$
Orthorhombic	0.65	39.54	8	$R\sqrt{3}$ [a] $R\sqrt{4}$ [b]
Tetragonal-spheroidal	0.435	30.19	10	$R\sqrt{3}$
Rhombohedral	0.35	25.95	12	$R\sqrt{2}$ [c] $R\sqrt{2/3}$ [d]

[a] Case 2.　　[b] Case 4.　　[c] Case 3.　　[d] Case 6.

The rhombohedral system is the most important theoretically, and usually is the basis for calculations. It is also the most important from a practical viewpoint, because it is the densest possible state.

In the Case 3 type of rhombohedral packing, each sphere is in contact with four spheres below, four above, and four in the same layer. In Case 6, each sphere has contact with three below, three above, and six in the same layer.

In the rhombohedral system, there are two types of voids:

1. Concave-cube void formed by six spheres of which four form a square, one lies in the hopper produced, and the sixth lies vertically below it; and

2. Concave-tetrahedron void formed by four spheres, one of which lies in the hopper-like depression formed by the other three.

The number of concave-tetrahedron voids is twice that of concave-cube voids in the rhombohedral system, but the distribution differs in the two cases. All voids are interconnected in such a way that the largest sphere that can pass through the circuit has a radius of $(2/\sqrt{3} - 1)R$ (39).

Graton and Frazer (32) show that there are several alternative arrangements of Case 6 packing analogous to multiple twinning in crystallography. This results from the fact that the unit of the rhombic layer (Fig. 1) has two hollows into either one of which a sphere may be placed.

The stability of the systems increases as the porosity decreases. The cubical system is the least stable, because each sphere is delicately supported at one point below and is only prevented from toppling by lateral support provided by the four neighboring spheres in the same layer. The orthorhombic and tetragonal-spheroidal systems have more stability, because each sphere has two points of support from below as it rests in the cusp formed by two adjacent spheres. A force having a component perpendicular to the plane of this cusp will tend to topple it. The rhombohedral system has complete stability: in Case 6 each sphere rests in the hopper-like depression formed by three spheres, whereas in Case 3 each sphere rests in the hopper-like depression formed by a square of four spheres. If Case 1 packing is disturbed slightly, it may pass through Case 2 to Case 3. This happens when each sphere leaves its position at the top of a lower sphere and falls into an adjoining cusp and thence into an adjacent hopper. In a similar manner, Case 4 may pass into the Case 5 state and finally into Case 6.

The cubical packing has the greatest potential energy, whereas the rhombohedral has the least. Because bodies try to attain the position of least potential energy, these systems tend to form the rhombohedral state, especially if a mechanical disturbance is applied to the system. However, the side walls of the container act against this tendency by preventing any lateral spreading of the system.

The question of the relative stability of a system is only one of the factors influencing the formation of a given packing. The relative stability concerns the vertical relationships, but there are other conditions which influence the horizontal relationships.

If equal spheres accumulate on a horizontal surface, there will be a strong tendency for a simple rhombic arrangement to show itself in the first layer (32). If this occurs there is considerably better than an even chance that this pattern will propagate upwards

to form Case 6 packing. It is, of course, highly unlikely that this will continue without interruption. There are bound to be many regions of haphazard packing, each such region being initiated by a sphere getting into the wrong place. Thus, in the building-up of the assemblage, there is a conflict between the tendency to form Case 6 packing and the tendency to produce haphazard packing. Haphazard packing may, purely by chance, result in a systematic or repetitive arrangement in some regions. Therefore, the probability is that the resulting assembly will consist of three-dimensional colonies of Case 6 packing and of intervening regions of haphazard arrangement.

There is an optimum rate of assembly to give maximum regularity of arrangement. Obviously, rapid dumping is unfavorable.

The angle which the side wall makes with the bottom influences the packing formation. A 90° angle will favor Cases 1, 2, 4, and 5; a 60° or 120° angle favors Cases 2 and 3, whereas a 70° 32' or 109° 28' angle favors Case 6. The packing is also influenced by the angles which the side walls make with each other. A 90° angle favors formation of the square pattern and, hence, Cases 1, 2, and 3. Intersection of the side walls at 60° with themselves and at 90° with the bottom favors Cases 4 and 6. Intersection of the side walls at 60° with themselves and at 70° 32' with the bottom strongly favors Case 6 packing.

The walls of the container give rise to a wall effect which causes the porosity in the vicinity of the wall to be greater than that in the body of the packing. This effect has been studied by Furnas (28) who obtained an expression for the voids, V_W, present in a ring at the wall of area $\pi \, d D / 2$:

$$V_W = \left\{ V + K (1 - V) \right\} \left(\frac{1 + 2Kd}{D} \right) - \frac{2Kd}{D} \tag{1}$$

in which d is the diameter of the particles, D is the diameter of container, V is the voids present in the interior, and K is an experimental factor found to be 0.3. The wall effect increases as the ratio d/D decreases.

If the wall effect may be neglected, the density of the system will be independent of the absolute size of the spheres. This is confirmed by the experimental studies of Westman and Hugill (94).

Kolbuszewski (49) carried out experiments on the effect of the rate of pouring of sand on the resulting porosity. As the rate of pouring from a given height decreased, the porosity decreased to a limiting value. This value itself decreased with increasing height of drop up to a certain height.

Systematic Packing of Spheres of Different Sizes

Horsfield (37) calculated the decrease in porosity resulting from the insertion into the voids of the rhombohedral system of successive spheres just large enough to fill the voids. The spheres filling the concave-cube voids are termed secondary spheres, whereas those filling the concave-tetrahedron voids are tertiary spheres. The quaternary spheres are inserted in the largest voids left after the secondary and tertiary spheres are in place, and so on through the different types. The results are given in Table 2. Of course, it is impossible to attain practically a system packed in such a manner.

Hudson (39) imagined the voids of the rhombohedral system to be filled with S spheres of equal radii, r, arranged in cubic symmetry. He calculated the density increment for values of S up to 27 (22, 39). The densest state was obtained when each concave-cube void contained 21 spheres with r = 0.1782R (in which R is the radius

TABLE 2

EFFECT ON POROSITY OF
SPHERES INSERTED IN
VOIDS OF RHOMBOHEDRAL SYSTEM

Sphere Type	Radius[a]	No. of Spheres	Porosity
Primary	1	1	25.95
Secondary	0.4142	1	20.69
Tertiary	0.2247	2	19.01
Quaternary	0.1766	8	15.74
Quinary	0.1163	8	14.81
Filler	0.0000	-	3.84

[a]Primary radius = 1.

of the primary spheres) and each concave-
tetrahedron void contained 4 spheres
with r = 0.1547R.

Dense Random Packing of
Unequal Spheres

Wise (101) studied mathematically a
dense random packing of unequal spheres
which is more representative of a real
densely packed system than the preceding
systematic models. This random packing
is obtained in the following manner.

A large sphere A is taken and other
smaller spheres are placed on its surface.
The first and second spheres must touch
each other and also A. Every new sphere
must touch A and at least two others that
touch each other. Figure 2 shows what
is seen looking out from A. If the center
of a sphere D is joined to the centers of
the spheres around D, a network of tri-
angles is formed, each of which lies in a
different plane. These triangles are the
faces of a polyhedron with the centers of
the spheres as its vertices. If these vertices are joined to the center of A, the whole
space inclosed by the polyhedron is partitioned into tetrahedra associated with the
given sphere D. Wise sets up a probability distribution function w for the four radii
in each tetrahedron and deduces general equations for w. The properties of the packing
are expressed in terms of w.

In the special case in which the logarithms of the radii of the spheres follow a normal
distribution of standard deviation, $\sigma = 0.4$, the mean radius is 1.08 and the mean porosity
of the packing is 0.2. The mean number of spheres in contact with a sphere of given
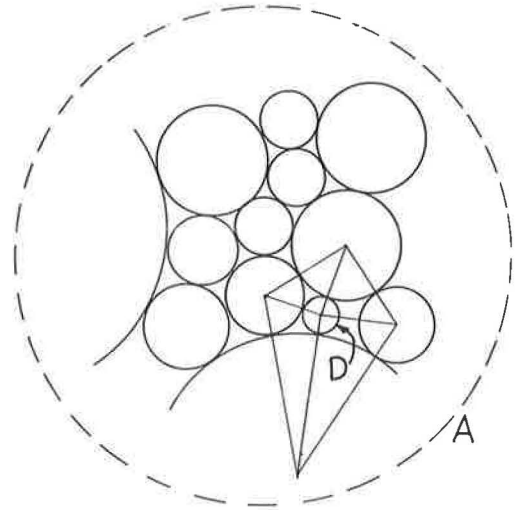radius can also be calculated and is shown in curve C of Figure 3.

Figure 2.   Dense random packing of unequal
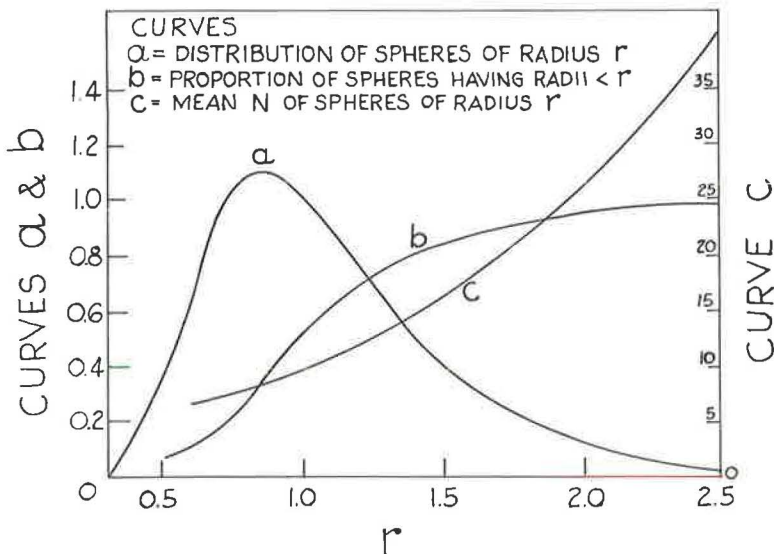spheres (101).

Figure 3.   Dense random packing of spheres having radii obeying a log-normal distribu-
tion of standard deviation $\sigma = 0.4$ (101).

Wise's main concept of tetrahedra is used by Kallstenius and Bergau (46) in determining by a graphical method the structure resulting from a random assembly of grains.

Another type of random packing was theorized by Brandt (7) and used in the calculation of the speed of a dilatational wave through a granular system. The primary spheres are packed randomly to a porosity, n, and smaller uniform spheres are packed to the same porosity in the voids of the primary system. Still smaller spheres are packed to the same porosity in the remaining voids and so on.

REAL GRANULAR SYSTEMS

In a real granular system, the coordination numbers of the spheres vary according to the position of each sphere.

W. O. Smith (82) suggested a simple method to determine the average coordination number, N, of a system having a certain porosity, n. N is considered to decrease linearly as the porosity increases from 25.95 percent (rhombohedral system) to 47.64 percent (cubic system). N can, therefore, be obtained by interpolation between the corresponding values of 12 and 6.
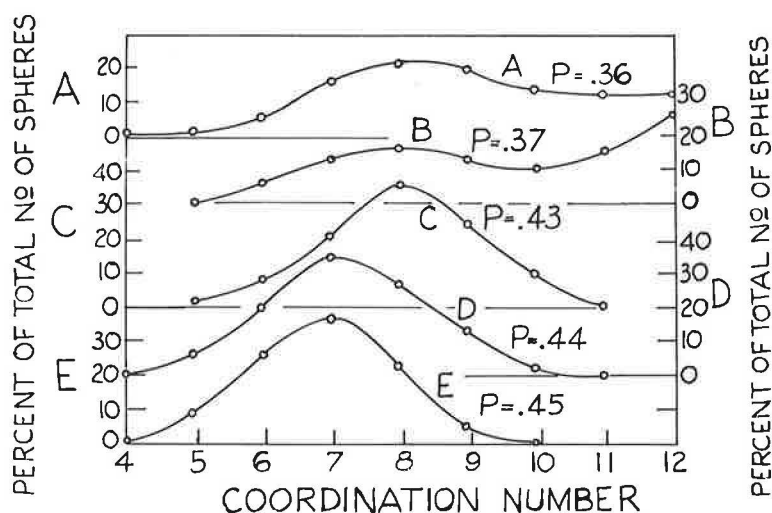

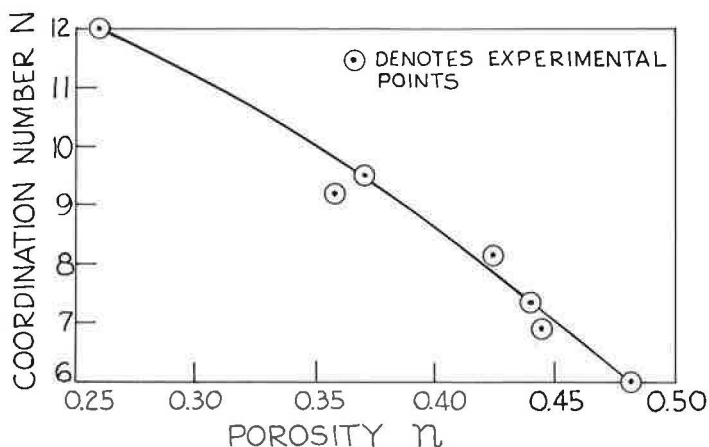Figure 4. Distribution of coordination number at several porosities (83).

Figure 5. Average number of contacts per sphere, N, as function of porosity n (83).

Later W. O. Smith et al. ([83]) determined experimentally the coordination numbers in a well packed aggregate of lead shot for various porosities. At a given porosity, the number of spheres having a given coordination number varied according to a Gaussian distribution (Fig. 4). At a porosity of 36 percent, the greatest number of spheres had a coordination number of 8, and the values of N ranged from 4 to 12. As the porosity increased, there was a shift toward the lower coordination numbers, as may be expected. These authors thought that the actual system might for statistical purposes be treated as composed of separate clusters of rhombohedral or cubic arrangements, these being present in such a proportion as to give the observed porosity of the assembly. This consideration leads to the following expression for the average coordination number, N, in terms of the porosity, n:

$$N = 26.4858 - \frac{10.7262}{1 - n} \tag{2}$$

The curve representing this is shown in Figure 5 and agrees well with the observed experimental values.

MECHANICAL BEHAVIOR OF GRANULAR SYSTEMS

A theoretical model for determining the mechanical behavior of a granular system is an arrangement of discrete spheres in direct elastic contact with one another.

Contact Theory

The classical Hertz theory of contact predicts that when two elastic spheres in contact are compressed by a force, N, along their line of centers, there will be a plane circular area of contact ([91]). The radius, a, of this circle is assumed to be small compared to the radius, $\bar{R}$, of either sphere and is given by

$$a = (\theta N R)^{1/3} \tag{3}$$

in which

$$\theta = 3(1 - \nu^2)/4E \tag{4}$$

and ν and E are Poisson's ratio and Young's modulus, respectively, of the spheres. The normal pressure σ at distance, ρ, from the center of contact ($\rho \leq a$) is given by

$$\sigma = \frac{3N}{2 \pi a^3} (a^2 - \rho^2)^{1/2} \tag{5}$$

which is a parabolic distribution (Fig. 6). The relative approach α of the sphere centers is

$$\alpha = 2 \left(\frac{\theta N}{R^{1/2}} \right)^{2/3} \tag{6}$$

from which the normal compliance C of the contact is

$$C = \frac{d\alpha}{dN} = \frac{4}{3} \left(\frac{\theta^2}{RN} \right)^{1/3} = \frac{1 - \nu}{2 \mu a} \tag{7}$$

in which μ is the shear modulus of the spheres. As apparent from Eqs. 3 and 6, a and α do not vary linearly with N. This fact introduces mathematical difficulties.

If the normal force, N, is kept constant and a tangential force is applied in the plane of contact and gradually increased from zero to T, slip will start at the circumference of the circle of contact and progress radially inward covering an annular area. The inner radius, c, of the annulus of slip was found by Mindlin ([56]) to be
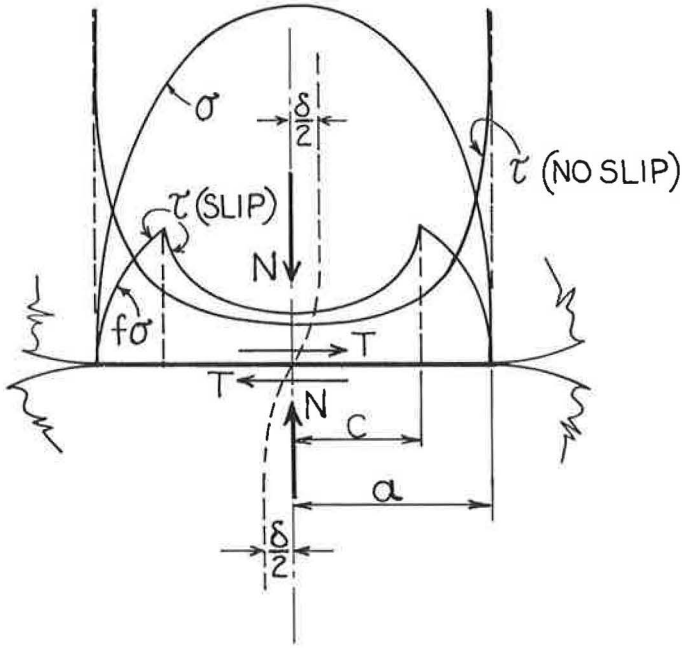
Figure 6. Distribution of normal, σ, and tangential, τ, components of traction on contact surface of two like spheres subjected to normal force followed by monotonic tangential force (22).

$$c = a \left(1 - \frac{T}{fN} \right)^{1/3} \tag{8}$$

in which f is the coefficient of static friction. The relative tangential displacement, δ, of the centers of the spheres is

$$\delta = \frac{3(2 - \nu)\, fN}{8\, \mu\, a} \left[1 - \left(1 - \frac{T}{fN} \right)^{2/3} \right] \tag{9}$$

The tangential compliance of the contact is

$$S = \frac{d\delta}{dT} = \frac{2 - \nu}{4\, \mu\, a} \left(1 - \frac{T}{fN} \right)^{-1/3} \tag{10}$$

On the annulus of slip, the tangential component of traction, τ, is assumed to be

$$\tau = f\sigma \tag{11}$$

As the tangential force T approaches fN, Eq. 8 shows that c tends to zero. When T = fN, rigid body sliding occurs.

It is important to note that the tangential compliance S is of the same order of magnitude as the normal compliance C.

If the tangential force acting on the two spheres under consideration is gradually reduced from a peak value T_1 $(0 < T_1 < fN)$, an annulus of counter slip will be formed,

starting from the edge of the area of contact, and will gradually spread radially inward. Its inner radius was found by Mindlin et al. (58) to be

$$b = a \left(1 - \frac{T_1 - T}{2fN} \right)^{1/3} \tag{12}$$

The corresponding relative displacement of the centers of the spheres during unloading is

$$\delta_u = \frac{3(2 - \nu) fN}{8 \mu a} \left[2 \left(1 - \frac{T_1 - T}{2fN} \right)^{2/3} - \left(1 - \frac{T_1}{fN} \right)^{2/3} - 1 \right] \tag{13}$$

This is shown by curve PRS in Figure 7. When T decreases to zero, there will remain a residual displacement, δ_R, and a certain annulus of slip. (This can be seen by setting T = 0 in Eq. 12, T = T_1 in Eq. 8 and noting that b - c > 0.) This indicates that the system is not elastic. The permanent set can be removed only by applying a tangential force in the reverse direction. When T = $-T_1$, b = c; that is, the slip has been annulled. An oscillation of the applied tangential force between the values T_1 and $-T_1$ causes the closed hysteresis loop PRSUP to be followed.

The area inclosed in the loop represents the frictional energy F dissipated in each cycle of loading:

$$F = \frac{9(2 - \nu)(fN)^2}{10 \mu a} \left\{ 1 - \left(1 - \frac{T_1}{fN} \right)^{5/3} - \right.$$

$$\left. \frac{5T_1}{6fN} \left[1 + \left(1 - \frac{T_1}{fN} \right)^{2/3} \right] \right\} \tag{14}$$

For small amplitudes of loading (i.e., $T_1/fN \ll 1$) Eq. 14 reduces to

$$F = \frac{(2 - \nu) T_1^3}{36 \mu afN} \tag{15}$$

The conclusions of this theory have been verified experimentally except for Eq. 15 in which F was found to vary as T_1^2 instead of T_1^3. This discrepancy may be explained by supposing that at small values of T_1, energy is dissipated as a result of plastic deformation of a small portion of the contact surface (22).

The two spheres are generally subjected to varying normal and tangential forces (i.e., a varying oblique force) when the granular system of which they are a part is acted on by varying external forces or is in a state of internal vibration. In such cases, as mentioned by Deresiewicz (22), the relation between the instantaneous tangential forces and displacements depends not only on the initial state of loading but also on the entire history of normal and tangential forces.
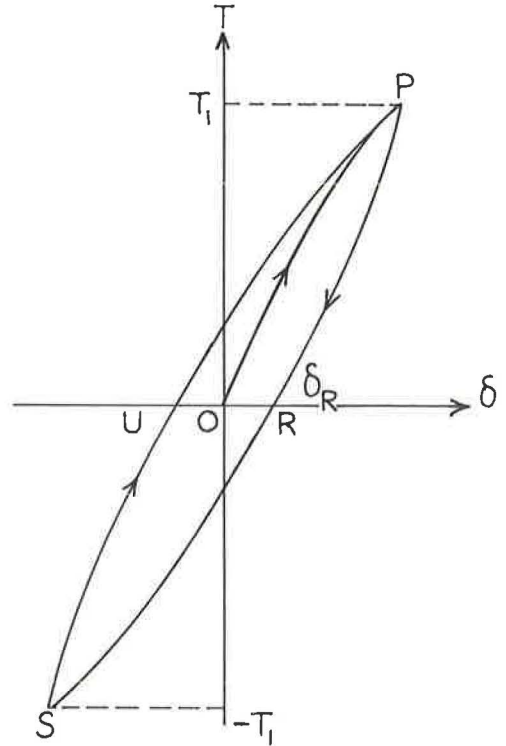

Figure 7. Theoretical hysteresis loop showing relative tangential displacement, δ, of centers of two spheres due to normal force (22).

Moreover, a variety of phenomena are involved which depend upon: whether either the normal or the tangential force is held constant while the other varies; whether they both vary and whether the sense of variation is such that one increases while the other decreases, both increase, or both decrease; whether the relative rate of change of the two forces is greater or less than the coefficient of friction; whether the immediately preceding history of loading was in the same or in the opposite sense as the current loading.

Deresiewicz (22) gives the solutions (i.e., the tangential compliances) for oblique forces applied in a certain manner, including the oblique force which maintains a constant direction but oscillates in magnitude between equal values—a problem connected with a vibration of a granular system. Deresiewicz also outlines the solution to the case of a twisting couple applied about the line of centers of two spheres in contact. The spheres are compressed by a constant normal force. The results are similar to those presented previously for a tangential force applied to the two spheres at constant normal force.

Velocity of Waves Through Granular System

To determine the velocity of compressional waves through a granular system, the grains have been assumed to be in elastic contact with each other and contact theory has been used.

Hara (34) studied the propagation of compressional waves of long wavelength in a system of equal spheres of cubic and rhombohedral (Case 3) arrangements. The direction of propagation was taken to be parallel to one of the edges of the unit lattice. The spheres were imagined to be replaced by mass-spring systems in series, in which the stiffness of each spring was computed from Hertz's theory of normal contact. If N is the normal force at each contact and R is the radius of each sphere, the velocity, C_1, of the compressional waves was found by Hara to be proportional to $(N/R^2)^{1/6}$. If the system is acted on by its own weight only, C_1 is proportional to the sixth root of the height of the system.

Gassmann (30) considered a rhombohedral (Case 6) system of equal spheres, each of radius, R. Taking as the origin the center of a sphere in the topmost layer (zero-layer) and taking the z-axis vertically downward, the following equations give the coordinates of the center of the sphere in the kth layer:

$$x = \frac{R}{2} \left[4i + 2j + (-1)^k + 1 \right] \tag{16}$$

$$y = \frac{\sqrt{3}}{4} R \left[4j + (-1)^k + 1 \right] \tag{17}$$

$$z = \frac{2\sqrt{6}}{3} R k \tag{18}$$

in which i and j are arbitrary integers.

Gassmann assumed there was zero pressure between spheres in the same layer and that a given sphere was subjected only to the weight of the spheres lying above it. The variations of the stress from its initial value are assumed to be small enough that the increments in the components of stress and strain are linearly related. If the number of layers and spheres is sufficiently large, the system at its initial state of stress can be considered a homogeneous anisotropic porous solid with the symmetry of Voigt's class No. 26 of crystals (53). In other words, the system has transversely isotropic symmetry (53), all directions perpendicular to the z-axis being equivalent with respect to elasticity. The matrix of the elastic constants is

C_1	$C_1 - 2C_5$	C_2	0	0	0
$C_1 - 2C_5$	C_1	C_2	0	0	0
C_2	C_2	C_3	0	0	0
0	0	0	C_4	0	0
0	0	0	0	C_4	0
0	0	0	0	0	C_5

in which $C_1 = \overline{C}$, $C_2 = C_4 = 4\overline{C}$, $C_3 = 16\overline{C}$, $C_5 = 0$ and

$$\overline{C} = \frac{1}{24\sqrt{2}} \left[\frac{6E^2 N_k}{(1-\nu^2)^2 R^2} \right]^{1/3} \tag{19}$$

N_k is the normal force on the contact between spheres of the kth and $(k+1)$th layers. If no load is assumed above the first layer

$$N_k = \frac{\pi}{3} R^2 \rho \, g \, z \tag{20}$$

assuming the density of the air filling the voids to be negligible in comparison with the density, ρ, of the spheres; g is the acceleration due to gravity. The partial differential equations of wave motion through the system can be obtained by substituting the elastic constants obtained previously into the general equations of motion of an elastic solid (53), assuming the wavelength to be large compared with R. The solution (30) gives the velocities of propagation of plane waves through the system. There exist in general three distinct wave velocities, corresponding to three different waves. Each velocity depends on the direction of wave propagation.

Gassmann calculated the variation of the largest velocity with depth using the elastic constants of granite and taking the z-axis as the direction of wave travel. The velocity varied as the sixth root of the pressure.

Deresiewicz (22) discusses the experimental work on the relation between the velocity, the pressure and the percentage of water filling the voids.

Brandt (7) considers a system of several sizes of spheres randomly packed. His model is closer to an actual granular system than are the regular models assumed by others. The largest (primary) spheres, of number, K_1, and radius, R_1, are assumed to be randomly packed to a porosity, n. The number, K_1, is taken to be large enough that the wall effect of the inclosure may be neglected. The volume V of the inclosure is

$$V = \frac{4\pi K_1 R_1^3}{3(1-n)} \tag{21}$$

Secondary spheres (K_2 in number and of radius, R_2) are assumed to be packed randomly in the voids of the primary system to the same porosity, n. In a similar manner, tertiary spheres are packed in the remaining voids, and finally quaternary spheres are randomly packed in the spaces that are left. If R_i/R_{i+1} is large enough

$$V_1 : V_2 : V_3 : V_4 = 1 : n : n^2 : n^3 \tag{22}$$

in which V_i is the total true volume of the ith set of spheres. This relation has been shown experimentally by Furnas (29) to be approximately true when $R_i/R_{i+1} \geq 5$.

If the volume of the inclosure containing the granular system is decreased so that the spheres deform, and Δ_1 is the decrease in the radius of each primary sphere, the new volume of the inclosure is

$$V_n = \frac{4\pi K_1 (R_1 - \Delta_1)^3}{3(1-n)} = \frac{4\pi K_1 R_1^3}{3(1-n)} - \frac{4\pi K_1 R_1^2 \Delta_1}{(1-n)} \tag{23}$$

neglecting terms involving Δ_1^2 as is done in the Hertz theory of contact. The decrease in the inclosure volume is

$$V_d = V - V_n = \frac{4\pi K_1 R_1^2 \Delta_1}{(1-n)} \tag{24}$$

The decrease in the volume of the spheres is of the order of Δ_1^2 and may be neglected. Hence, V_d may be taken as the decrease in void volume, that is, the decrease in the bulk volume of the secondary system of spheres resulting in a decrease Δ_2 in the radius of each secondary sphere. Repetition of this reasoning gives the relation

$$\frac{\Delta_2}{\Delta_1} = \frac{1}{nU} \tag{25}$$

in which $U = R_1/R_2$. Assuming $U = R_i/R_{i+1}$ $(i = 1, 2, 3, 4)$, this procedure yields

$$\frac{\Delta_i}{\Delta_1} = \frac{1}{(nU)^{i-1}} \tag{26}$$

Brandt then considers a case where the flexible inclosure of the granular system is subjected to an all-round pressure, p_0, while a liquid is introduced at a pressure P_L. An energy balance may then be set up in which the energy, E_T, required to decrease the bulk volume of the system is equated to the sum of the energy, E_S, used in deforming the spheres and the energy, E_L, employed to compress the interstitial liquid:

$$E_T = \frac{4 \pi K_1 R_1^2}{1 - n} \int_0^{\Delta_1} p_0 dx \tag{27}$$

and

$$E_S = \sum_{i=1}^{4} NK_i \int_0^{\Delta_i} F_i dx \tag{28}$$

in which N is the average coordination number of the spheres and is assumed to be the same for the four sets, which are packed to the same porosity, n, and F_i is the average force at the contact of a sphere in the ith set. The energy balance gives rise to a cubic equation in F_1. The approximate solution obtained by Brandt after insertion of the experimental value $N = 8.84$ is

$$F_1 = \frac{2.34 R_1^2 \left(p_0 - P_L \right)}{C_\varphi \left[1 + \frac{30.75 B^{3/2} (1 - \nu^2)}{E(p_0 - P_L)^{1/2}} \right]} \tag{29}$$

in which B is the bulk modulus of the liquid, ν, is the Poisson's ratio of the spheres and $(C_\varphi)^{1/3} = 2/3 n^{1/2}$, approximately. From this value of F_1, Δ_1 and the new bulk volume, V_n, of the system can be determined. V_n, can in turn be used to find the speed C_d of a dilatational wave in the system from the known equation

$$C_d = \left[\frac{3g}{\rho} (-V \frac{dp}{dV}) \left(\frac{1-\nu}{1+\nu} \right) \right]^{1/2} \tag{30}$$

in which ρ is the density of the total system including the interstitial fluid.

For a system with air in the voids (its density being neglected) Brandt obtains

$$C_d = \left[\frac{2g}{3 \rho n (1-n)} \left(\frac{1-\nu}{1+\nu} \right) \right]^{1/2} \frac{P_0^{1/6}}{K^{1/3}} \tag{31}$$

at low pressures, K being a constant.

Experimental data support the theoretical result of the proportionality of C_d to $P_0^{1/6}$ at low pressures but depart from it at high pressures. The point of transition between the behavior at low and high pressures probably represents the upper limit of applicability of the classical Hertz theory of contact (22).

Although the theoretical results of Hara, Gassmann and Brandt are in qualitative agreement with these experimental data, they predict values of the velocity of wave propagation less than those obtained by experiment because they consider only the normal

components of the forces at the points of contact and neglect the tangential components. Because the tangential stiffness of a contact has the same order of magnitude as its normal stiffness, it must be considered. This has been done for certain idealized granular systems.

Stress-Strain Solutions for Idealized Granular Systems

Tangential forces or twisting moments at the contacts between the grains of a granular system cause the load-displacement relations to be nonlinear and inelastic. Therefore, the mechanical response of the system depends not only on the initial loading but also on the history of loading and the stress-strain relations at any point of the system must be expressed as increments of stress related to increments of strain.

Duffy and Mindlin ($\underline{23}$) obtained a solution for a rhombohedral system (Case 3) of spheres subjected to a certain simple program of loading. The system is assumed to be initially subjected to an isotropic compressive stress, σ_O. An arbitrary incremental stress, small in relation to σ_O, is then applied. The initial contact forces are all purely normal and equal to each other. Also the compliances are nearly the same for all the contacts. The incremental stress-strain relations obtained are

$$
\begin{aligned}
d\sigma_{11} &= C_{11}d\epsilon_{11} + C_{12}d\epsilon_{22} + C_{12}d\epsilon_{33} \\
d\sigma_{22} &= C_{12}d\epsilon_{11} + C_{11}d\epsilon_{22} + C_{12}d\epsilon_{33} \\
d\sigma_{33} &= C_{12}d\epsilon_{11} + C_{12}d\epsilon_{22} + C_{11}d\epsilon_{33} \\
d\sigma_{23} &= 2C_{44}d\epsilon_{33} \\
d\sigma_{13} &= 2C_{44}d\epsilon_{13} \\
d\sigma_{12} &= 2C_{44}d\epsilon_{12}
\end{aligned}
\tag{32}
$$

in which

$$
C_{11} = \frac{2(4-3\nu)}{\nu} \quad C_{12} = 2C_{44} = \frac{4-3\nu}{2-\nu} \left(\frac{3\mu^2\sigma_O}{2(1-\nu)^2} \right)^{1/3}
\tag{33}
$$

The equations are referred to rectangular coordinate axes parallel to the edges of the unit cube of the system. The form of these relations corresponds to those in a crystal with cubic symmetry. From them, the velocity of wave propagation may be derived, assuming that the variations in the stress accompanying the propagation are small compared to the initial stress in the system. Strictly speaking, integration of Eq. 32 should be limited to increments in which the stress remains isotropic. When this is not the case, the compliances will vary from contact to contact and it will become necessary to consider the history of loading of each contact.

Duffy and Mindlin ($\underline{23}$) have also obtained solutions for the case when the system is subjected to a loading giving rise to an isotropic pressure, σ_O, and a uniaxial pressure, σ_a, parallel to one of the edges of the unit cube. The subsequent increments in loading are supposed to be variations in either σ_O or σ_a. The differential stress-strain relations have the same form as those of a tetragonal crystal with six independent elastic moduli. In this case, there are two types of contacts, each with a different loading history.

MECHANICAL RESISTANCE PROPERTIES OF GRANULAR SYSTEMS

As a result of Coulomb's studies, the shearing strength, s, of a granular system is commonly expressed as $s = \sigma \tan \phi$ in which σ is the normal pressure on the failure plane and ϕ is the so-called angle of internal friction. The resistance to shear is due to a combination of effects, including sliding friction, rolling friction and interlocking ($\underline{88}$). Tan ϕ, the shearing strength per unit normal stress, is not constant but depends on a number of factors. Methods of measurement of tan ϕ and their comparative merits are discussed in various references ($\underline{9}$, $\underline{12}$, $\underline{41}$, $\underline{51}$, $\underline{70}$, $\underline{74}$, $\underline{80}$, $\underline{87}$, $\underline{93}$).

Dependence of Tan ϕ on Void Ratio

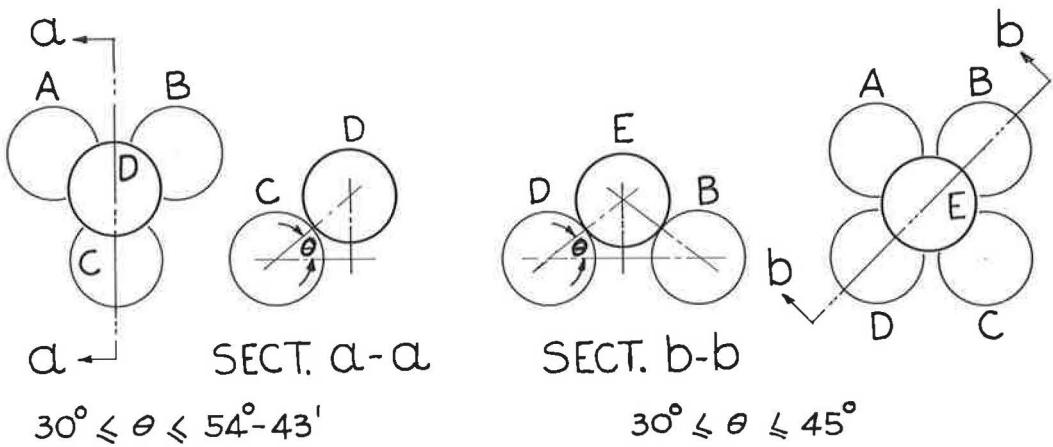At a constant normal stress, tan ϕ (i.e., peak value) increases as the initial void

CASE 6

CASE 3

Figure 8. Units of generalized rhombohedral system.

ratio decreases. When a dense granular system is sheared, it expands, because the closely interlocked grains need sufficient space to be able to roll or slide over one another. The increase in volume means that work is done against the normal pressure which reflects itself in a higher tan ϕ. In a loose system containing many arches, the volume will decrease during shear as the arches are broken down and the grains rearrange themselves to a denser state. Eventually the critical void ratio is attained at which shear continues at constant volume (14, 88). Winterkorn suggests that in shear, granular systems behave as macromeritic liquids (98). The comparison with ordinary molecular liquids gave rise to the following formula (100):

$$\tan \phi = \frac{C'}{V - V_{min}} \qquad (34a)$$

which is equivalent to

$$\tan \phi = \frac{C}{e - e_{min}} \qquad (34b)$$

in which C' and C are constants, e is the void ratio, V is the volume of the system in the given state, and e_{min} and V_{min} are the corresponding values with the system in the densest possible state. Winterkorn's formula is verified by comparing its predictions with experimental data obtained by various workers.

Idel (42) considered a generalized rhombohedral system (Case 6) of equal spheres. In this system every three spheres forming a hollow to support a fourth sphere were generally not in contact with each other (Fig. 8). This resulted in a higher porosity than the 26 percent of the normal rhombohedral system in which the three supporting spheres are in contact with each other. Idel defined the contact angle θ as the angle made with the horizontal by the normal at the point of contact between the upper and a lower sphere (Fig. 8). The following relation was obtained:

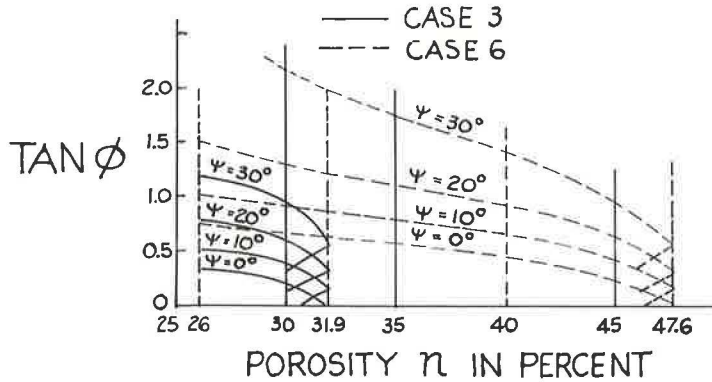$$n = 1 - \frac{\pi}{9\sqrt{3}} \frac{1}{\sin \theta \cos^2 \theta} \qquad (35)$$

Figure 9. Wittke's solution for tan ϕ of rhombohedral system as function of porosity for different values of coefficient of friction f, i.e., tan ψ (102).

in which n is the fractional porosity. For the usual (densest) rhombohedral system (Case 6), $\theta = 54°43'$. For the Case 3 generalized rhombohedral system (four supporting spheres) Wittke obtained

$$n = 1 - \frac{\pi}{12} \frac{1}{\sin \theta \cos^2 \theta} \tag{36}$$

In this case $\theta = 45°$ for the densest state when n = 26 percent. The least possible value of θ for either case is $30°$.

From statical considerations, Wittke (102) obtained the following relation for the angle ϕ of the general rhombohedral system (either case) under the stress conditions of the triaxial test:

$$\tan^2\left(\frac{\phi}{2} + 45°\right) = 2 \tan \theta \tan (\theta + \psi) \tag{37}$$

in which tan ψ = f, the coefficient of friction between the spheres. Because θ is related to n by Eqs. 35 or 36, tan ϕ may be related by Eq. 37 to n. Curves of tan ϕ against n can thus be drawn for given values of tan ψ (Fig. 9). These curves differ for Cases 3 and 6 of the rhombohedral system, because Eqs. 35 and 36 are different.

Wittke performed experiments on glass beads packed in the generalized rhombohedral state. The measured tan ϕ values were about 50 percent lower than the theoretical values according to Eq. 37. The major part of this discrepancy was attributed to friction developed between the end layers of the system (top and bottom) and the bounding plates.

The theory developed by Wittke is based on a particular idealized granular system. Because, as indicated by Figure 9, tan ϕ depends considerably on the arrangement of the system, Wittke's solution for tan ϕ as a function of n cannot be considered applicable directly to a general granular system, such as a sand. In the shear zone of a dense granular system, there is a loosening up as compared to the rest of the system (93, 102). The over-all volume changes taking place during shearing are considered by Newland and Allely (65) and by Poorooshasb (69).

Dependence of Tan ϕ on f

A number of expressions have been derived relating tan ϕ to the coefficient of friction between the grains, f. Caquot (13) considered an irregular system composed of grains of various sizes and shapes in random distribution and found that tan $\phi = (\pi/2)f$.

Bishop (2) obtained approximate expressions for ϕ from energy considerations. In the case of triaxial compression in which $\sigma_2 = \sigma_3 < \sigma_1$,
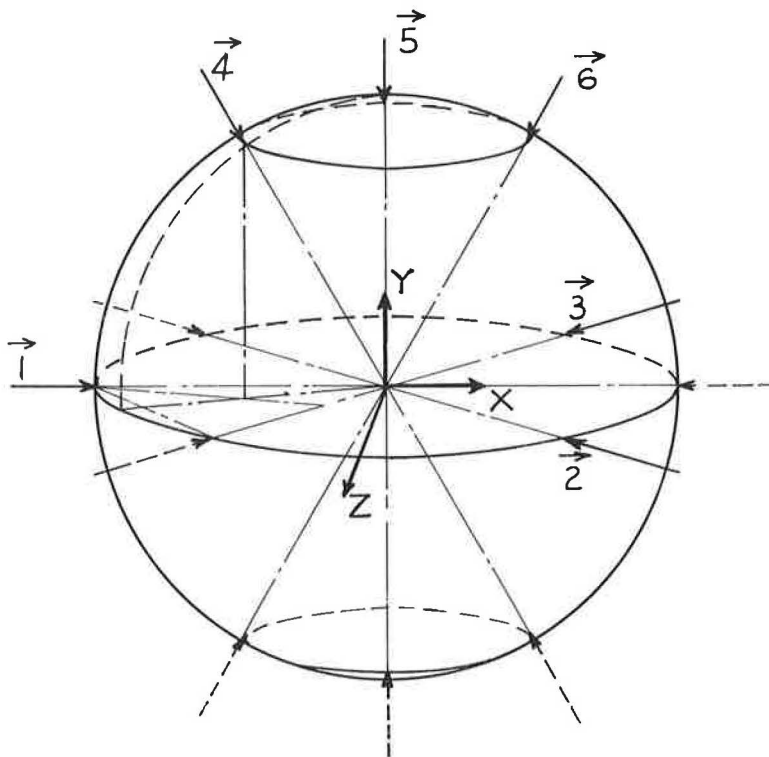
Figure 10. Normal unit vectors at 12 tangent points of sphere in Case 6 rhombohedral system (20).

$$\sin \phi = \frac{15 f}{10 + 3 f} \quad (\sigma_1 = \text{normal stress}) \tag{38}$$

For plain strain where $\sigma_2 = \dfrac{\sigma_1 + \sigma_3}{2}$,

$$\sin \phi = 3/2 \, f \tag{39}$$

The expressions of both Bishop and Caquot give $\tan \phi = 0$ when $f = 0$ (Fig. 12). This cannot be true for void ratios below the critical value, because in such cases a finite amount of work must be done against the normal forces as the system expands.

Considering a rhombohedral (Case 6) system of equal spheres, Dantu (20) obtained relations between $\tan \phi$ and f in the following manner. Each sphere has 12 points of contact with neighboring spheres and the direction cosines of the unit normal vectors (Fig. 10) are given in Table 3.

Assuming the system is subjected to normal stresses, σ_x, σ_y, σ_z, and to shear stresses, τ_{xy}, τ_{yz}, τ_{zx}, the usual notation for the subscripts being used, the normal reactions between the grains can be calculated from considerations of statics.

Assuming zero friction between the spheres:

TABLE 3

DIRECTION COSINES OF
UNIT NORMAL VECTORS[a]

Normal Vector	α	β	δ
$\overline{1}$	1	0	0
$\overline{2}$	$-1/2$	$+\sqrt{3/2}$	0
$\overline{3}$	$-1/2$	$-\sqrt{3/2}$	0
$\overline{4}$	$+1/2$	$+\sqrt{3/6}$	$-\sqrt{6/3}$
$\overline{5}$	0	$-\sqrt{3/3}$	$-\sqrt{6/3}$
$\overline{6}$	$-1/2$	$+\sqrt{3/6}$	$-\sqrt{3/6}$

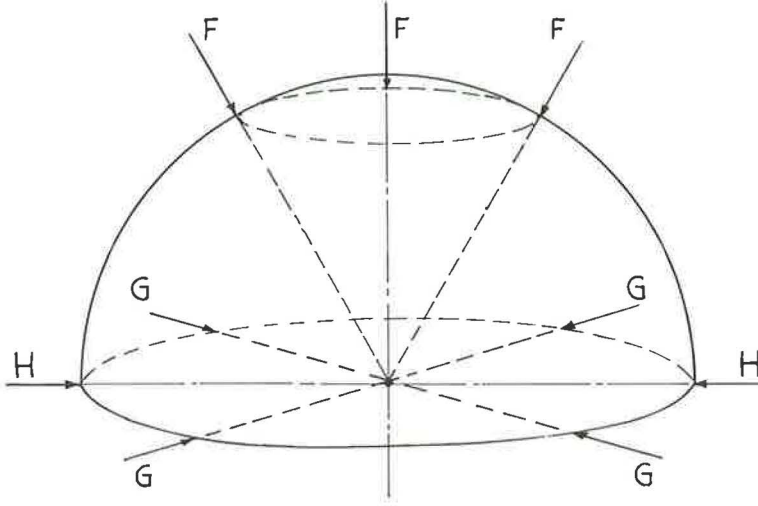[a] α, β, and δ are the direction cosines referred to the x, y, and z axes, respectively (Fig. 10).

Figure 11. Normal reactions acting on sphere in Case 6 rhombohedral system when system is subjected only to normal stresses, σ_x, σ_y and σ_z (20)

1. If $\tau_{xy} = \tau_{yz} = \tau_{zx} = 0$,

$$F = R^2 \sqrt{2}\, \sigma_z, \quad G = \frac{R^2 \sqrt{2}}{3}\, (4\sigma_y - \sigma_z), \quad H = \frac{R^2 \sqrt{2}}{3}\, (6\sigma_x - \sigma_z - 2\sigma_y) \qquad (40)$$

in which R is the radius of the spheres and F, G, H are the normal reactions between the spheres (Fig. 11);

2. If $\tau_{xy} = \tau_{yz} = \tau_{zx} = 0$, and $\sigma_x = \sigma_y = \sigma_r$, as in the triaxial test

$$F = R^2 \sqrt{2}\, \sigma_z, \quad G = H = \frac{R^2 \sqrt{2}}{3}\, (4\sigma_r - \sigma_z) \qquad (41)$$

3. If $\tau_{xy} = \tau_{yz} = \tau_{zx} = 0$, and $\sigma_x = \sigma_y = \sigma_z = \sigma$, corresponding to application of a hydrostatic pressure to the system, then

$$F = G = H = R^2 \sqrt{2}\, \sigma \qquad (42)$$

In Case 2, failure of the system will occur when G = H = 0, i.e., when $\sigma_z/\sigma_r = 4$. This corresponds to $\tan \phi = 0.750$ or $\phi = 36°52'$. Assuming a coefficient of friction, f, between the spheres, Dantu finds by statics for this case that

$$F = \frac{2R^2}{\sqrt{2} + f}\, \sigma_z, \quad G = H = \frac{8\,R^2\sqrt{2}}{6}\, \left(\sigma_r - \sigma_z\, \frac{\sqrt{2}}{4}\, \frac{1 - \sqrt{2}\,f}{\sqrt{2} + f} \right) \qquad (43)$$

The condition of limiting equilibrium corresponds to G = 0 when

$$\frac{\sigma_z}{\sigma_r} = 4\, \frac{\sqrt{2} + f}{\sqrt{2} - 2f} \qquad (44)$$

from which

$$\sin \phi = \frac{\sigma_z - \sigma_r}{\sigma_z + \sigma_r} = 3\, \frac{\sqrt{2} + 2f}{5\sqrt{2} + 2f} \qquad (45)$$

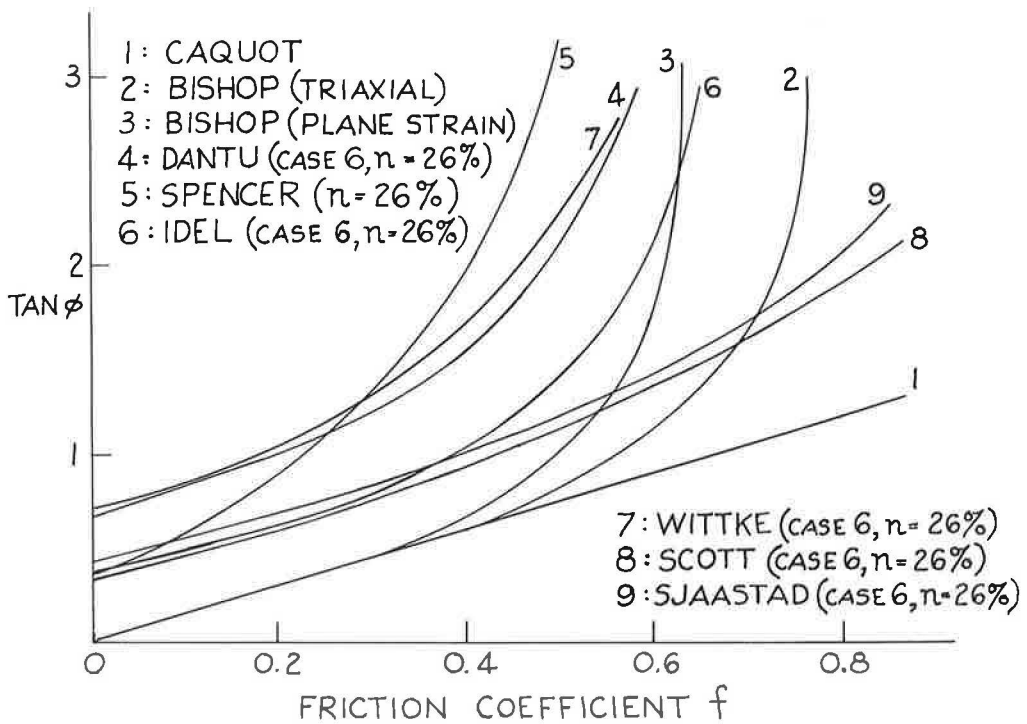The curve representing $\tan \phi$ against f is compared in Figure 12 with curves obtained

Figure 12. Different theoretical solutions for tan ϕ of regular system of spheres in terms of coefficient of friction f of spheres.

by others. Tan ϕ tends to infinity ($\phi = 90°$) when $f = \sqrt{2}/2 = 0.71$. Physically this means that for values of f greater than 0.71, the granular system can have vertical sides and at the same time support a vertical load without any lateral support. Failure occurs by actual crushing of the grains when the load has attained a sufficiently high value.

Considering an ideal packing of equal spheres, Spencer (84) obtained a relation between ϕ, f and n.

In his study of the generalized rhombohedral system (Case 6), inclosed in a cylinder as in a triaxial test, Idel (42) obtained from statical considerations the following expression:

$$\sin \phi = \frac{1.5 \tan (\psi = \theta) - 1}{1.5 \tan (\psi + \theta) + 1} \tag{46}$$

in which $\tan \psi = f$. Because n is related to θ by Eq. 35, this expression gives the variation of tan ϕ with f at different porosities. Eq. 46 is different from Eq. 37 from which Wittke's curve is drawn.

Extending the theoretical calculations of Thurston and Deresiewicz (90) on the mechanism of failure of a rhombohedral system of equal spheres, Scott (75) obtained

$$\tan \phi = \frac{\sqrt{3} + (4\sqrt{2})f}{2(\sqrt{6} - f)} \tag{47}$$

Sjaastad (79) considered a Case 6 system and ignored the contribution to shear strength of rolling friction as compared to that of sliding friction. Failure of the system occurs when one distinct layer of spheres, together with all those above it, slides over the layer immediately below, which remains at rest together with all the lower layers. Considering a typical sphere resting in the hollow formed by the three spheres below it, it is apparent that there are two extreme modes of failure: (a) type 1 in which
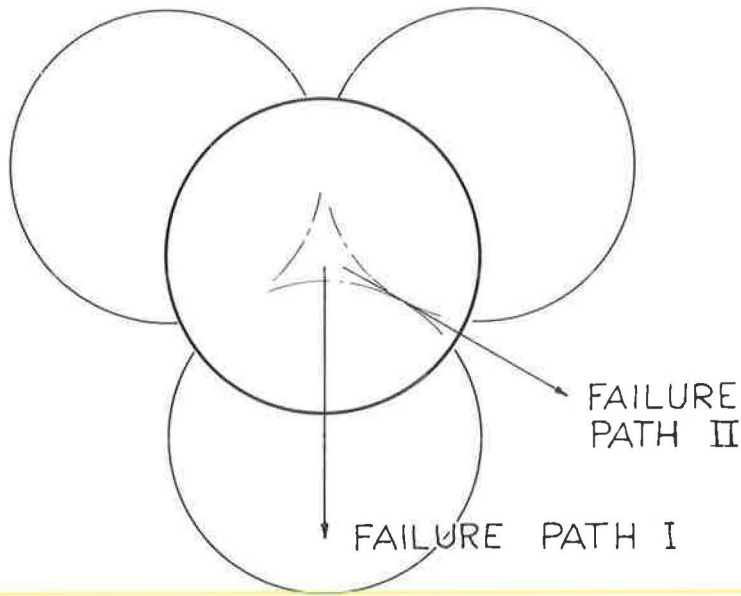
Figure 13. Two extreme failure paths in Case 6 rhombohedral system (79).

the top sphere slides directly over the top of one of the bottom spheres, and (b) type 2 in which the top sphere slides through the cleavage between two of the lower spheres (Fig. 13). Two conditions must be considered in each mode of failure: (a) the static case in which failure is about to occur, and (b) the kinetic case existing after a very small displacement when the top sphere has lost contact with one or two of the underlying spheres. The expressions obtained by Sjaastad are as follows:

1. Type 1, static case

$$\tan \phi = \frac{1}{\sin \theta - f \cos \theta} \left[\cos \theta + \frac{f}{3(\sin \theta + f \cos \theta)} \right] \tag{48}$$

and kinetic case

$$\tan \phi = \frac{\cos \theta + f \sin \theta}{\sin \theta - f \cos \theta} \tag{49}$$

in which $\theta = 54°43'$.

2. Type 2, static case

$$\tan \phi = \left[\frac{2f}{3(\sin \theta + f \cos \theta)} + \sin \alpha \right] / \left[\cos \alpha - \frac{f \sin \alpha}{\sin 60} \right] \tag{50}$$

and kinetic case

$$\tan \phi = \frac{\sin \alpha \sin 60° + f \cos \alpha}{\cos \alpha \sin 60° - f \sin \alpha} \tag{51}$$

in which $\theta = 54°43'$ and $\alpha = 19°30'$.

For each type a mean curve is obtained (Fig. 14) by taking the average of the kinetic and static values. Assuming equal probability for any sphere to move along either failure path, Sjaastad obtained the curve for 26 percent porosity shown in Figure 12. Another assumption was that of equal partition of energy between the two extreme failure paths. Because less energy is required for type 2 failure, the probability ratio
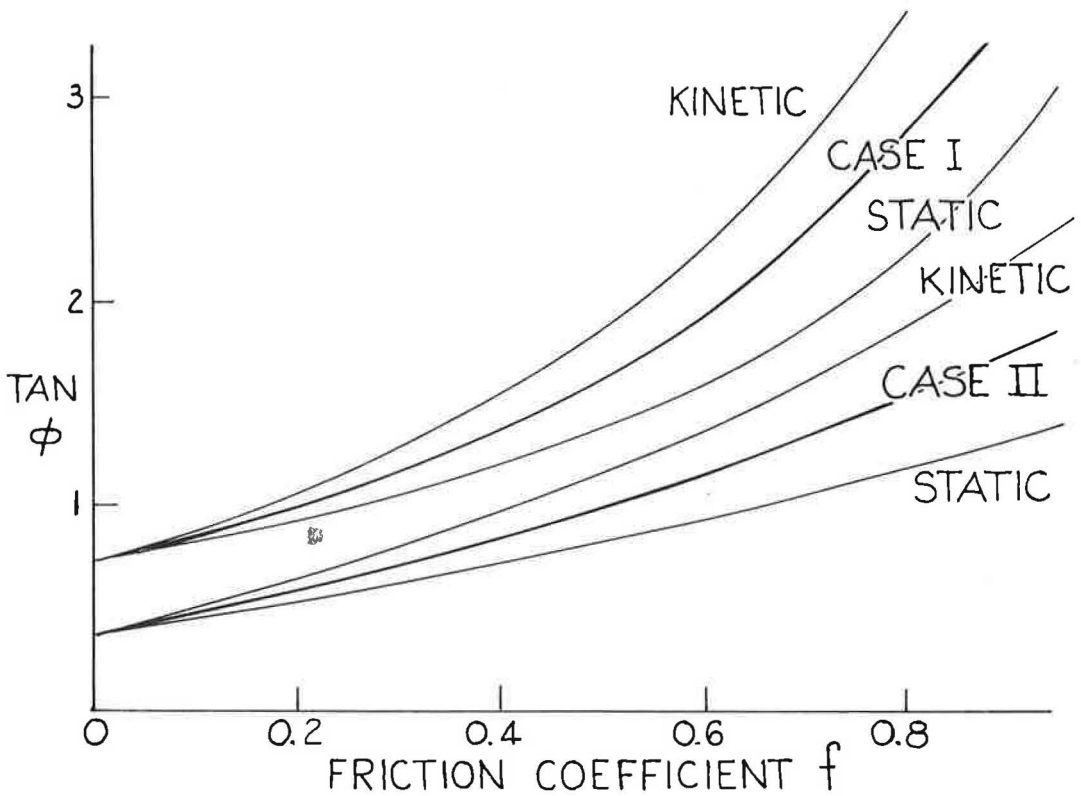
Figure 14. Sjaastad's theoretical solutions for tan ϕ of Case 6 rhombohedral system in terms of friction coefficient f (79).

is about 2 to 1 in favor of it. However, very little difference was found between the curve resulting from this assumption and that based on equal probability.

Sjaastad assumed that for the regular packing at the upper limit of porosity, the cubic, tan ϕ is equal to f. Therefore, curves at intermediate porosities could be obtained (Fig. 15) by assuming further that ϕ is proportional to the relative density. The latter assumption is based on data published by Burmister.

Some of the results obtained experimentally by various workers on systems with nearly perfect and equal spheres are plotted in Figure 15 in which there is satisfactory agreement with Sjaastad's equal partition solution in the range f = 0.1 to 0.5. In particular, although Sjaastad's data on glass beads at 38 percent porosity are somewhat greater than theoretical values, the line joining them is almost parallel to the theoretical curve at n = 38 percent. On the other hand, Sjaastad's data do not show such an agreement with the solutions of Spencer, Idel and Wittke. Considering all the data shown in Figure 15, they fit Spencer's solution best at the lower values of f, but Sjaastad's over a wider range.

None of these solutions are completely verified by the data now available. To determine which is the most accurate, values of tan ϕ at f $\geq$ 1 must be measured on granular systems approaching the ideal. Because the solutions diverge considerably at the higher values of f, such data should easily show which is the most valid.

All solutions except Caquot's show a rapid increase of tan ϕ with f. An increase in f is obtained when the system is subjected to a vacuum and some heat is applied, so that the adsorbed layers of gas are mostly removed and there is more intimate contact between the particles. Sjaastad's experiments (79) have proved this increase in f.
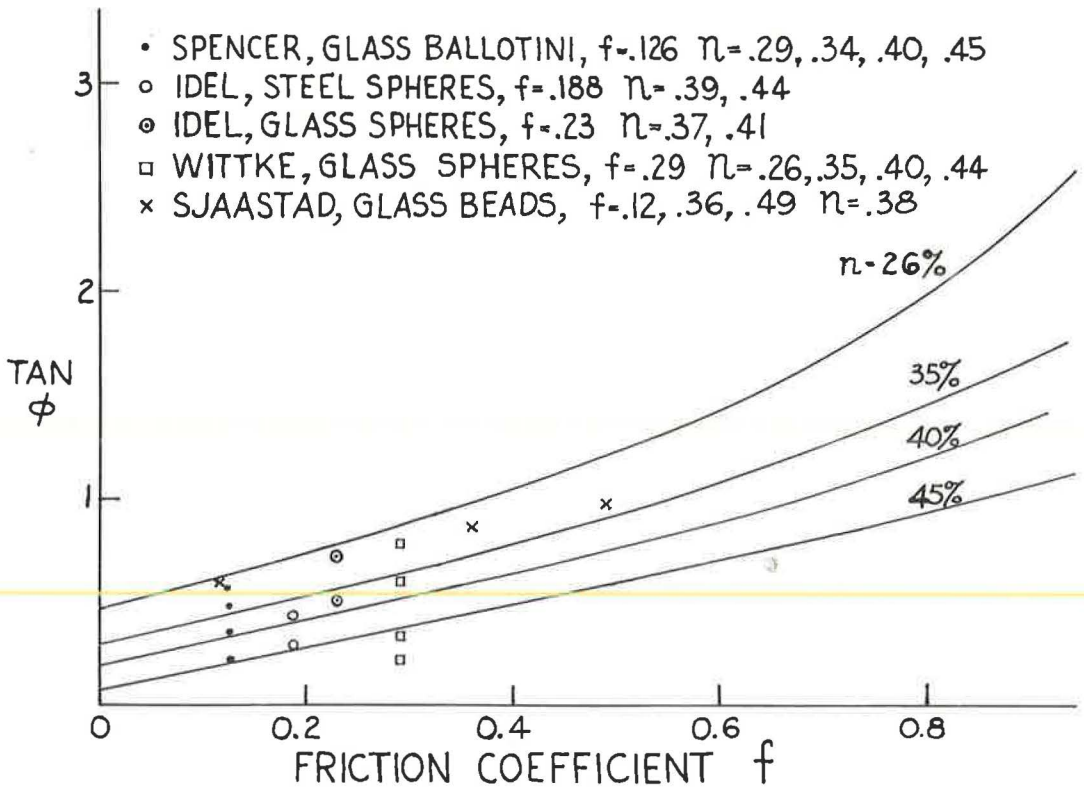
Figure 15. Experimental data on nearly ideal systems vs Sjaastad's Equal Partition of Energy solution (79).

Effect of Grain Size on Tan φ

According to the expressions for tan φ obtained by various workers on the basis of idealized granular systems, tan φ is independent of the absolute grain size of the system. To determine conclusively whether tan φ depends on the grain size, controlled tests on systems with regular arrangements of spherical grains of uniform size and surface characteristics should be performed. The results obtained until now are inconclusive, because the systems tested have generally departed more or less from uniformity in size, shape and condition of surface of their grains. Also care was not generally taken to obtain the same initial void ratios for the samples tested so as to afford a true basis for comparison. Wittke's (102) experiments are an exception, but the grain sizes used by him do not differ widely. Sjaastad (79) used a wider size range and also maintained the same initial void ratio, but his system was less ideal than that of Wittke.

Hennes (35) measured the shear strength of samples of rounded gravel of approximately uniform size. Tan φ was found to increase appreciably with grain size up to $\frac{1}{4}$ in., beyond which there was little variation (Fig. 16). The shapes of the grains varied considerably within each sample and from sample to sample. The results, therefore, do not show the influence of grain size alone. The samples were densified before testing in the same manner by tamping and vibration, causing widely differing values of the initial void ratio. However, Table 4 indicates that the largest size ($\frac{3}{4}$ to $\frac{1}{2}$ in.) had a considerably greater initial void ratio than the smaller sizes. Because tan φ increases as the void ratio decreases, the largest size may be expected to show a value of tan φ greater than 1.17 at the same void ratios as the smaller sizes. This indicates a tendency of tan φ to increase with grain size in the tested range, but it is not conclusive owing to nonuniformity of the samples in size and shape. The resistance
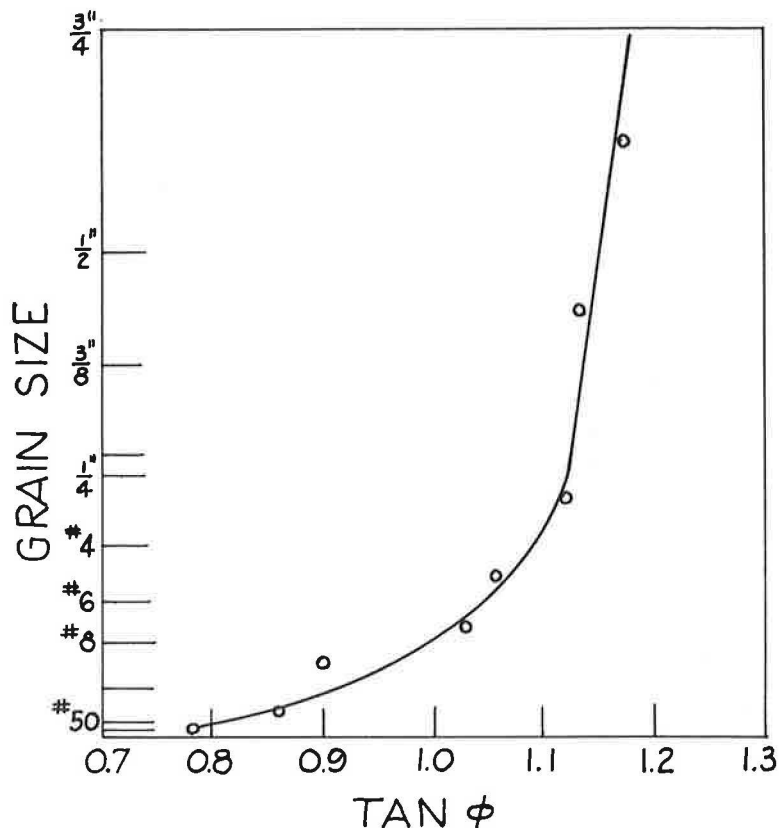
Figure 16. Hennes' experimental curve showing effect of grain size on tan ϕ for rounded gravel (35).

to shear depends considerably on the state of packing, particularly along the plane of sliding, and the packing is influenced by the gradation and shape characteristics.

From tests on crushed quartz in loose state, Parsons (68) found that tan ϕ had a minimum value at a grain size of 0.75 mm (Fig. 17). The samples were placed in the shear box by pouring from the same height. The results are inconclusive, because the degree of angularity or sharpness of the grains varied with the grain size.

Kjellman and Jakobson (48) obtained a higher value of ϕ at a larger grain size (Table 5) using samples of round pebbles. The initial void ratio, e_o, of the coarser samples was larger (i.e., smaller unit weight), so that if corrected to the same e_o the difference between the values of ϕ for the fine and coarse material would become greater. Here again the results are inconclusive, because secondary effects may have played a part.

Using samples of sand, Wu (103) obtained decreasing values of ϕ with increasing grain size in the range from 0.1 to 3 mm. This is at least partly due to the greater nonuniformity of the coarser samples (42). For systems at the same void ratio, tan ϕ decreases as the nonuniformity increases.

From triaxial tests on glass beads and quartz sand, Idel (42) concluded that tan ϕ was independent of grain size. The size of the glass beads tested varied from 3 to 35 mm, whereas that of the

TABLE 4

HENNES' EXPERIMENTAL DATA (35)[a]

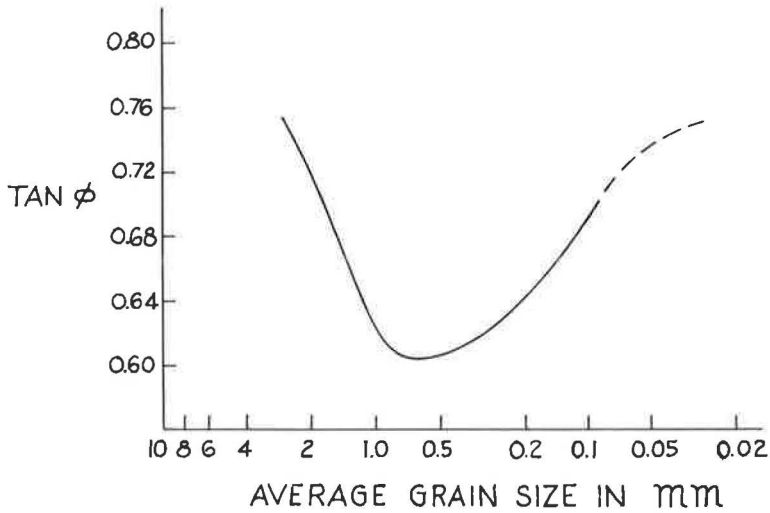| Grain Size	Direct Shear Tan ϕ	Init. Void Ratio	Triaxial Tan ϕ	Init. Void Ratio
Nos. 8-16	0.903	0.698	0.91	0.61
Nos. 3-4	1.12	0.622	0.93	0.61
3/4-1/2 in.	1.17	0.85	1.03	0.58

[a]On samples of rounded gravel.

Figure 17. Parsons' experimental curve showing effect of grain size on tan φ for crushed quartz (68).

quartz sand varied from 0.4 to 5 mm. Idel's results, however, showed a considerable scatter in the measured values of tan φ. For instance, in the case of the glass beads at a porosity of 39.5 percent, the measured values of tan φ ranged from 0.55 to 0.70.

Wittke (102) developed an ingenious experimental technique for obtaining a system of practically uniform glass beads in a rhombohedral packing (Case 3 or 6) and for testing it triaxially in that state. With a porosity of 26 percent, the value of tan φ for three sizes of glass beads (15.0, 14.8 and 11.85 mm) stayed nearly constant at 0.37 in the Case 3 state. With Case 6 packing (porosity also 26 percent), tan φ varied slightly from 0.78 to 0.86 for the three sizes. However, Wittke's results do not permit generalization, because the sizes used varied only over a narrow range.

Bishop's measurements (3) on Chesit Bank pebbles and on Ham River sand showed that the two materials had nearly the same tan φ at equal porosities. The ratio of the two sizes was 1:60. Casagrande (15) reports a similar constancy of tan φ with grain size.

Sjaastad (79) performed direct shear tests on five nearly uniform samples of glass beads. Each sample passed one U. S. standard sieve and was retained on the next sieve. The mean sizes varied from 0.46 to 3.1 mm, and the initial void ratio was kept constant at 0.608. The results (Fig. 18) support the argument that tan φ is independent of grain size. The considerably higher φ value shown by the 1.1-mm sample was attributed to its greater uniformity compared with the others, shown by microscopic observation.

In summary, there is some evidence indicating an increase of tan φ with grain size. However, the evidence is inconclusive, because this increase may well be due solely to secondary effects such as shape and nonuniformity of the component particles and variation in their surface characteristics. There exists more and better evidence suggesting that tan φ is independent of grain size.

Other Factors Influencing Tan φ

It has been established experimentally

TABLE 5

KJELLMAN AND JAKOBSON'S
EXPERIMENTAL DATA (48)[a]

Pebble Type	Size (mm)	Init. Unit (t/m³)	φ (deg)
Fine[b]	8 – 11	1.54	36.2
Coarse[b]	38 – 53	1.43	37.1
Fine[c]	8 – 11	1.63	42.9
Coarse[c]	38 – 53	1.53	44.1

[a]On samples of round pebbles.
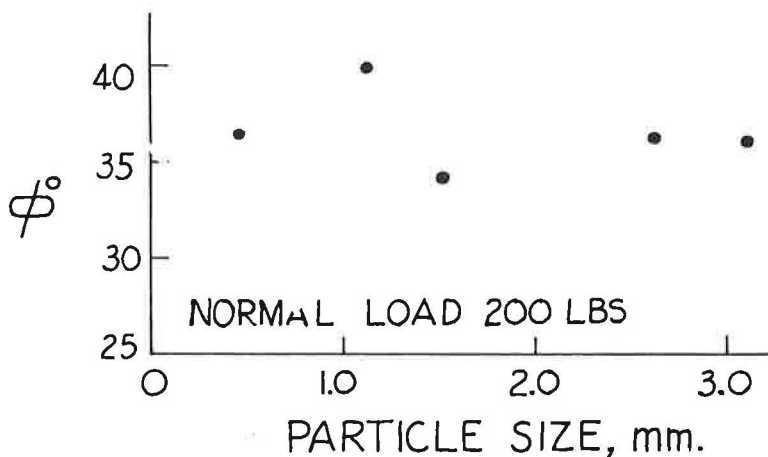[b]Loose state. [c]Dense state.

Figure 18. Sjaastad's experimental data showing effect of grain size on ϕ for glass beads (79).

for granular soil systems that tan ϕ decreases with the applied normal pressure (88). It is also found that tan ϕ increases with increasing angularity of the grains, i.e., with decreasing sphericity (15, 16, 35, 88).

A uniform granular system with constant void ratio and a certain friction coefficient, f, may have different values of tan ϕ depending on its mode of packing. Wittke (102) found theoretically that a system of uniform spheres in the Case 3 packing had about half the value of tan ϕ as the same system in Case 6 packing. This was also verified experimentally. Because Case 6 may be turned into Case 3 by a suitable rotation in space, Wittke's findings indicate anisotropy. That is, the value of tan ϕ depends on the direction of the applied stresses.

Wittke's theory also shows that the stress and strain conditions affect tan ϕ. Thus, for example, his theory gives a value of 1.0 for a Case 6 system at an f of 0.1 when the conditions are those of a plane-strain test, whereas for the same system under the conditions of a triaxial test, tan ϕ equals 0.9. This finding provides an explanation for the higher experimental values of tan ϕ of a granular soil obtained by the box shear test as compared with those obtained by triaxial testing (35, 88).

Whitman (96) has shown experimentally that tan ϕ is independent of the rate of strain in the triaxial test when the failure-time is varied from 5 msec to 5 min.

Certain experimental variables, such as the ratios of the dimensions of the sample tested and the ratio of its diameter to that of the inclosing cylinder, may affect the measured tan ϕ (102). These are not discussed here, because they do not pertain to the system as such but only to the experimental technique.

Granular Systems with Different Grain Sizes

Figure 19 shows the porosities obtained for granular systems containing two grain sizes when the systems are subjected to equal amounts of compactive effort. For a system of given grain size ratio, there is a certain composition that gives the least porosity. The further the system is from uniformity, i.e., the smaller the ratio d_{min}/d_{max}, the easier it is to obtain smaller porosities. Comparison of the shear strengths of different granular systems at the same porosities shows that uniform systems have the greatest shear strength, other factors such as grain shape and roughness being equal (16, 35, 100, 105).

Assuming that tan ϕ varies linearly with n between 26 percent and 43 percent (justified according to Wittke's (102) solution), Idel (42) comes to the conclusion that all granular systems of two grain sizes should have the same tan ϕ when in the densest possible state, no matter what their percentage composition or grain size ratio (of course, assuming
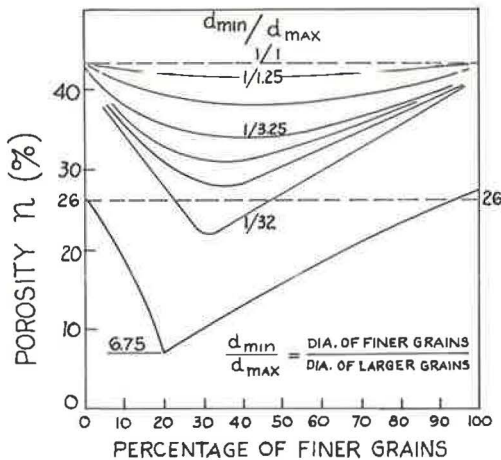
Figure 19. Porosities of systems composed of grains of two sizes and subjected to equal amounts of compactive effort (42).

equal shapes and f values). This conclusion is expected by Idel to hold for systems of more than two sizes. The same would apply to the systems in their loosest state. For an intermediate porosity, Idel assumes that the corresponding tan ϕ value can be found by linear interpolation. The nearer the system is to uniformity, the larger is the rate of change of tan ϕ with n.

The term relative density is used to indicate the position of the system between its loosest and densest states, these latter being obtained by arbitrarily fixed procedures (10, 49). Relative density = $(n - n_d)/(n_\ell - n_d)$ at a porosity n in which n_ℓ, n_d are the loosest and densest porosities. A comparison in importance has been made of n_ℓ and n_d to the liquid and plastic limits of a clay. The relative density determines, among other things, the supporting value of the system and its compressibility (10).

Burmister (10) gives results showing a linear variation of ϕ with the relative density of a given system. Wu (103) obtains similar results.

Hennes' (35) experimental results show that increasing angularity (i.e., nonsphericity of the grains) causes a greater increase in the shear strength of a graded system than in that of a system with uniform grain size.

TESTING OF MACROMERITIC SYSTEMS THEORY

According to the macromeritic theory, a granular system of identical spheres is in a potentially liquid state when it has a void ratio of 0.62 (the critical value) or higher (98, 100). The critical void ratio (CVR) thus corresponds to the melting point of simple chemical substances. Winterkorn (100) derived Eq. 34a on the basis of Batschinski's formula for the viscosity of simple molecular liquids at different temperatures. However, Eq. 34a can be expected to hold strictly only for the macromeritic liquid state, i.e., for systems above the CVR. It is, however, equivalent to Eq. 34b, whose predictions have been compared with data obtained from shear tests (direct or triaxial) on cohesionless soils (25).

Data from direct shear tests on Ottawa standard sand (88, p. 349) produced a curve for a normal pressure of 3 tons/sq ft in which $\phi = 32.3°$ when e = 0.57, and $\phi = 29.5°$ when e = 0.61. Substitution of these values in Eq. 34b yields values for C and e_{min} of 0.226 and 0.212, respectively. The formula can then be used to calculate values of tan ϕ at any void ratio, and the same normal pressure, as in Table 6 which shows good agreement between values. Whenever the experimental data at high void ratios are higher than the calculated ones, partial collapse to a lower void ratio during the testing may be suspected. Table 7 shows the values of e_{min} and C calculated at different normal pressures by means of Eq. 34b. At each normal pressure, two values of e were applied together with the corresponding measured ϕ values. The table indicates that at different normal pressures C does not deviate by more than 12 percent. These calculations have been made using data from experimental curves arbitrarily drawn as mean curves through points showing considerable scatter (89, Fig. C-5). Thus, a 12 percent deviation of C is not excessive.

The values of e_{min} in Table 7 are rea-

TABLE 6

CALCULATED VS EXPERIMENTAL
TAN ϕ VALUES[a]

Void Ratio e	Tan ϕ		Dev. ($\%$)
	Cal.	Exp.	
0.56	0.650	0.649	+ 0.2
0.59	0.598	0.596	+ 0.3
0.62	0.554	0.554	0.0
0.64	0.528	0.539	- 2.0
0.66	0.505	0.531	- 4.9

[a]Experimental data from Taylor (88, p. 349).

sonable when compared with the value 0.35 for the void ratio of the densest (rhombohedral) state of an assembly of equal spheres. The samples on which the data were obtained were only approximately uniform in size and their grains were not spherical. Therefore, they may be expected to have a "densest state" of lower void ratio than 0.35.

Data from triaxial tests on washed Fort Peck sand (88, p. 350) at a minor principal stress, σ_3, of 34 psi, produced experimental values of $\phi = 41.6°$ at $e = 0.62$, and $\phi = 34.0°$ at $e = 0.825$. From these and Eq. 35, $e_{min} = -0.028$ and $C = 0.575$ giving the calculated values of tan ϕ in Table 8. Though a negative e_{min} value is used in the formula, it gives good predictions.

Data from direct shear and triaxial tests on Sand B (87, p. 1061) are summarized in Table 9. For each type of test the values of C show good agreement. A comparison of the two types, however, shows that the value of C depends on the kind of test used for measuring the shear strength. Table 9 shows that the triaxial test gives higher values of C and this is confirmed by calculations with other experimental data (25). This variation of C with method of test is probably due to the different stress conditions imposed on the system.

De Beer (21, p. 281) obtained data by means of triaxial tests on sand at constant σ_3. The experimental curves show the variation of ϕ with n at various values of σ_3 from 0.02 kg/cm^2 to 50 kg/cm^2. The curve at $\sigma_3 = 1$ kg/cm^2 gives the following values: (a) at n = 0.39 (e = 0.640), $\phi = 41.7°$; and (b) at n = 0.45 (e = 0.818), $\phi = 34.0°$. These values give $e_{min} = 0.083$ and C = 0.496 from Eq. 34b which is then used at other void ratios to obtain the calculated tan ϕ values in Table 10. The agreement with the experimental data is very good. Table 11 gives the values of C and e_{min} calculated from the data at different σ values.

It is seen that in the large stress range from 0.02 to 50 kg/cm^2, C is practically constant, as it should be. As σ_3 increases, e_{min} shows a consistent decrease.

Burmister's data from direct shear tests performed on Ottawa standard sand (9, pp. 1073-75) have been applied to Eq. 34b to give Table 12. Here again the constancy of C is confirmed.

Wu's data (103) from triaxial tests on three specimens of sand referred to as 134, 121, 133, respectively, give Table 13. For each specimen, the value of C is approximately the same at the two values of σ_3.

TABLE 7

VALUES OF C AND e_{min} [1]

Normal Pressure (ton/sq ft)	e	e_{min}	C	Dev.[2] (%)
1/2	0.58, 0.62	0.235	0.236	+ 8.2
3	0.57, 0.61	0.212	0.226	+ 3.7
8	0.55, 0.59	0.235	0.192	- 11.9

[1] From Taylor (88, p. 349).
[2] Of C from mean value.

TABLE 8

CALCULATED VS EXPERIMENTAL TAN ϕ VALUES[a]

Void Ratio e	Tan ϕ		Dev. (%)
	Calc.	Exp.	
0.65	0.848	0.853	- 0.6
0.70	0.790	0.798	- 1.0
0.75	0.740	0.747	- 0.9

[a] From Taylor (88, p. 350).

TABLE 9

VALUES OF C AND e_{min} [1]

Test[2]	σ_3 (psi)	e_{min}	C
Direct shear	18	0.055	0.504
	34	0.083	0.465
Triaxial	18	- 0.128	0.653
	34	- 0.123	0.621

[1] From Taylor (87, p. 1061).
[2] Using values of e of 0.60 and 0.70 in all tests.

TABLE 10

CALCULATED VS EXPERIMENTAL TAN ϕ VALUES[a]

Porosity n	Void Ratio e	Tan ϕ		Dev. (%)
		Calc.	Exp.	
0.36	0.562	1.058	1.018	+3.9
0.41	0.695	0.810	0.813	-0.4
0.43	0.755	0.738	0.743	-0.7
0.47	0.886	0.617	0.636	-3.0

[a] Experimental data from De Beer (21, p. 281).

TABLE 11

VALUES OF C AND e_{min}[1]

Confining Stress σ_3 (kg/cm²)	e	e_{min}	C	Dev.[2] (%)
0.02	0.640, 0.818	0.132	0.533	+5.3
0.1	0.640, 0.818	0.118	0.520	+2.8
0.2	0.640, 0.818	0.110	0.515	+1.8
1	0.640, 0.818	0.083	0.496	-2.0
2	0.640, 0.818	0.051	0.497	-2.2
5	0.613, 0.785	0.000	0.504	-0.4
10	0.613, 0.785	-0.030	0.501	-1.0
50	0.613, 0.754	-0.085	0.485	-4.3

[1]From De Beer (21, p. 281).
[2]Of C from mean.

TABLE 12

VALUES OF C AND e_{min}[1]

Normal Pressure (kg/cm²)	e	e_{min}	C	Dev.[2] (%)
2.033	0.483, 0.637	0.208	0.278	+1.5
1.533	0.501, 0.651	0.204	0.224	+7.3
1.033	0.506, 0.663	0.264	0.261	-4.7
0.533	0.499, 0.656	0.274	0.262	-4.4

[1]From Burmister (9, pp. 1073-1075).
[2]Of C from mean.

TABLE 13

VALUES OF C AND e_{min}[1]

Sand Specimen	σ_3 (kg/cm²)	e	e_{min}	C
121	1.40	0.452, 0.637	-0.805	1.202
	2.80	0.445, 0.605	-0.770	1.146
133	1.40	0.371, 0.553	-0.881	1.173
	2.80	0.352, 0.550	-0.670	0.999
134	1.40	0.600, 0.823	-0.460	0.978
	2.80	0.606, 0.805	-0.525	1.048

[1]From Wu (103).

TABLE 14

CALCULATED VS EXPERIMENTAL TAN ϕ VALUES[a]

Porosity n	Void Ratio e	Tan ϕ Calc.	Tan ϕ Exp.	Dev. (%)
0.39	0.640	0.860	0.863	-0.3
0.41	0.695	0.785	0.776	+1.2
0.43	0.754	0.719	0.707	+1.7

[a]Experimental data from Nash (64, p. 163, Fig. 6).

TABLE 15

CALCULATED VS EXPERIMENTAL TAN ϕ VALUES[a]

Porosity n	Void Ratio e	Tan ϕ Calc.	Tan ϕ Exp.	Dev. (%)
0.40	0.667	0.821	0.827	-0.7
0.42	0.725	0.764	0.774	-1.3
0.46	0.851	0.665	0.635	+4.7

[a]Experimental data from Bjerrum et al. (5, p.33, Fig. 7).

TABLE 16

CALCULATED VS EXPERIMENTAL TAN ϕ VALUES[a]

Void Ratio e	Tan ϕ Calc.	Tan ϕ Exp.	Dev. (%)
0.60	0.690	0.690	0.0
0.70	0.623	0.627	-0.6

[a]Experimental data from Rutledge (74, p. 56, Table 2).

TABLE 17

CALCULATED VS EXPERIMENTAL TAN ϕ VALUES[a]

Porosity n	Void Ratio e	Tan ϕ Calc.	Tan ϕ Exp.	Dev. (%)
0.32	0.470	0.897	0.936	-4.2
0.40	0.667	0.619	0.674	-8.2

[a]Experimental data from Bishop (3).

Nash's triaxial tests on a nearly uniform sand (64, p. 163, Fig. 6) yield the following data: (a) at e = 0.667 (n = 0.40), ϕ = 39.4°; and (b) at e = 0.818 (n = 0.45), ϕ = 33.3°. These give C = 0.498 and e_{min} = 0.061 from which the calculated values of tan ϕ in Table 14 are obtained.

The following are data taken from the results of drained triaxial tests on sand made by Bjerrum et al. (5, p. 33, Fig. 7): (a) at e = 0.613 (n = 0.38), ϕ = 41.4°; and (b) at e = 0.785 (n = 0.44), ϕ = 35.5°. These give C = 0.640 and e_{min} = -0.112 which are used for Table 15.

Rutledge's data obtained by triaxial tests on Sardis dam sand (74, p. 56, Table 2) yield (a) at e = 0.55, ϕ = 36.1°; and (b) at e = 0.80, ϕ = 29.7°. These give C = 0.656 and e_{min} = -0.352, used in Table 16.

Bishop's data obtained by direct shear tests on Walton gravel (3) yield: (a) at e = 0.428 (n = 0.30), ϕ = 44.8°; and (b) at e = 0.545 (n = 0.353), ϕ = 37.5°. These give C = 0.394 and e_{min} = 0.031, used in Table 17.

Eq. 34b has also been tested against additional data (25) published by Taylor (87, 88), De Beer (21), Burmister (9, 10, 12), Wu (103), Nash (64), Bjerrum et al. (5), Rutledge (74), Bishop (3), and Caquot and Kerisel (13). The results are similar to those preceding.

GENERAL CONCLUSIONS

Eq. 34b reproduces rather accurately the tan ϕ values of granular systems within a given range of strain energy, expressed as normal pressure or minor principal stress. The constants C and e_{min} are derived from tan ϕ determinations at two different void ratios, with the system being at the same level of strain energy as in the contemplated use.

The value of C has been found to be approximately constant at different strain energy levels provided that the same type of test--plane shear or triaxial—is employed. Physically, the C-factor is of a composite nature. It can be conceived as expressing primarily particle-particle interaction; hence, C should also express the ease with which a system of high void ratio will collapse to the CVR and of the ease or difficulty with which pores or "holes" from other parts of the system will migrate to the shear failure planes or zones during the shear process. Furthermore, because C is of the essence of a "free energy consuming" factor, its value should express also the various mechanisms for energy consumption, such as translation and translation plus rotation, mobilized in the system during the shearing process.

The values for e_{min} generally decreased as the strain energy of the system increased. The strain energy is of the nature of a free energy; shear in the type of system considered is an irreversible process and the main characteristic of such processes is the production of entropy. Hence, increase in strain energy of the system should favor the shear process and be reflected in either the C or e_{min} values or both. These considerations indicate the direction which must be followed for theoretical refinement of the simple formula for tan ϕ. The need for such refinement is indicated by the fact that at high strain energies the calculated e_{min} values may become negative. It is remarkable, however, and important from a practical point of view, that even negative e_{min} values did not prevent the simple formula from yielding rather accurate data.

The relative constancy of factor C and the rather accurate predictions of tan ϕ that can be made by means of the acknowledgedly oversimplified Eq. 34b show the essential validity of the assumption of physical analogy between macromeritic and molecular systems and their respective conditions of state—solid and liquid with relatively low internal friction for pure systems of identical component particles and liquids with wide range of internal friction for systems with particles of different sizes, shapes and character. There exists, however, a definite need for more exact evaluation of the physical significance of factor C and of the apparent variation of e_{min} with increasing strain energy of the granular system. Such evaluation may even make important contributions to our theoretical understanding of the behavior of true, i. e., molecular, liquids.

From this point of view of the macromeritic systems theory, the CVR at constant volume represents the volumetrically defined melting point of the system. Identification of the various types of CVR, is made by Taylor (88) and more recently by Geuze (31) and Fahmy (24). Winterkorn (98) has shown that the CVR (any type) decreases linearly as log σ_3 increases. This relationship was checked and confirmed by Farouki (25) using other data given by Taylor (87, 88) and Burmister (9). Hence for any given system one may write

$$CVR = a - b \log \sigma_3 \qquad (52)$$

in which a and b are constants. In this equation, the minor principal stress, σ_3, may be replaced by the normal stress, σ_1.

In normal molecular liquids, the melting point increases with increasing pressure. Where the opposite is the case, as with normal ice and water, this is due to a structural arching effect arising from the directional nature of the H-bonds of the H_2O molecule. The decrease of the volumetrically defined melting point of macromeritic systems with increasing strain energy makes their behavior more comparable to that of water than that of normal molecular liquids. This may be one of the reasons why the laws of macromeritic assemblies, developed originally for noncohesive granular systems, maintain their intrinsic validity even in typical cohesive soil-water systems.

ACKNOWLEDGMENTS

REFERENCES

1. Bagnold, R. A. , "The Physics of Blown Sand and Desert Dunes." William Morrow and Co. , New York (1943).

2. Bishop, A. W. , "Correspondence on Shear Characteristic of a Saturated Silt, Measured in Triaxial Compression." Geotechnique, 4:43-45.

3. Bishop, A. W. , "A Large Shear Box for Testing Sands and Gravels." Proc. 2nd Internat. Conf. on Soil Mech. and Found. Eng. , Rotterdam, 1:207-211 (1948).

4. Bishop, A. W. , and Eldin, A. K. G. , "The Effect of Stress History on the Relation Between ϕ and Porosity in Sand." Proc. 3rd Internat. Conf. on Soil Mech. and Found. Eng. , Zurich, 1:100 (1953).

5. Bjerrum, L. , Kringstad, S. , and Kummenije, O. , "The Shear Strength of a Fine Sand." Proc. 5th Internat. Conf. on Soil Mech. and Found. Eng. , Paris, 1:29-37 (1961).

6. Boerdijk, A. H. , "Some Remarks Concerning Close-Packing of Equal Spheres." Philips Res. Rept. , 7:303-313 (1952).

7. Brandt, H. , "A Study of the Speed of Sound in Porous Granular Media." J. Appl. Mech. , 22:479-486 (1955).

8. Brown, R. L. , and Hawksley, P. G. W. , "Packing of Regular (Spherical) and Irregular Particles." Nature, 156:421-422 (1945).

9. Burmister, D. M. , "Some Investigations of the Shearing Resistance of Cohesionless and Cohesive Materials." Sym. on Shear Testing of Soils, Proc. ASTM, 39:1071-1083 (1939).

10. Burmister, D. M. , "The Importance and Practical Use of Relative Density in Soil Mechanics." Proc. ASTM, 48:1249-1268 (1948).

11. Burmister, D. M. , "The Importance of Natural Controlling Conditions upon Triaxial Compression Test Conditions." ASTM Spec. Tech. Publ. 106, p. 248 (1950).

12. Burmister, D. M. , "The Place of the Direct Shear Test in Soil Mechanics." ASTM Sym. on Direct Shear Testing of Soils (1952).

13. Caquot, A. , and Kerisel, J. , "Traite de Mecanique des Sols." 3rd ed. , Gauthier-Villars, Paris (1956).

14. Casagrande, A. , "Characteristics of Cohesionless Soils Affecting the Stability of Slopes and Earth Fills." Jour. Boston Soc. of Civil Eng. , 23:1, 13-32 (Jan. 1936).

15. Casagrande, A. , "Notes on the Shearing Resistance and the Stability of Cohesionless Soils and Their Relation to the Design of Earth Dams." Disc. , Proc. 1st Internat. Conf. on Soil Mech. and Found. Eng. , Cambridge, Mass. , 3:58-60 (1936).

16. Chen, L. , "An Investigation of Stress-Strain and Strength Characteristics of Cohesionless Soils by Triaxial Compression Tests." Proc. 2nd Internat. Conf. on Soil Mech. and Found. Eng. , Rotterdam, 5:35-43 (1948).

17. Converse, F. J. , "The Use of the Direct Shear Testing Machine in Foundation Engineering Practice." ASTM Sym. on Direct Shear Testing of Soils (1952).

18. Dallavalle, J. M. , "Micromeritics." 2nd ed. , Pitman (1948).

19. Dantu, P. , "Contribution a l'Etude Mecanique et Geometrique des Milieux Pulverulents." Proc. 4th Internat. Conf. on Soil Mech. and Found. Eng. , London, 1:144-148 (1957).

20. Dantu, P. , "Etude Mecanique d'un Milieu Pulverulent Forme de Spheres Egales de Compacite Maxima." Proc. 5th Internat. Conf. on Soil Mech. and Found. Eng. , Paris, 1:61-70 (1961).

21. De Beer, E., "Neuere Erkenntnisse über den Bruchwiderstand Kohäsionsloser Böden unter Flachgründungen." Sym. on Soil Mechanics, T. H., Aachen (1961).

22. Deresiewicz, H., "Mechanics of Granular Matter." Off. of Naval Res. Columbia Univ. Rept., Contract Nonr-266(09); Tech. Rept. 25 (1957).

23. Duffy, J., and Mindlin, R. D., "Stress-Strain Relations and Vibrations of a Granular Medium." Columbia Univ. Rept., Contract Nonr-266(09); Off. of Naval Res. Tech. Rept. 17 (1956).

24. Fahmy Mohamed, A., "Zur Definition der kritischen Dichte von Sanden." Veröffent. des Inst. für Bodenmechanik und Grundbau der T. H. Fridericiana in Karlsruhe, 5 (1960).

25. Farouki, O. T., "A Comparison of Experimental Data Obtained by Various Workers on the Frictional Properties of Granular Materials with Values Calculated on the Basis of the Concept of the Solid and Liquid States of Macromeritic Systems." Princeton Univ., Dept. of Civil Eng. (Jan. 1963).

26. Farouki, O. T., "Properties of Granular Systems." Princeton Univ., Dept. of Civil Eng. Res. Rept. (March 1963).

27. Fuller, W. B., and Thompson, S. E., "The Laws of Proportioning Concrete." Trans. ASCE 59, 67 (1907).

28. Furnas, C. C., "Flow of Gases Through Beds of Broken Solids." U.S. Bur. of Mines Bull. 307 (1929).

29. Furnas, C. C., "Grading Aggregates. Mathematical Relations for Beds of Broken Solids of Maximum Density." Ind. and Eng. Chem., 23:1052-1058 (1931).

30. Gassmann, F., "Elastic Waves Through a Packing of Spheres." Geophysics, 16:673-685 (1951); 18:269 (1953).

31. Geuze, E. C. W. A., "Critical Density of Some Dutch Sands." Proc. 2nd Internat. Conf. on Soil Mech. and Found. Eng., Rotterdam, 3:125-130 (1948).

32. Graton, L. C., and Frazer, H. J., "Systematic Packing of Spheres, with Particular Relation to Porosity and Permeability." Jour. Geol., 43:785-909 (1935).

33. Hansen, B., "Shear Box Tests on Sand." Proc. 5th Internat. Conf. on Soil Mech. and Found. Eng., Paris, 1:127-131 (1961).

34. Hara, G., "Theorie der Akustischen Schwingungs Ausbreitung in Gekörnten Substanzen und Experimentelle Untersuchungen an Kohlepulver." Elekt. Nach.— Tech., 12:191-200 (1935).

35. Hennes, R. G., "The Strength of Gravel in Direct Shear." ASTM Sym. on Direct Shear Testing of Soils (1953).

36. Holtz, W. G., and Gibbs, H. J., "Triaxial Shear Tests on Pervious Gravelly Soils." Jour. Soil Mech. and Found. Div. SMI 867, Proc. ASCE 82 (1956).

37. Horsfield, H. T., "The Strength of Asphalt Mixtures." Jour. Soc. Chem. Ind., 53:107T-115T (1934).

38. Housel, W. S., "Shearing Resistance of Soil—Its Measurement and Practical Significance." Proc. ASTM, 39:1084 (1939).

39. Hudson, D. R., "Density and Packing in an Aggregate of Mixed Spheres." Jour. Appl. Phys., 20:154-162 (1949).

40. Hutchinson, B., and Townsend, D., "Some Grading-Density Relationships for Sand." Proc. 5th Internat. Conf. on Soil Mech. and Found. Eng., Paris, 1:159-163 (1961).

41. Hvorslev, M. J., "Torsion Shear Tests and Their Place in the Determination of the Shearing Resistance of Soils." Sym. on Shear Testing of Soils, Proc. ASTM, 39:999-1022 (1939).

42. Idel, K., "Die Scherfestigkeit rolliger erdstoffe." Veröffent. des Inst. für Bodenmechanick und Grundbau der T. H. Fridericiana in Karlsruhe, 2 (1960).

43. Jakobson, B., "Some Fundamental Properties of Sand." Proc. 4th Internat. Conf. on Soil Mech. and Found. Eng., London, 167 (1957).

44. Jumikis, A. R., "The Shape of Rupture Surface in Dry Sand." Proc. 5th Internat. Conf. on Soil Mech. and Found. Eng., Paris, 1:693-698 (1961).

45. Jurgenson, L., "Shearing Resistance of Soils." Contrib. to Soils Mechanics. Boston Soc. Civil Eng., pp. 184-225 (1925-1940).

46. Kallstenius, T., and Bergau, W., "Research on the Texture of Granular Masses." Proc. 5th Internat. Conf. on Soil Mech. and Found. Eng., Paris, 1:165-170 (1961).

47. Kirkpatrick, W. M., "The Condition of Failure for Sands." Proc. 4th Internat. Conf. on Soil Mech. and Found. Eng., London, 1:172-178 (1957).

48. Kjellman, W., and Jakobson, B., "Some Relations Between Stress and Strain in Coarse-Grained Cohesionless Materials." Proc. Royal Swedish Geotech. Inst. 9 (1955).

49. Kolbuszewski, J. J., "An Experimental Study of the Maximum and Minimum Porosities of Sands." Proc. 2nd Internat. Conf. on Soil Mech. and Found. Eng., Rotterdam, 1:158-165 (1948).

50. Kolbuszewski, J. J., "Fundamental Factors Affecting Experimental Procedures Dealing with Pressure Distribution in Sands." Brussels Conf. 58 on Earth Pressure Prob., 1:71-83 (1958).

51. Lambe, T. W., "Soil Testing for Engineers." Wiley, New York (1951).

52. Leva, M., "Fluidization." McGraw-Hill (1959).

53. Love, A. E. H., "A Treatise on the Mathematical Theory of Elasticity." 4th ed., Dover, New York (1944).

54. Matzke, E. B., "Volume-Shape Relationships in Lead Shot and Their Bearing on Cell Shapes." Amer. Jour. Bot., 26:288-295 (1939).

55. Melmore, S., "Densest Packing of Equal Spheres." Nature, 159:817 (1947).

56. Mindlin, R. D., "Compliance of Elastic Bodies in Contact." Jour. Appl. Mech., 16:259-268 (1948).

57. Mindlin, R. D., and Deresiewicz, H., "Elastic Spheres in Contact Under Varying Oblique Forces." Jour. Appl. Mech., 20:327-344 (1953).

58. Mindlin, R. D., Mason, W. P., Osmer, T. F., and Deresiewicz, H., "Effects of an Oscillating Tangential Force on the Contact Surfaces of Elastic Spheres." Proc. 1st Nat. Cong. Appl. Mech., Chicago, pp. 203-208 (1951).

59. Mogami, T., "On the Law of Friction of Sand." Proc. 2nd Internat. Conf. on Soil Mech. and Found. Eng., Rotterdam, p. 51 (1948).

60. Mogami, T., "On Professor Winterkorn's Theory of Macromeritic Liquids." Univ. of Tokyo, Repts. of the Inst. of Sci. and Technol., 8:(4) (1954).

61. Moran, D. E., "Experimental Loadings on Granular Material." Jour. Franklin Inst., 199:493-501 (1925).

62. Morris, H. C., "Effect of Particle Shape and Texture on the Strength of Noncohesive Aggregates." ASTM Spec. Tech. Publ. 254 (1959).

63. Muurinen, E., "Theoretical and Practical Aspects of the Workability of Granular Mixtures." Master's Thesis, Princeton Univ. (1961).

64. Nash, K. L., "The Shearing Resistance of a Fine Closely Graded Sand." Proc. 3rd Internat. Conf. on Soil Mech. and Found. Eng., Zurich, 1:160-164 (1953).

65. Newland, P. L., and Alley, B. H., "Volume Changes in Drained Triaxial Tests on Granular Materials." Geotechnique, 7 (1):17-34 (March 1957).

66. Nutting, P. G., "The Deformation of Granular Solids." Jour. Wash. Acad. Sci., 18:123-126 (1928).

67. Osterman, J., "A Theoretical Study of the Failure Conditions in Saturated Soils." Proc. Royal Swedish Geotech. Inst. 20 (1962).

68. Parsons, J. D., "Progress Report on an Investigation of the Shearing Resistance of Cohesionless Soils." Proc. Internat. Conf. on Soil Mech. and Found. Eng., Harvard, 2, 133 (1936).

69. Poorooshasb, H., and Roscoe, K. H., "The Correlation of the Results of Shear Tests with Varying Degrees of Dilation." Proc. 5th Internat. Conf. on Soil Mech. and Found. Eng., Paris, 1:297-304 (1961).

70. "Procedures for Testing Soils." ASTM (1950).

71. "Proceedings of the Conference on the Measurement of Shear Strength of Soils in Relation to Practice." Geotechnique, 2 (2, 3) (1950, 1951).

72. Rayleigh, W. R., "On the Influence of Obstacles Arranged in Rectangular Order Upon the Properties of a Medium." Phil. Mag., 34:481-502 (1892).

73. Reynolds, O., "On the Dilatancy of Media Composed of Rigid Particles in Contact." Phil. Mag. (Ser. 5), 20:469-481 (1885).

74. Rutledge, P. C., "Soil Mechanics Fact Finding Survey." U.S. Army Corps of Engineers, Vicksburg, Miss. (April 1947).

75. Scott, R. F., "Principles of Soil Mechanics." Addison-Wesley, Reading, Mass. (1963).

76. Schockley, W. G., "Correlation of Some Physical Properties of Sand." Proc. 3rd Internat. Conf. on Soil Mech. and Found. Eng., Zurich, 1:203-206 (1953).

77. Schultze, E., and Moussa, A., "Factors Affecting the Compressibility of Sand." Proc. 5th Internat. Conf. on Soil Mech. and Found. Eng., Paris, 1:335-340 (1961).

78. Siedek, P., and Voss, R., "Über die Lagerungsdichte und den Verformungswiderstand von Korngemischen." Strasse und Autobahn, 8, 273-277 (1955).

79. Sjaastad, G. D., "The Effect of Vacuum on the Shearing Resistance of Ideal Granular Systems." Ph. D. Thesis, Princeton Univ., Dept. of Civil Eng. (June 1963).

80. Skempton, A. W., and Bishop, A. W., "The Measurement of the Shear Strength of Soils." Geotechnique, 2(2):90-133 (Dec. 1950).

81. Slichter, C. S., "Theoretical Investigation of the Motion of Ground Waters." U.S. Geol. Survey, 19th Ann. Rept., Part 2, pp. 301-384 (1899).

82. Smith, W. O., "Capillary Flow Through an Ideal Uniform Soil." Physics, 3:139-146 (1932).

83. Smith, W. O., Foote, P. D., and Busang, P. F., "Packing of Homogeneous Spheres." Phys. Rev., 34:1271-1274 (1929).

84. Spencer, M. E., "The Relationships Between Porosity and Angle of Internal Friction." Disc. on Paper $\frac{1}{5}$, Proc. 5th Internat. Conf. of Soil Mech. and Found. Eng., Paris, 3:138-140 (1961).

85. Supnik, F., "On the Dense Packing of Spheres." Trans. Amer. Math. Soc., 65:14-26 (1949).

86. Takahashi, T., and Sato, Y., "On the Theory of Elastic Waves in Granular Substances." Bull. Earthquake Res. Inst. (Tokyo Univ.), 27:11-16 (1949); 28:37-43 (1950).

87. Taylor, D. W., "A Comparison of Results of Direct Shear and Cylindrical Compression Tests." Sym. on Shear Testing of Soils, Proc. ASTM, 39:1058-1070 (1939).

88. Taylor, D. W., "Fundamentals of Soil Mechanics." J. Wiley, New York (1948).

89. Taylor, D. W., and Leps, T. M., "Shearing Properties of Ottawa Standard Sand as Determined by the M. I. T. Strain-Control Direct Shearing Machine." Proc. of the Soils and Found. Conf. of the U.S. Eng. Dept., Boston, Mass., pp. C-1—C-17 (June 1938).

90. Thurston, C. W., and Deresiewicz, H., "Analysis of a Compression Test of a Model of a Granular Medium." Jour. Appl. Mech., 26, Trans. ASME, 81, 251-258 (1959).

91. Timoshenko, S., and Goodier, J. N., "Theory of Elasticity." McGraw-Hill, New York (1951).

92. Traxler, R. N., and Baum, L. A. H., "Permeability of Compacted Powders. Determination of Average Pore Size." Physics, 7:9-14 (1936).

93. Watson, J. D., "A Triaxial Compression Apparatus for the Determination of the Stress-Deformation Characteristics of Soils." Sym. on Shear Testing of Soils, Proc. ASTM, 39:1046-1057 (1939).

94. Westman, A. E. R., and Hugil, H. R., "The Packing of Particles." Jour. Amer. Ceram. Soc., 13:767-779 (1930).

95. White, H. E., and Walton, S. F., "Particle Packing and Particle Shape." Jour. Amer. Ceram. Soc., 20:155-166 (1937).

96. Whitman, R. V., and Healey, K. A., "Shear Strength of Sands During Rapid Loadings." Jour. Soil Mech. and Found. Div., Proc. ASCE, Paper 3102, pp. 99-132 (April 1962).

97. Wikramaratna, P. H. D. S., Disc. on Paper $\frac{1}{10}$ by Dantu, Proc. 5th Internat. Conf. on Soil Mech. and Found. Eng., Paris, 3:150-151 (1961).

98. Winterkorn, H. F., "Macromeritic Liquids." ASTM Spec. Tech. Publ. 156, pp. 77-89 (1953).

99. Winterkorn, H. F., "Theory and Practice of Soil Densification." Power Apparatus and Systems 39, pp. 1060-1069 (1958).

100. Winterkorn, H. F., "Introduction to Engineering Soil Science." Chaps. 4, 5, 11. Princeton Univ. (1960).

101. Wise, M. E., "Dense Random Packing of Unequal Spheres." Philips Res. Rept., 7:321-343 (1952).

102. Wittke, W., "Über die Scherfestigheit Rolliger Erdstoffe." Veröffent. des Inst. für Bodenmechanik und Grundbau der T. H. Fridericiana in Karlsruhe, 11 (1962).

103. Wu, T. H., "Relative Density and Shear Strength of Sands." Jour. of the Soil Mech. and Found. Div., Proc. ASCE, Paper 1161, 83 (Jan. 1957).

104. Yamagauchi, H., "Strain Increments and Volume Change in the Plastic Flow of a Granular Material." Proc. 5th Internat. Conf. on Soil Mech. and Found. Eng., Paris, 1:413-417 (1961).

105. Zeller, J., and Wullimann, R., "The Shear Strength of the Shell Materials for the Göschenenalp Dam, Switzerland." Proc. 4th Internat. Conf. on Soil Mech. and Found. Eng., London, 2:399-404 (1957).

Discussion

ARPAD KEZDI, Professor, Technical University, Budapest, Hungary. —Every investigation of the behavior of granular systems used to start with the examination of ideal packings of spheres. This is an idealization of nature and not directly applicable in practice; however, these studies may lead to a better understanding of nature, the realization of some important facts and the establishment of some, at least qualitative, statements. The concept of grain assemblies as macromeritic liquids, introduced by Winterkorn, throws a new light on the investigations of packings of equal spheres because the laws of physics, with respect to liquids, can thereby be applied to grain assemblies.

When comparing the characteristics of different states of matter, Winterkorn includes the grain assemblies as a separate state along with the solid, liquid and gaseous states (113). Sands and gravels may also be listed with liquids. The variation of the coefficient of lateral pressure, K_0 (known in soil mechanics as coefficient of earth pressure at rest), shows clearly the fields for every condition of state. If a solid body displays a very great cohesion ($c \rightarrow \infty$), K_0 tends to zero. With decreasing binding forces between the elementary particles (caused by an increase of temperature, by vibration, or electric effects), the K_0 value increases to 0.4 to 0.5, which is characteristic for grain assemblies. Greater values occur with the viscous liquids, in which the internal shearing resistance is much smaller and finally $K_0 = 1$ is reached for ideal liquids with zero internal friction. In the case of gases K_0 exceeds 1, due to the atomic particle movements. The increase of K_0 can be achieved by transmitting energy to the system, either as mechanical energy forcing particles out of the solid, as vibration energy decreasing the number of contacts between the particles, thus reducing the inner resistance in a transient manner, or as thermal energy which enlarges the distances between the particles and increases their speed, thus transforming a solid to a liquid or a liquid to a gas. By applying a common yardstick for the different kinds of energy, it will be possible to plot the K_0 values as a function of the stored energy in the system, thus giving the range for the different conditions of state (Fig. 20). The greater the stored energy, the easier the migration of the "holes" in the system and, therefore, the greater the coefficient of lateral pressure.

Some Properties of Packings of Uniform Spheres

The first systematic treatment of packings of uniform spheres was given by Slichter (81). He established the different arrangements of the spheres and gave formulas to
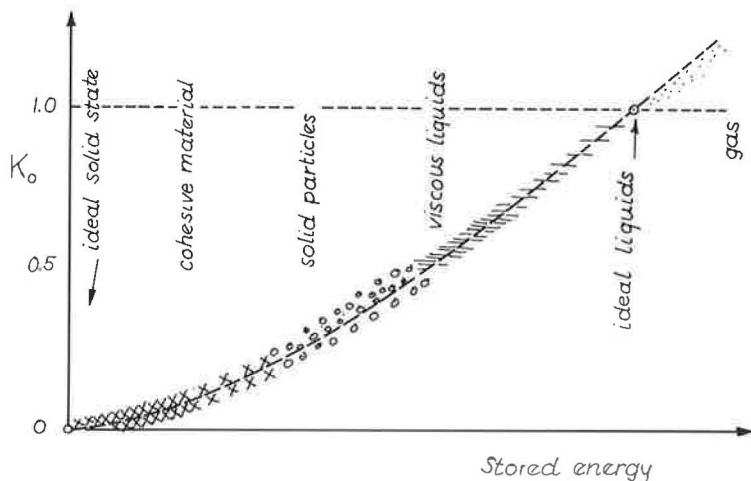
Figure 20. Relation between condition of state and pressure coefficient.

calculate their density based on the following assumptions: (a) the spheres are ideally rigid and undeformable; (b) the system of spheres is of infinite extent; and (c) there are no adhesive forces between the spheres; frictional forces will be mobilized by movements only.

A packing of spheres can be either continuous or discontinuous, compressible or incompressible. It is continuous, if, by starting on the surface of a sphere, selected at random, any sphere may be reached by crossing on surface contact points only. Dry granular soils obviously form a continuous packing.

A packing is compressible if a hydrostatic pressure, applied on plane surfaces, limiting a closed volume of the packing, can cause a compression of the system. Compressible systems are stable in unloaded state only if adhesive forces act between the spheres, as in clay and silt soils. Packings suffering no compression on the application of hydrostatic pressure are incompressible; this state is best approached by natural sands and gravels. This does not imply, however, that the simultaneous application of hydrostatic and shearing stresses cannot cause any compression of the system. In incompressible systems, there is at least one point of contact on every half sphere. The following investigations are limited to continuous and incompressible packings.

The density of a packing may be either uniform or variable. Uniform density results when an infinite system may be formed from finite unit cells without gaps and voids between the cells. In a more rigorous definition of uniformity, in the same—congruent—position every sphere must be with respect to its neighbors.

To construct uniform packings, a certain configuration in the plane is chosen such that the plane may be covered completely with an infinite number of unit cells without overlapping. Points on the borderlines that serve as centers of spheres are fixed so that the spheres do not intersect each other. The plane of the spheres' centers is the middle plane of the layer. An identical layer is placed on the first with middle planes parallel. A third similar layer is placed. The distance between the first and second layers, and the second and third layers, respectively, may be different. The whole system is composed of layers constructed in this manner. The fourth layer is in every respect identical with the first one; therefore, only three layers need be investigated. One sphere is selected in the middle layer and the number of spheres in contact with it in the lower, middle and upper layers are designated u, m, ℓ. The symbol $[u, m, \ell]$ is used to characterize the construction procedure. The coordination number of the system is given by $N = u + m + \ell$. Cubic packing, the loosest state of uniform incompressible packings, has the symbol $[1, 4, 1]$ and rhombohedral packing, the densest state, has the symbol $[3, 6, 3]$ (Fig. 21). The symbol of the orthorombic system is $[2, 4, 2]$ and that of the tetragonal-spheroidal is $[2, 6, 2]$. It is evident that packings
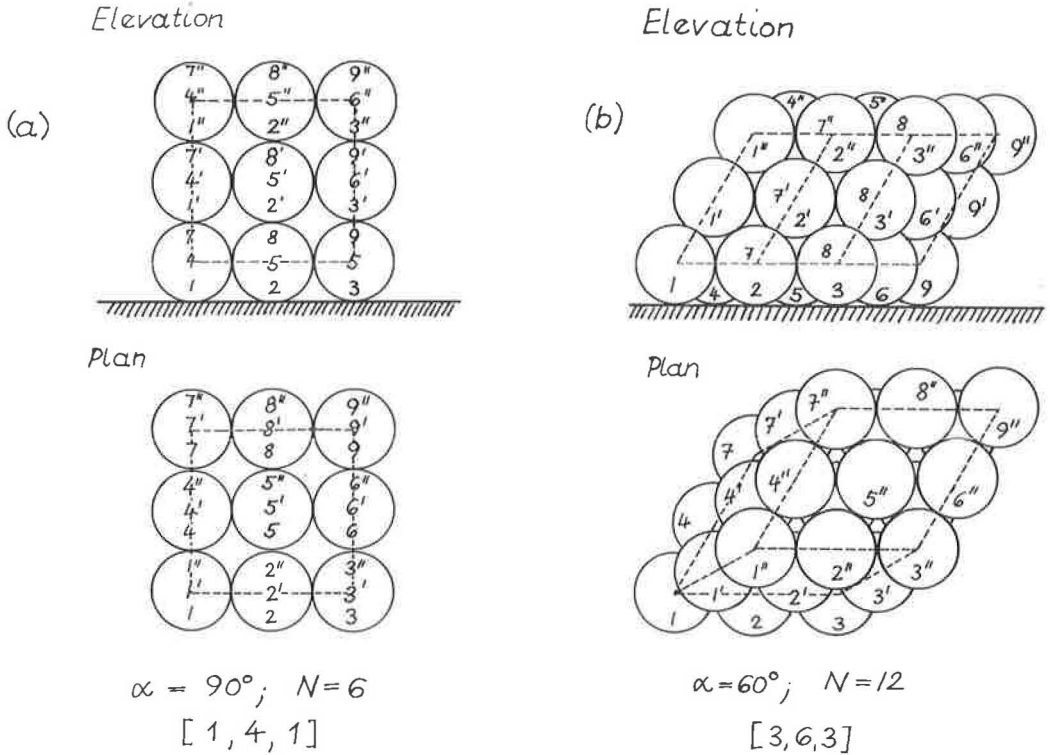
Figure 21. Cubic (a) and rhombohedral (b) packing of spheres.

for every coordination number between 6 and 12 can be constructed in several ways and the densities of packings with the same coordination number are not necessarily the same (107).

A continuous, incompressible, and uniform packing with coordination number as low as 4 is constructed as follows: The base figure is a hexagon, with every second corner the center of a sphere. The length of the side is smaller than D; the diagonals are greater than D. The spheres are not in contact; therefore, $m = 0$. The lower layer is constructed so that every sphere contacts three spheres in the middle layer. The upper layer is constructed by establishing one point of contact with the sphere of the middle layers. Then $u = 1$, and the symbol of the system is [1, 0, 3] (Fig. 22).

The porosity of this system is given by the relation

$$n = 1 - \frac{D^3 \pi}{6} \frac{2\nu}{A(m_1 + m_2)} \tag{53a}$$

in which D is the diameter of the spheres, ν is the number of spheres on the base figure given by normal projection of the packing to the base plane, A is the area of the base figure, and m_1 and m_2 are the distances between the three planes. For example, in the packing [3, 6, 3]

$$n = 1 - \frac{\pi}{3\sqrt{2}} = 0.259 \tag{53b}$$

when

$$\nu = 1 + 6 \times \tfrac{1}{3} = 3,$$
$$m_1 = m_2 = 2r\sqrt{2}/\sqrt{3}, \text{ and}$$
$$A = 6r^2\sqrt{3}.$$

The porosity of packings with the same coordination number depends on the distance between the parallel planes used in the construction; it varies, therefore, between given limits. Data on different packings are listed in Table 18. As can be seen, there are continuous and incompressible systems with porosities above 70 percent; the value, $n = 47.46$ percent, generally taken as the maximum, is smaller than the porosity of many packings.

The cubic system is the simplest packing and has a porosity of 47.46 percent. This system may be transformed to an orthorhombic and to a rhombohedral one. In the first case, every sphere of a given layer glides on a sphere of the lower layer, with the direction of movement parallel to the straight line connecting the centers of the given row of spheres. The unit cell, consisting of eight spheres, is transformed from a cube to a rhombohedron (Fig. 21). The amount of movement can be given by the variation of the orientation angle, α, between $60°$ and $90°$ (Fig. 23). At $\alpha = 60°$, the system is orthorhombic.

The porosity of the system in terms of α is

$$n = 1 - \frac{\pi}{6 \sin \alpha} \qquad (54)$$

The volume of the unit cell varies with $\sin \alpha$. The same relation applies to the height of the unit cell. The variation of V and n is shown in Figure 24. If $n = (V - V_s)/V$, and V_s is the volume of solids in the cell

Figure 22.   Packing with   coordination No. N-4.

TABLE 18

SYSTEMATIC PACKING OF SPHERES

Coordination No. N	Symbol	Porosity n	Relative Vol V
4	[1,1,2]	0.718	1.853
5	[1,0,4]	0.558	1.185
6	[3,0,3] = [1,4,1]	0.476	1.000
7	[1,5,1]	0.439	0.932
8	[1,6,1]	0.395	0.864
9	[1,6,2]	0.352	0.807
10	[2,6,2]	0.302	0.750
11	[2,6,3]	0.281	0.728
12	[3,6,3]	0.259	0.707

$$V_S = V(1 - n) = \pi/6 \qquad (55)$$

The volume of the spheres in the unit cell remains constant during the movement. This case may be considered that of plane deformation, the unit cell being deformed in one direction only.

In the second basic case, several types of movement must be applied to the system. There must be additional movement in the direction normal to that of the plane deformation. The movement is carried out uniformly; i.e., the deformation and compression of the unit cell occur at a uniform rate. The angle of orientation (that is, the angle between two edges of the same side on the unit cell) is the same for every two edges (Fig. 25). Assuming this, movement may be described with the help of α, and the volume of the unit cell and the porosity can be given as functions of α.

The formula for the porosity has been given by Slichter as early as 1889:

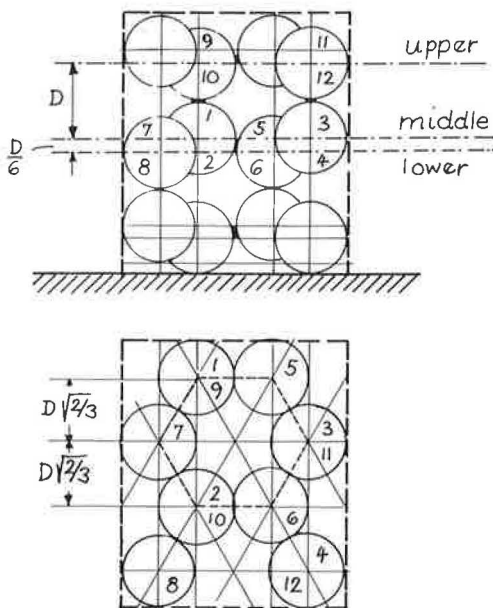$$n = 1 - \frac{\pi}{6(1 - \cos \alpha)\sqrt{1 + 2 \cos \alpha}} \qquad (56)$$
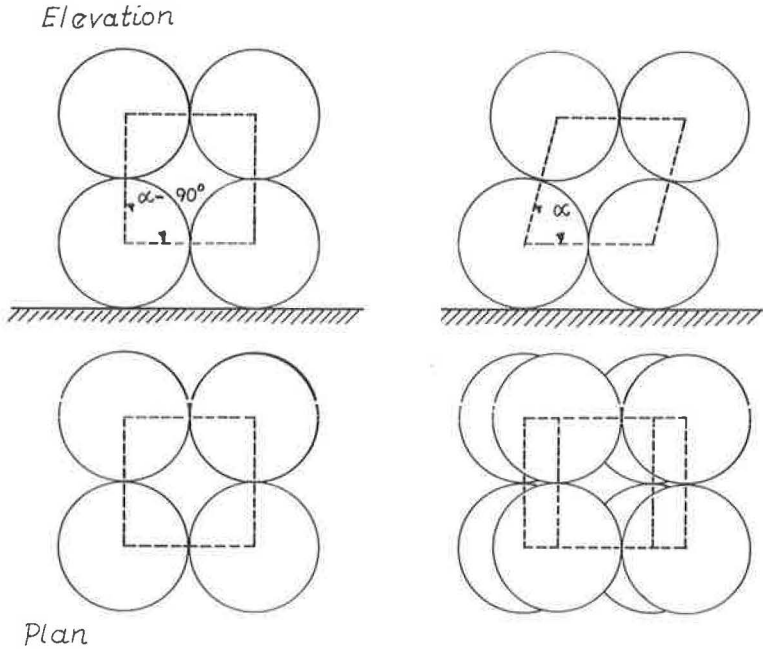
Elevation

Plan

Figure 23. Orthorhombic packing of spheres.

The volume of the unit cell is

$$V = (1 - \cos \alpha) \sqrt{1 + 2 \cos \alpha} \tag{57}$$

and the volume of solids is given by Eq. 55. The void ratio is, therefore,

$$e = \frac{n}{1 - n} = \frac{6V}{\pi} - 1 \tag{58}$$

The height of the unit cell varies with α (Fig. 26): $h = D \sin \delta$ with $D \cos \delta = D \cos \alpha / \cos (\alpha/2)$ which yields

$$h = D \sqrt{1 - \frac{\cos^2 \alpha}{\cos^2 \alpha/2}} = D \frac{(1- \cos \alpha) \sqrt{1 + 2 \cos \alpha}}{\sin \alpha} \tag{59}$$

Figure 27 shows the variation of V, F and h for D = 1 in terms of α.

The coordination number of the system does not vary continuously during the movement; it takes the final value only after performing the described movement. Smith et al. (83), with the intention of applying the results derived for uniform spheres to actual particle systems, assumed that the actual system may for statistical purposes be treated as composed of separate clusters of rhombohedral or cubic arrangements, these being present in such a proportion as to give the observed porosity of the assembly. This consideration leads to the following expression for the average coordination number, N, in terms of the porosity, n:

$$N = 26.4858 - \frac{10.7262}{1 - n} \tag{60}$$

The curve representing this (Fig. 28) agrees well with the observed experimental values. From the relationship between the angle of orientation and the porosity, the curve N = f(α), i.e., the relationship between the angle of orientation and the coordi-
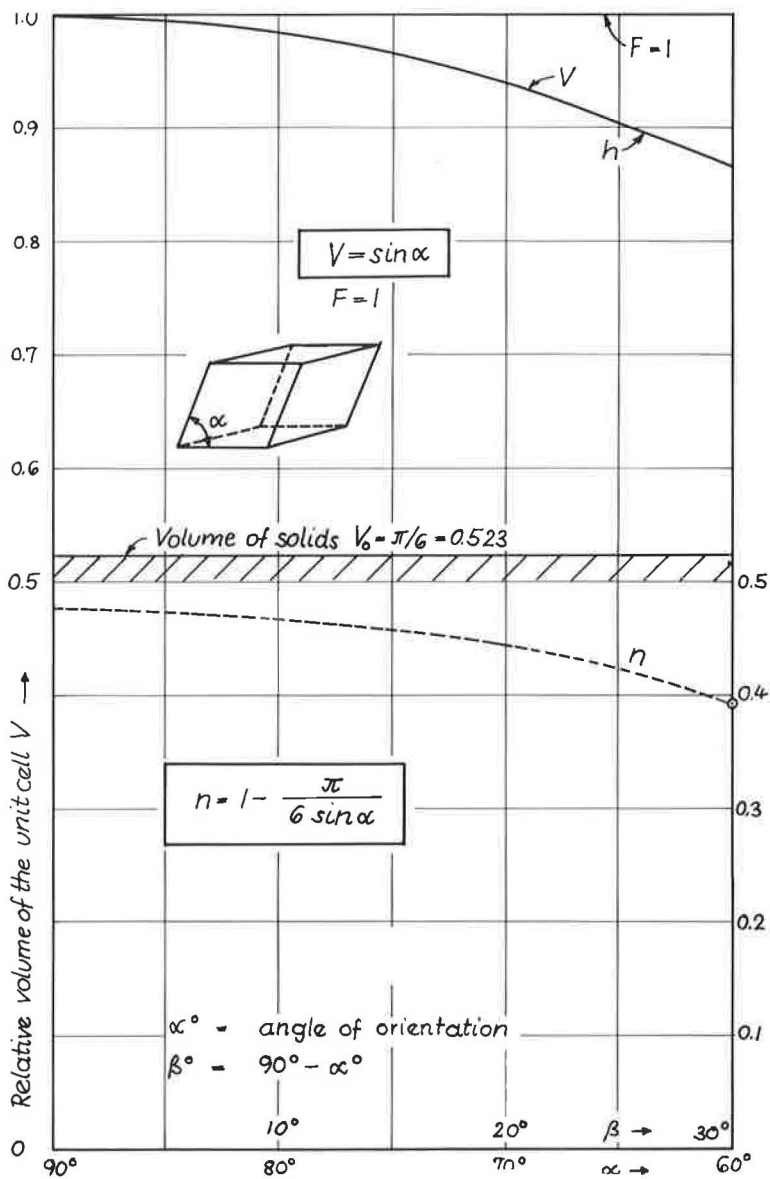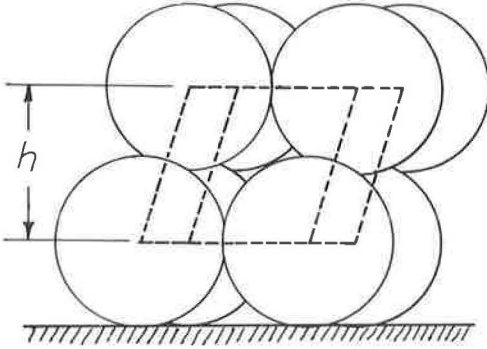
Figure 24. Relative volume of unit cell vs angle of orientation.
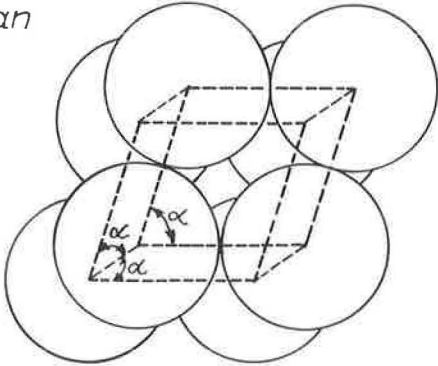
Elevation

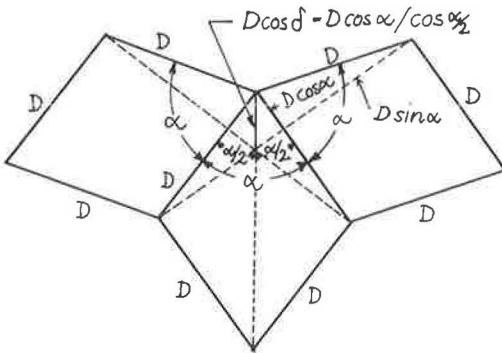
Plan

Figure 25. Rhombohedral packing.

Figure 26. Height of unit cell.

nation number (Fig. 28b), may be constructed. The plot of N as a function of the relative volume of the unit cell (Fig. 29) is a straight line that represents, most likely, Eq. 60 in another form. The equation of the straight line is:

$$N = 6 + 6(2 + \sqrt{2})(1 - V) = 6(4.41 - 3.41 V) \quad (61)$$

Coordination number and porosity may also be related by plotting the values given in Table 18. Porosities and the relative volumes of the unit cell are shown in Figure 30. The plot consists, of course, of isolated points for the integers N; the connecting dotted line is given only to show the trend of variation. It is interesting to show that Figure 31, giving $N = f(\alpha)$ and constructed on the base of the curves in Figure 32, does not differ much from the data shown in Figure 28b.

Extending the interpretation of α beyond $60°$ results in decreasing values of n, and the spheres intersect each other. The rate of decrease is considerable, because the volumes of the intersecting parts have to be considered twice. When this volume equals the volume of the remaining voids, theoretically n = 0. This occurs at $\alpha = 49°$, where the volume of the unit cell is equal to $V = 0.523 = \pi/6$. The variation of n with α for the range $90° \geq \alpha \geq 49°$ is given in Figure 33. The part $60° > \alpha \geq 49°$ of the curve may be used to determine the angle of orientation for packings of nonuniform spheres with porosities greater than 25 percent. This angle may be taken as a characteristic of the substitute packing of uniform spheres. Efforts to find a physical meaning for values of α greater than $90°$ have not been successful. (At $\alpha = 120°$, n again equals zero; however, the part of the curve for values between 90 and $120°$ is not the same as that between 60 and $90°$.

Shearing Resistance of Packings

The following is an attempt to determine the stresses necessary to bring the cubic system into the rhombohedral system. The shearing resistance of the densest packing (N = 12), filling the entire space, will be infinitely great, thus forming a closed system. An increase of the volume cannot take place, even if the shearing stresses increase to infinity. The porosity of a certain arrangement in the infinite space can decrease only as the effect of shearing stresses; any combination of stresses causes a tendency of densification.

As shown in Figures 24 and 27, the unit cell suffers a compression and a distortion during the movements that transform a cubic system (N = 6) into a rhombohedral one (N = 12). The decrease of volume can be achieved by the application of a uniform all-
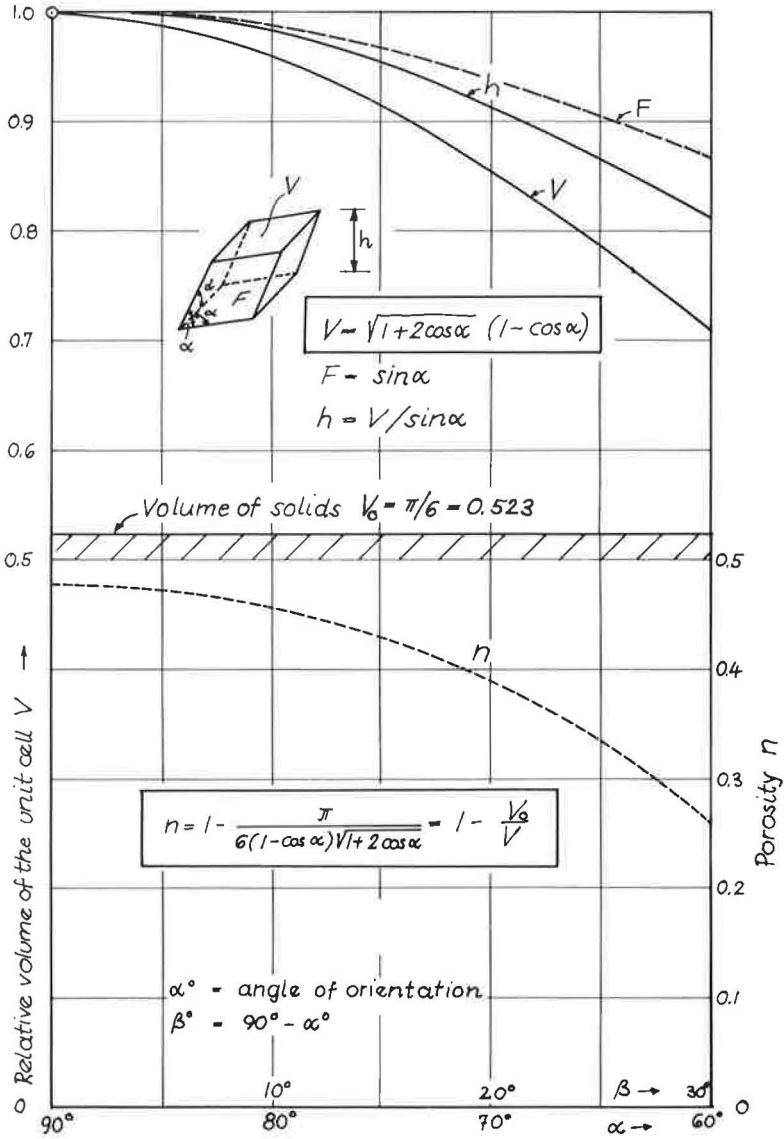
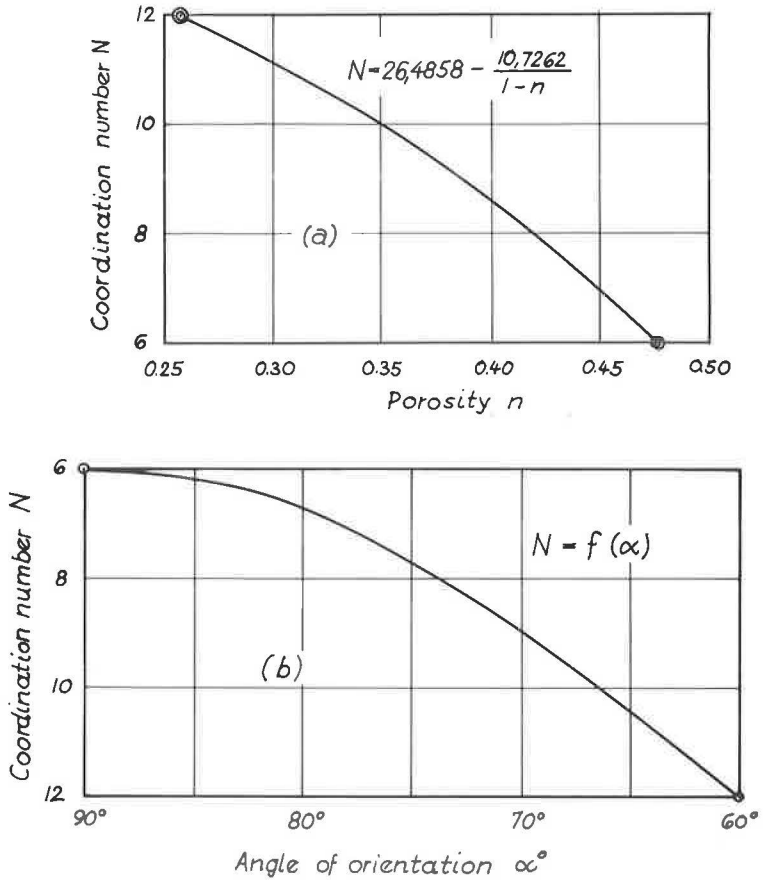Figure 27. Relative volume of unit cell vs angle of orientation.

Figure 28. Coordination number according to assumption of Smith.
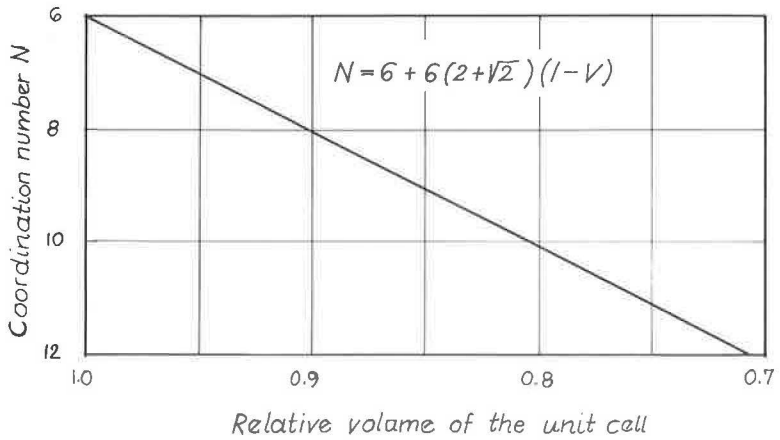

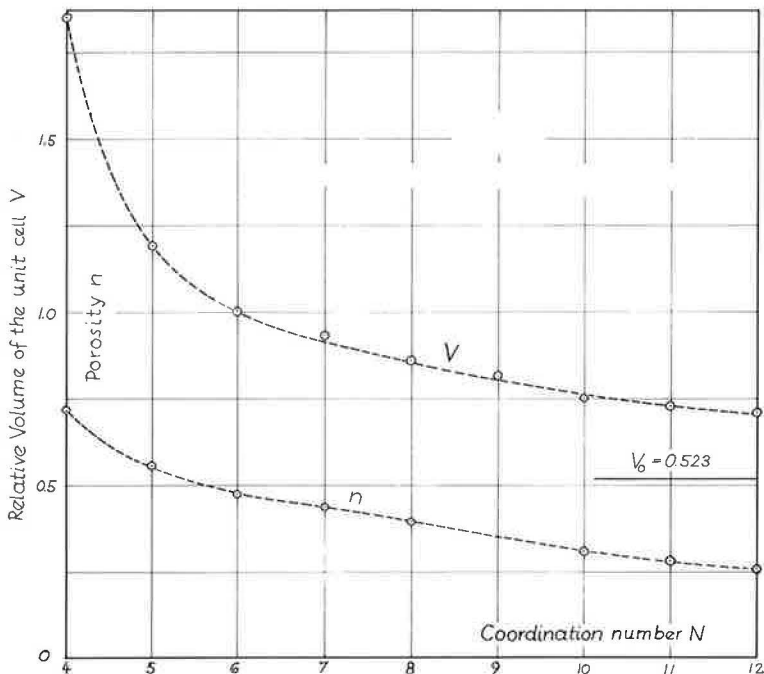Figure 29. Coordination number as function of relative volume.

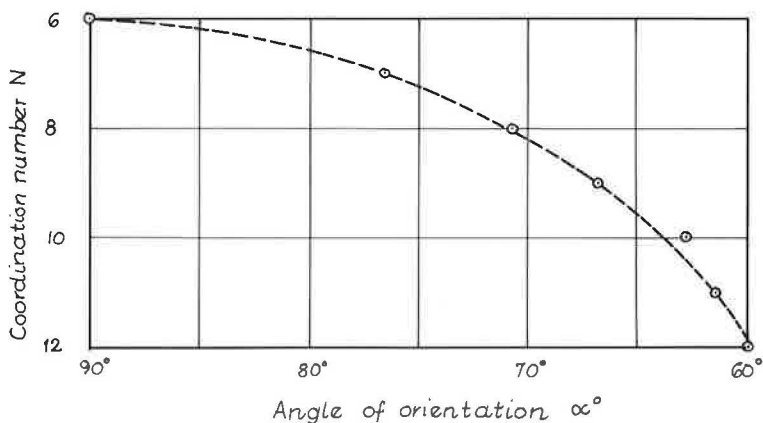Figure 30. Coordination number and relative volume.

Figure 31. Coordination numbers for packings given in Table 1.

round pressure; the decrease of the angle of orientation may be caused by uniform shear (Fig. 33). The relation between volume change and shear strain and the respective stresses may be determined by use of the general laws related to liquids.

As a first approximation, a linear relationship is assumed to exist between volume change and hydrostatic pressure. The volume in consideration—the volume of the unit cell—is occupied partly by voids and partly by sphere parts. For the present, a substitute liquid filling the unit cell is assumed. The volume change from $\alpha = 90°$ to $\alpha = 60°$ is given by

$$\frac{V - V_0}{V_0} = \frac{\Delta V}{V_0} = \frac{\sigma}{C} \tag{62a}$$
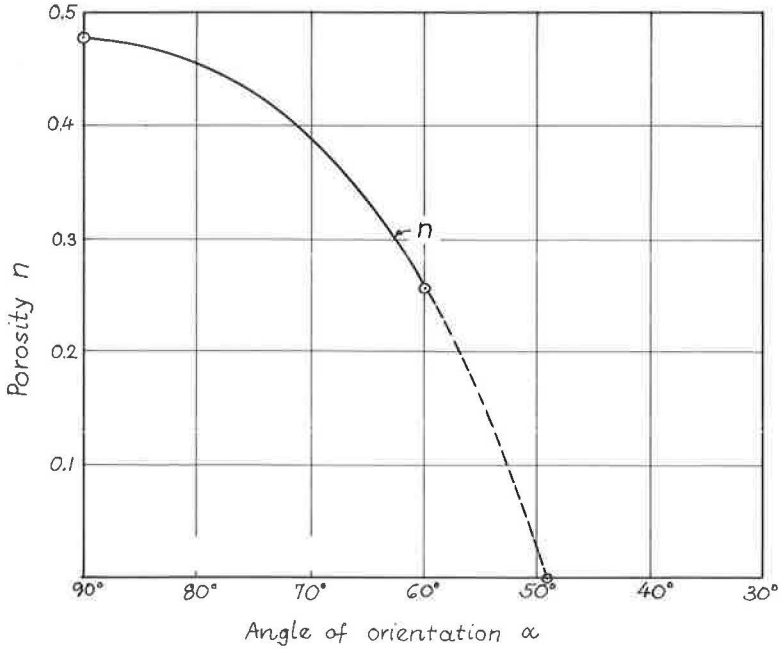
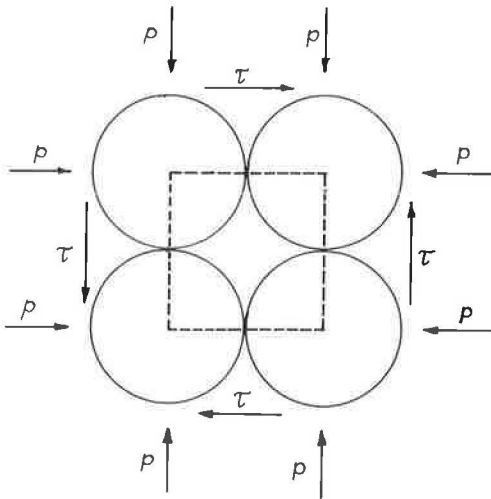Figure 32. Variation of porosity with angle of orientation.

and

Figure 33. Packing of spheres loaded by hydrostatic and shearing stresses.

$$\sigma = \frac{c}{V_0} (V - V_0) =$$

$$C_1 (V - V_0) \qquad (62b)$$

in which C is the bulk modulus of compressibility (depending on the surface properties of the spheres) and V_0 is the volume at $\alpha = 60°$ $(V_0 = \pi/6)$.

The deformation caused by shearing stresses consists of the change of α accompanied by the decrease of porosity. In the theory of liquids (108), the shearing stress is given by

$$\tau = -\frac{\partial F}{\partial \beta} \qquad (63)$$

in which $\beta = 90° - \alpha$ and $F(\beta, T)$ is the free energy of the lattice referred to one sphere. It is a function of variation of the height of the unit cell and of the temperature. Because these are isothermic processes, this term can be taken as the potential energy of one sphere with respect to the sphere immediately below. It is, then, given by $h - h_0$, where h is the height of the unit cell at α and h_0 is the minimum value at $\alpha = 60°$ or $D\sqrt{2/3}$ (Fig. 26, Eq. 59). Assuming again, as a first approximation, a linear relationship for $h = h(\alpha)$ (connecting $h = 1$ for $\alpha = 90°$ and $h = h_0$ for $\alpha = 60°$), $h = 1 - C_2\beta$ or

$$\frac{\partial F}{\partial \beta} = \frac{\partial h}{\partial \beta} = C_2 \qquad (64)$$

and, therefore, τ = const. = C_2.

The shearing resistance of the medium can be given (Fig. 34) as

$$\tan \phi = \tau/\sigma = \frac{\tau}{\sigma} \frac{C_2}{C_1(V - V_0)} = \frac{C}{V - V_0} \quad (65)$$

which is in complete agreement with the equation of Winterkorn suggested by the analogy between liquids and grain assemblies (106).

Values, calculated on the basis of the concept of the solid and liquid state of macromeritic systems (Eq. 65) have been compared with experimental data

Figure 34. Determination of angle of friction.

obtained by various dependable workers on the friction properties of granular materials (26).

It must be emphasized that this formula represents the first approximation. Besides the substitution of the relations V = f (p) and h = h (β) with straight lines—which actually, as it can be seen from Figures 24 and 27, may be considered justified—it neglects an important factor. This approximation is also involved in Batschinski's formula: namely, the activation energy for the diffusion of holes in the liquid and in the particle assembly has been disregarded. It should be borne in mind also that the application of the equation to higher pressures can hardly give exact values, because the dependence of the volume on the pressure and of the energy on the volume deviates from a linear law in this region.

Eq. 65 can be used to verify the difference between plane shear and shear in three dimensions. Considering Figures 5 and 8, respectively, with the term V_0 (volume of solids) the same in both cases, the difference in τ or h must be taken into account.

$$\tau \text{ plane} = \frac{1 - 0.866}{\pi/6} = 0.255 \quad (66a)$$

and

$$\tau \text{ space} = \frac{1 - 0.815}{\pi/6} = 0.353 \quad (66b)$$

yield

$$\frac{\tan \phi \text{ plane}}{\tan \phi \text{ space}} = \frac{0.255}{0.353} = 0.725 \quad (67)$$

This may explain the discrepancies in the value of tan ϕ as determined by direct shear or by triaxial test, respectively. It means that if the latter amounts, for instance, to ϕ = 40°, the direct shear is likely to give ϕ = arc tan (0.725 tan ϕ) = 32°. Many test results in the literature show similar deviations (111).

To arrive at a better approximation in the evaluation of the inner resistance of a macromeritic liquid, the dependence of V on σ, instead of Eq. 62b, must be considered, according to an empirical equation proposed long ago by Tait (108). This relation states that there is a strain-hardening during the process of compression. For a given amount of compression, greater all-round stresses must be applied if there is already a stress of this type acting. This means that the bulk modulus of compressibility is not a constant, but a function of the all-round pressure itself. If

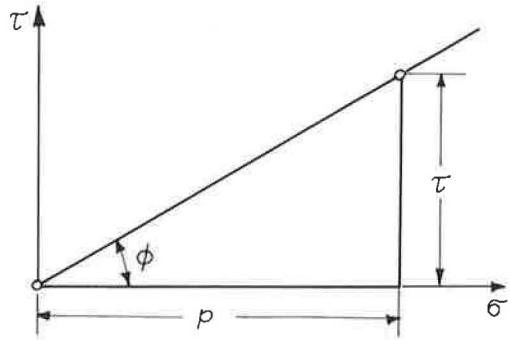$$C = \frac{dp}{d\epsilon} = \frac{p + b}{ab} \quad (68)$$

the volume change is

$$V - V_0 = a \log \left(\frac{p + b}{b} \right) \tag{69}$$

This equation is of the same form as that for the compression of soils proposed by Terzaghi (112).

The term $(V - V_0)$ is given as a trigonometric function of β; it may be replaced without loss of accuracy by a parabola of the second degree. The deviation from the exact value can be made smaller than 1 percent. Then

$$V - V_0 = C_1 \beta^2 \tag{70}$$

and from Eq. 69

$$p = b \left[\left(\exp \frac{V - V_0}{a} \right) - 1 \right] = b \left[\left(\exp \frac{C_1 \beta_1^2}{a} \right) - 1 \right] \tag{71}$$

Eq. 59, giving a measure for the available potential energy, may be replaced also by a parabola of the second degree. Then

$$F = 1 - C_2 \beta^2 \tag{72}$$

and

$$\tau = \partial F / \partial \beta = 2 C_2 \beta \tag{73}$$

The shearing resistance is given by

$$\tan \phi = \frac{\tau}{\rho} = \frac{2 C_2 \beta}{b \left[\left(\exp \frac{C_1 \beta^2}{a} \right) - 1 \right]} \tag{74}$$

Because the relation between the porosity and the angle of orientation ($\alpha = 90° - \beta$) is known, Eq. 74 furnishes the solution to the problem. However, the physical meaning of the laws expressed by this equation will be better understood, if instead of β, the void ratio ϵ is used (notation used to replace the usual e, in order to avoid confusion with the base of the natural logarithm). Then, Eq. 70 yields

$$\beta = \sqrt{\frac{V - V_0}{C_1}} = \sqrt{\frac{\epsilon - \epsilon_{min}}{C_1}} \tag{75}$$

and

$$\tan \phi = \frac{2 C_2 \sqrt{(\epsilon - \epsilon_{min})/C_1}}{b \left[\left(\exp \frac{\epsilon - \epsilon_{min}}{a} \right) - 1 \right]} = \frac{C \sqrt{\epsilon - \epsilon_{min}}}{\left(\exp \frac{\epsilon - \epsilon_{min}}{a} \right) - 1} \tag{76}$$

Eq. 76 should be checked against available shear test data obtained by dependable research workers. In Figure 35 data from direct shear tests on Ottawa standard sand (88) have been plotted as $\tan \phi = f(\epsilon)$; the curve according to Eq. 76 is also shown using the constants $\epsilon_{min} = 0.2$ a = 0.5, and C = 1.26. The deviations are small (Table 19).

It is likely that a more precise determination of the constants would result in a still better agreement; this sample calculation has been presented to show the general trend of Eq. 76. It may be assumed that the constants ϵ_{min} and a vary within close limits.

A third approximation is also available to evaluate the function $\tan \phi = f(\epsilon)$. The variation of the volume of the unit cell with the variation of the imaginary coordination
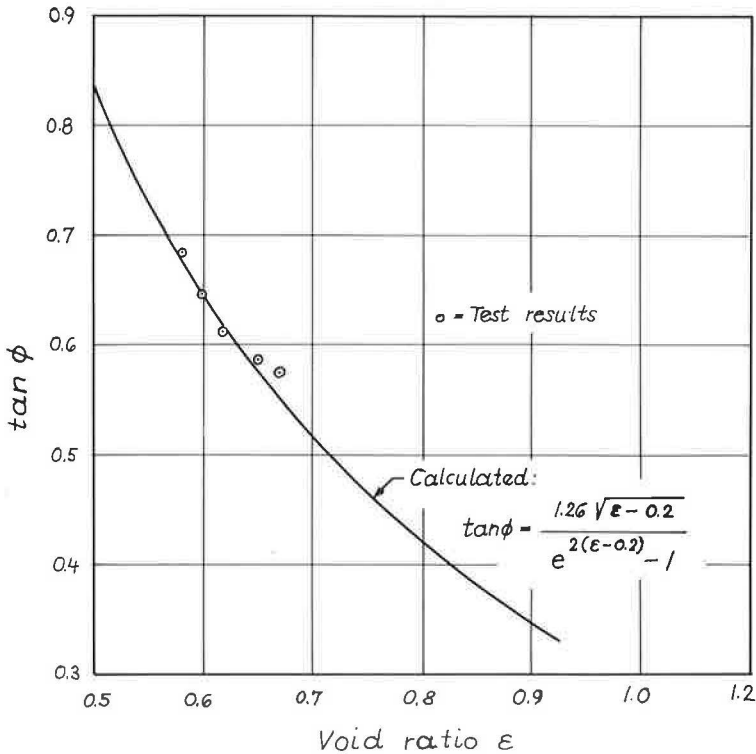
Figure 35. Experimental vs calculated data.

number is a linear relationship. The shearing stress, necessary to produce movement by overcoming the friction on the surface of the spheres, may be assumed to be directly proportional to $(N - 6)$. In the case of the cubic arrangement of the spheres $(N = 6)$, the shearing resistance is zero (melting point). Then Eq. 61 yields

$$N - 6 = 6 (2 + \sqrt{2}) (1 - V) \qquad (77)$$

and

TABLE 19

EXPERIMENTAL VS CALCULATED DATA ON SHEARING STRENGTH

Void Ratio ϵ	Tan ϕ		Dev.	Dev. (%)
	Calc.	Exp.		
0.58	0.684	0.682	-0.002	-0.29
0.60	0.651	0.648	-0.003	-0.46
0.62	0.620	0.614	-0.006	-0.98
0.64	0.593	0.589	-0.004	-0.67
0.66	0.570	0.579	+0.009	+1.38

$$\tau = C (N - 6) = C_1 [a - b (V - V_0)] \qquad (78)$$

Assuming, as in the first approximation,

$$\sigma = C_2 (V - V_0) \qquad (79)$$

the result is

$$\tan \phi = \frac{C}{V - V_0} - B \qquad (80)$$

This equation differs from Winterkorn's Eq. 34a only in the term $(-B)$. This may account for the activation energy neglected in Batschinski's equation. It would be
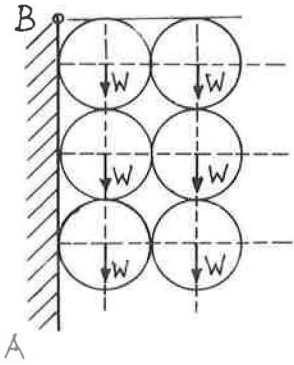
Figure 36. Lateral pressure of cubic packing.
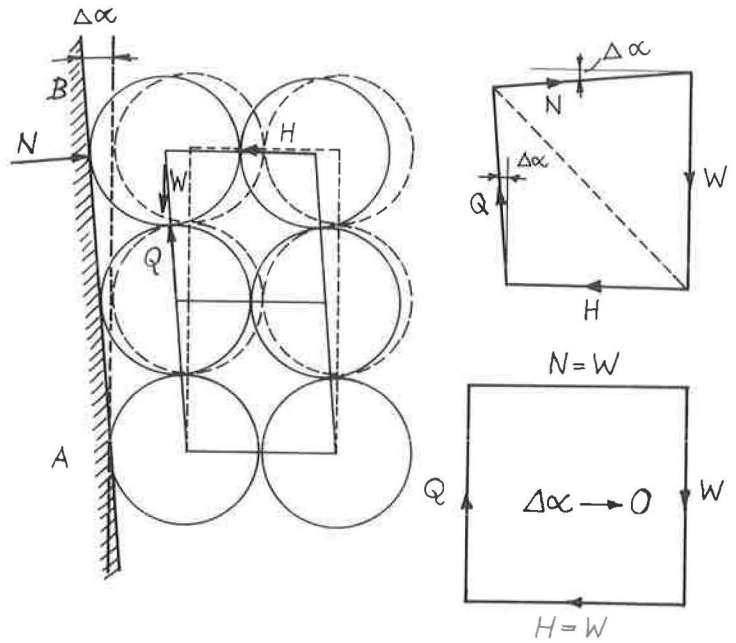
Figure 37. Cubic packing as limiting state.

$$K_o h \gamma_s = \frac{2\Sigma}{h}$$
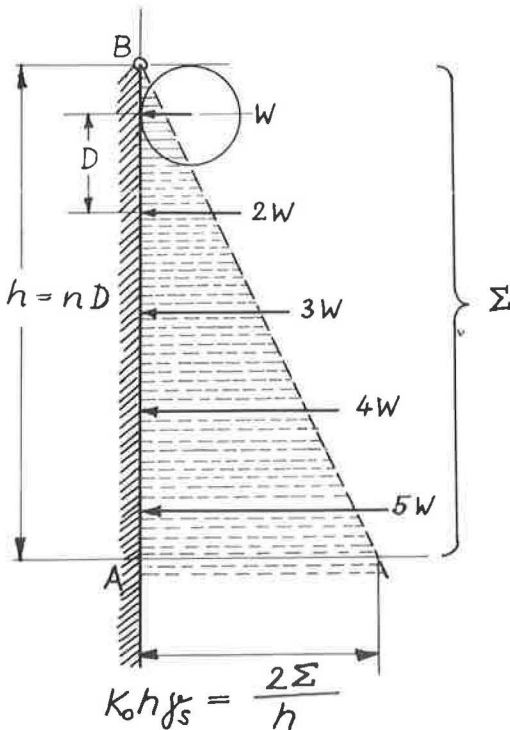
Figure 38. Substitution of isolated forces.

worthwhile to check this equation against experimental data; it is not impossible that cases yielding negative values for ϵ_{min}, which is physically difficult to visualize, would fit Eq. 80.

LATERAL PRESSURES OF PACKINGS

The study of systematic packings can be extended to the investigation of lateral pressures exerted by them. This investigation furnishes some interesting results that may be of value for the better understanding of earth pressure phenomena (110).

If in cubic packing, there is, according to Winterkorn's conception, a melting point of the grain assembly, the coefficient of lateral pressures, as interpreted in the theory of earth pressure, has to be unity (Fig. 20). This packing, however, gives at the first glance zero value (Fig. 36); there are no horizontal forces between the spheres. The slightest tilting of the wall AB will produce, however, lateral forces; if there is no friction between the spheres, this horizontal force, H, if $\Delta \alpha \to 0$, in the first row is W (Fig. 37). In the second row, H is 2W, and so on, until in the n-th row H is nW. The coefficient of earth pressure is

$$K_0 = \frac{E_0}{h^2 \gamma} = \frac{\sigma_X}{\sigma_Z} \tag{81}$$

This definition assumes a continuous distribution of the forces transmitted through the particles; that is, the number of contacts becomes infinity. To calculate, the packing must be substituted by a continuous mass. This can be accomplished in the following manner (Fig. 38):

$$DE_0 = W + 2W + \ldots + nW = \frac{1}{2} n (n + 1) W \tag{82}$$

$$W = \frac{\pi}{6} D^3 \gamma_s \tag{83}$$

$$E_0 = \frac{1}{2} n (n + 1) \frac{\pi}{6} D^2 \gamma_s \tag{84}$$

in which D is the width of the back of wall. This gives a triangular distribution for the horizontal stresses, with an intensity

$$\sigma_X = \frac{2\Sigma E}{h} = (n + 1) \frac{\pi}{6} D \gamma_s \tag{85}$$

because h is nD.

The vertical force exerted by a vertical row of spheres is

$$N = nW = \frac{\pi}{6} D \gamma_s \tag{86}$$
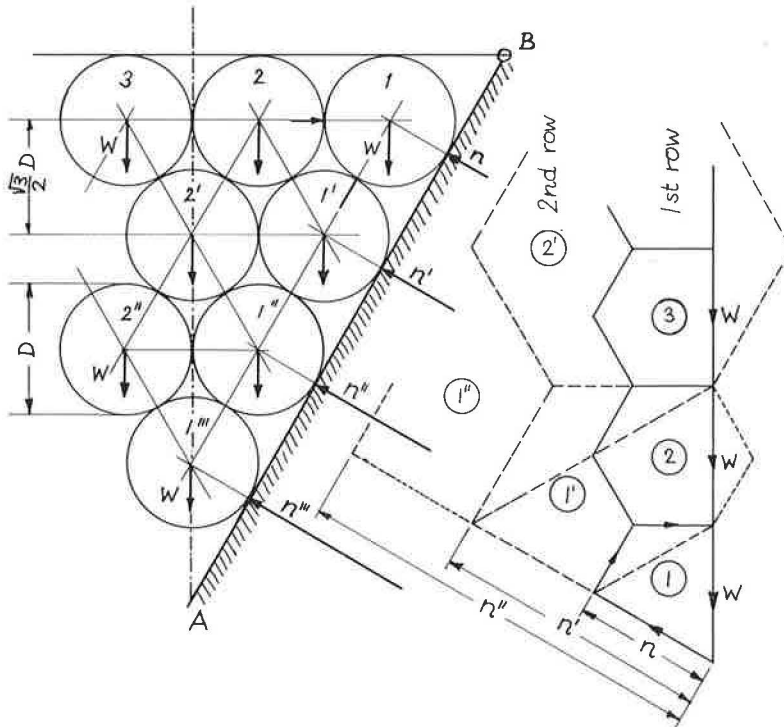

Figure 39. Forces in orthorhombic system.

58

giving a uniform pressure

$$\frac{N}{D^2} = n D \frac{\pi}{6} \gamma_s \tag{87}$$

and a coefficient of the earth pressure at rest

$$K_0 = \frac{\sigma z}{\sigma_Z} = 1 + \frac{1}{n} \tag{88}$$

which, if $n \to \infty$, is 1.

Although a simpler expression for this coefficient is

$$-K_0 = \frac{H}{N} = \frac{nW}{nW} = 1 \tag{89}$$

the more complicated way shown here is useful for the treatment of other cases.

The density of the orthorhombic system is midway between that of the densest and the loosest ([3, 6, 3] and [1, 4, 1]) systems. It is, in fact, the densest of the plane systems. The determination of forces between the spheres and those acting on a plane with the angle of $\alpha = 60°$, respectively, is shown in Figure 39.

With the same procedure as before, the resultant force on $\overline{AB}$ is

$$DE_0 = \frac{1}{2} n (n + 1) \frac{\pi}{6} D^3 \gamma_s \tag{90}$$

and

$$E_0 = K_0 \frac{s^2 \gamma_s}{2} \tag{91}$$

Therefore

$$K_0 = \left(1 + \frac{1}{n}\right) \frac{\pi}{6} = 0.523 \ (n \to \infty) \tag{92}$$

and, for the vertical plane

$$DE_{oh} = \frac{1}{2} n (n + 1) \frac{1}{0.866^2} \times H \tag{93}$$

$$H = W \tan 30° \tag{94}$$

$$K_{oh} = \left(1 + \frac{1}{n}\right) \frac{1}{0.866^2} \times \frac{\pi}{6} \times 0.577 = 0.404 \tag{95}$$

These results are in very good agreement with the measured values for sand of middle density.

REFERENCES

106. Batschinski, Z., Phys. Chem. 84:643 (1913).
107. Filep, L., "Egyenlo Gombokbol Allo Halmazak." Vizugyi Kozlemenyek, Budapest (1936).
108. Frenkel, J., "Kinetic Theory of Liquids." Dover Publ., New York (1955).
109. Kezdi, A., "Erddruck Theorien." Springer Verlag, Berlin, Gottingen, Heidelberg (1962).
110. Kezdi, A., "Baugrundmechanik." Verlag fur Bauwesen, Berlin (1964).
111. Peltier, J., Proc. 84th Internat. Conf. Soil Mech. Found. Eng., London, 3 (1958).
112. Terzaghi, K. V., "Erdbaumechanik auf bodenphysikalischer Grundlage." F. Deuticke, Leipzig, Vienna (1925).
113. Winterkorn, H. F., "Macromeritic Liquids." ASTM Sym. on Dynamic Testing of Soils (July 1953).

Stabilization of Soils with Fly Ash Alone

MANUEL MATEOS
  Project Engineer, Torán y Cia., Madrid, Spain: formerly Research Associate,
  Engineering Experiment Station, Iowa State University, Ames

Fly ash reacts with lime to form a cementing material used to strengthen soils for the construction of bases and subbases for pavements. To sustain the cementitious reaction, lime must be added or supplied to the fly ash. Nevertheless, a survey of fly ashes revealed that some of them contain cementing materials—lime or other products—in a quantity sufficient for good strength. The stabilization of soils with fly ashes that do not need added lime should be a very competitive method when the transportation cost of the fly ash is within economical limits. This paper presents the results obtained with several fly ashes used without lime to stabilize several soils with different textures.

•SOIL STABILIZATION, a relatively new science, aims at the improvement of the engineering characteristics of soils, either by physical means or by treating the soils with different products. Some of the successful stabilizing agents are cement, lime, and lime plus fly ash. Fly ash, an artificial pozzolan, reacts with lime to produce strength through cementation (1).

The stabilization of soils with lime and fly ash is a well-known process used in the construction of pavements for roads, airfields and parking lots. The advantages of this method of soil stabilization stem from the fact that fly ash is a waste product of power plants and is available at a low price. However, from 2 to 9 percent lime is added, bringing this method to a cost comparable to that of other methods of soil stabilization.

Although the general understanding is that fly ash reacts only with lime, exploratory studies showed that some fly ashes produce strength without the addition of lime (2). Extensive studies made with two cementitious fly ashes in the stabilization of several soil materials are presented in this investigation.

MATERIALS

Fly Ashes

Preliminary studies were made using several fly ashes selected from a group of 21 fly ashes extensively studied by the author (3, 4, 5). Five fly ashes were found to produce an adequate cementation of a sandy soil, and two of these fly ashes gave such high strengths that they were further evaluated with a variety of soil materials. The analyses of the five fly ashes are given in Table 1.

Fly Ash A. —This sample was collected by mechanical precipitators (cyclone type). The coal was from Missouri and was pulverized and burned in suspension in Combustion Engineering boilers. The sample was from Montrose Station Power Plant of the Kansas City, Mo., Power and Light Company.

Fly Ash B. —This sample was collected by mechanical precipitators (multicone dust collectors). The coal was from Iowa, unwashed, pulverized and tangential fired. The sample was from the Des Moines Power Plant of the Iowa Power and Light Company.

TABLE 1

ANALYSIS OF FLY ASHES

Fly Ash Designation	Analysis (%)							Passing No. 325 Sieve (%)	Spec. Grav. (g/cm³)	Spec. Surf. (cm²/g)
	SiO₂	Fe₂O₃	Al₂O₃	CaO	MgO	SO₃	C			
A	39.2	30.2	11.9	11.6	0.8	1.9	2.8	57.4	2.33	1,730
B	40.1	36.6	13.1	5.8	0.3	2.4	0.2	31.8	2.82	1,460
C	35.3	43.4	7.8	5.3	0.9	1.4	3.8	64.8	2.69	2,048
D	40.5	20.8	12.4	10.6	0.3	2.0	7.8	57.6	2.44	2,109
E	51.2	20.2	10.0	6.3	1.6	1.7	1.0	80.7	2.34	2,539

TABLE 2

ANALYSES OF SOILS

Soil	Passing Sieve (%)[a]						Liquid Limit (%)	Plasticity Index
	¾ in.	No. 4	No. 10	No. 40	No. 100	No. 200		
Sonon limestone	100	32	15	6	4	3	-	NP
Rapid limestone	100	30	17	8	7	6	-	NP
Limestone screenings	100	98	68	48	29	19	-	NP
Bottom furnace ash	100	100	65	18	7	3	-	NP
Dune sand	100	100	100	ND	ND	4	-	NP
Colfax sand-loess mix	100	100	100	ND	ND	29	19	3
Friable loess	100	100	100	100	99	98	32	7
Gumbotil	100	100	100	97	93	81	76	50

[a]ND = Not determined.

TABLE 3

COMPRESSIVE STRENGTH RESULTS OF DUNE SAND-FLY ASH MIXTURES[a]

Fly Ash	Curing Period (days)	Compressive Strength (psi)			
		80:20[b]	73:27[b]	65:35[b]	100:0[b]
A	7	102	138	172	310
	28	193	273	378	746
	90	288	440	606	982
B	7	46	51	51	150
	28	138	217	288	665
	90	272	452	593	1,110
C	7	26	41	43	ND
	28	43	89	145	392
	90	74	175	298	702
D	7	60	69	74	ND
	28	110	152	192	276
	90	244	267	350	475
E	7	33	66	95	ND
	28	43	101	167	196
	90	51	138	201	238

[a]Cured at 71 F.   [b]Sand to fly ash.

Fly Ash C. —This sample was collected by mechanical precipitators (cyclone type). The coal was from Missouri and Kansas mines. The coal was pulverized and burned in suspension in Combustion Engineering boilers. The sample was sent from the Hawthorne Station Power Plant of the Kansas City, Mo., Power and Light Company.

Fly Ash D. —This sample was sent by the Kansas City, Mo., Power and Light Company. No data are available on the source.

Fly Ash E. —This sample was collected by electrical precipitators. The coal was from southern Illinois and was crushed in a bowl crusher. The sample was from the Meramec Station Power Plant of the Union Electric Company of Saint Louis, Mo.

Soils

Eight different kinds of soil materials and aggregates were selected to represent a wide variety in physical and chemical characteristics; their analyses are given in Table 2.

PROCEDURES

The soils were air dried and the soil aggregations broken down by grinding. The dried soils were mixed with the dry fly ash in a laboratory mixer for 0.5 min. Test specimens of the two crushed limestone soils, 4 in. in diameter by 4.6 in. in height were molded according to ASTM Specification D 558-57 (6). Test specimens of the other six soils, 2 in. in diameter by 2 in. in height, were molded with the Iowa State Compaction Apparatus (1, 2, 3, 4, 7) to a maximum density close to that of the other samples. Specimens were molded at several moisture contents.

After molding, the specimens were wrapped in waxed paper, sealed with cellophane tape, and stored for curing in a moist room at 71 ± 3 F and greater than 90 percent RH. The specimens were cured for 7, 28 and 90 days, followed by immersion in water for 1 day. They were then tested under unconfined compression to determine their maximum water stable strength.

RESULTS

Part of the preliminary studies made using fly ashes and a dune sand soil are presented in Table 3. The results indicate that some fly ashes alone can cement soil particles. Two of the five fly ashes (A and B) gave such high strengths that they could be used with the dune sand in the construction of base and subbase courses for pavements.

These two fly ashes were further evaluated with more soils (Figs. 1 to 4). Strengths of 400 psi or more were obtained after 28 days curing with six of the soils. The only two soils that gave 28-day strengths lower than 400 psi were the friable loess and the gumbotil (Fig. 4). However, these soils are not satisfactory, stabilized even with fly ash plus added lime (1, 5).

In recent studies with soil-cement mixtures (8), it has been found that a 7-day laboratory unconfined compressive strength of 453 ± 22 psi is adequate for a base course. If it is assumed that the same strength requirements are valid for soil and

Figure 1. Immersed unconfined compressive strength of soil-fly ash mixtures moist cured for 7, 28 and 90 days.

Figure 2. Immersed unconfined compressive strength of soil-fly ash mixtures moist cured for 7, 28 and 90 days.

fly ash mixtures cured for 28 days, fly ashes A and B can be used with six of the soils in the construction of base courses for pavements.

It should be emphasized that the strength of most of the soils treated continued to increase after 28 days, reaching strengths of 1,000 psi or more after 90 days of curing. The 7-day strengths are very low, usually about 100 psi, but this is true also for soils stabilized with lime plus fly ash (1, 5).

MECHANISM

Fly ash is a by-product of the power plants burning powdered coal. The suspended noncombustibles during the burning process are subjected to very high temperatures, such that individual mineral grains melt to form individual grains of fly ash. Possibly marly materials in the fly ash suffer changes in structure during the burning process similar to those in the formation of portland cement clinker, although this is highly speculative and has not been verified by X-ray analysis. Fly ash can thus be a kind
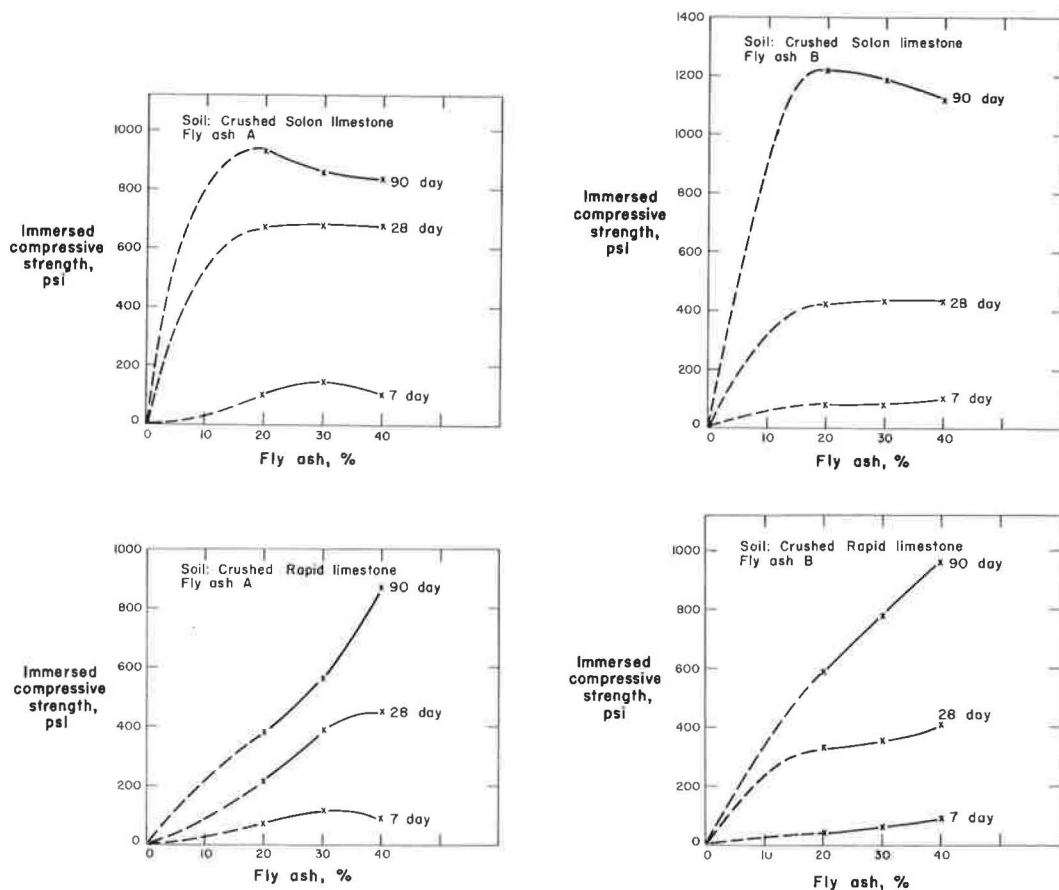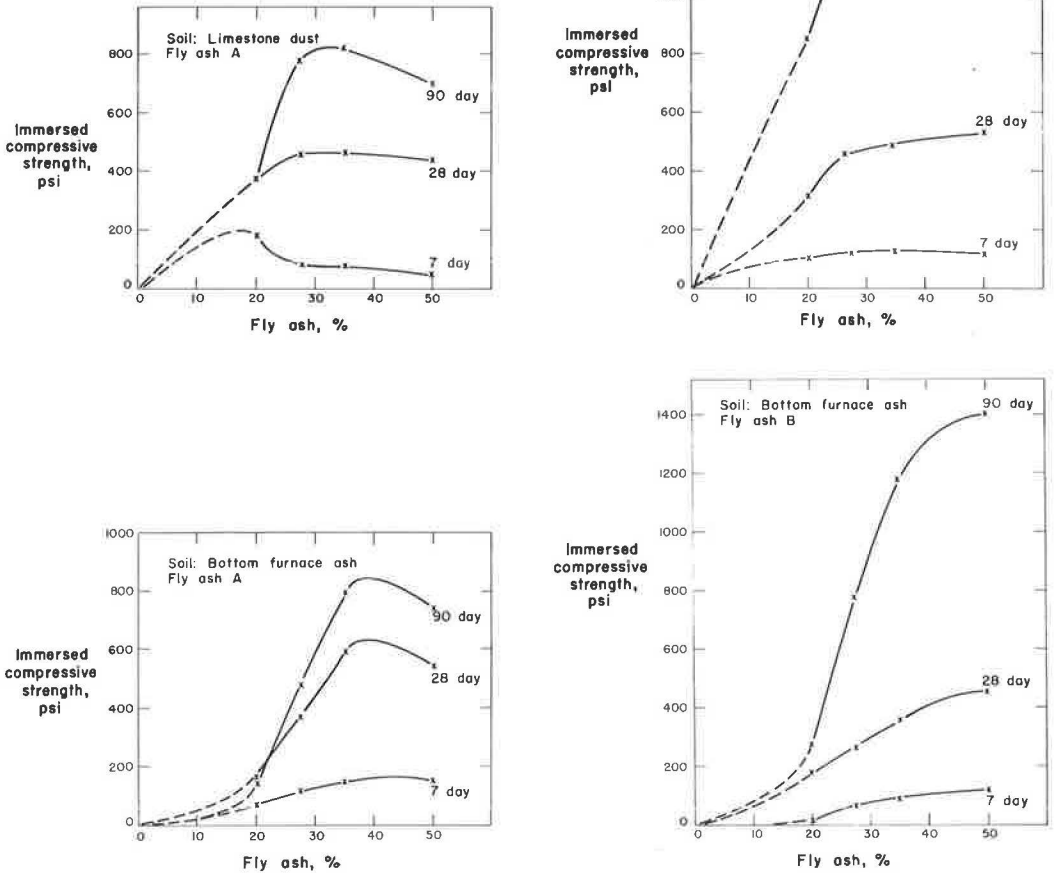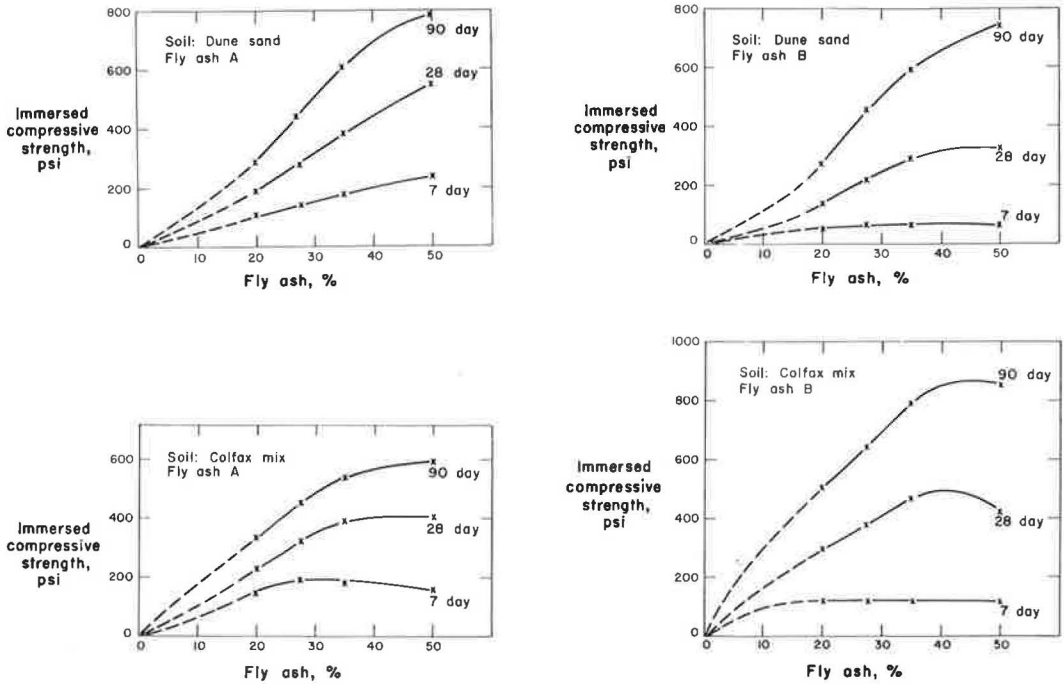
Figure 3. Immersed unconfined compressive strength of soil-fly ash mixtures moist cured for 7, 28 and 90 days.
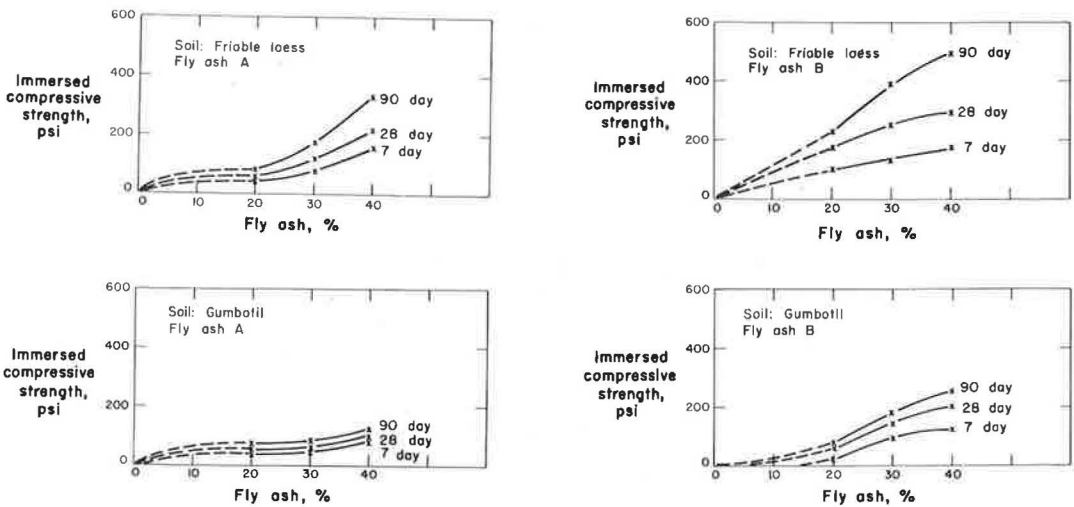

Figure 4. Immersed unconfined compressive strength of soil-fly ash mixtures moist cured for 7, 28 and 90 days.

of cement similar to ground clinker. Because the fly ash is minute, the particles may not require grinding to act with water as a cementing agent.

Free lime may already be present in the reactive fly ashes, so that none must be added for the lime-fly ash reaction to occur. Small amounts of free lime were found by chemical analysis (Table 1), and $Ca(OH)_2$ has been found in X-ray traces.

TABLE 4

COMPRESSIVE STRENGTH RESULTS OF SPECIMENS OF FLY ASH[a]

Fly Ash	Compressive Strength (psi)	
	1 Day	3 Days
A	878	923
B	687	827
C	445	570
D	205	242
E	167	220

[a]Curing period under steam at 248 F and 1 atm pressure.

SELECTION OF FLY ASHES

The choice of a fly ash to be used in concrete or in mixtures with lime is difficult because the strength and other requirements of fly ash are difficult to predict from physical or chemical characteristics (3). The ASTM has set standards for selecting a fly ash for such uses, but these standards need revision (3, 4).

A fly ash to be used alone in the stabilization of a soil should be carefully chosen. The best way to determine the suitability of a fly ash is to mold specimens under different moisture contents for several soil and fly ash combinations and cure them under standard conditions, up to 90 days. Selection can be made more simply by a quick test using steam to cure the specimens (4, 9). Specimens of fly ash for this quick test are prepared in the Iowa State Compaction Apparatus, giving five blows to each side of the specimen with the 5-lb hammer. The specimens are then wrapped in polyvinylidene chloride and sealed with cellophane tape. The specimens are preheated for about 2 hr in a 140 F oven and then autoclaved at 248 F and 1 atm pressure. The specimens are preheated to make the increase in temperature more gradual. After 24 hr of curing, the specimens are removed from the autoclave and placed in distilled water for 2 hr. They are then tested for unconfined compressive strength. Those fly ashes giving a strength of 600 psi or more may be considered good cementing materials for stabilizing soils for base and subbase courses of pavements (Table 4). The fly ashes with more than 600 psi under the quick test should be further evaluated with the actual soils to be used.

Another correlation found is that those fly ashes showing greatest strengths without added lime are more alkaline than others (2). The alkalies may make the fly ashes as reactive without lime as mixtures with lime (10, 11, 12). Until more information is obtained, the quick test should be used for the preliminary selection of a cementitious fly ash.

CONCLUSIONS

1. Some fly ashes possess cementitious qualities in themselves without addition of lime.

2. Some fly ashes can be used to stabilize soils. The soils that respond best are nonplastic coarse-grained soils, such as gravel, sand and slag. Strengths of 400 psi or more can be reached after 28-days curing with some combinations of soil and fly ash. These combinations are sufficient in strength to be used for the base courses of pavements.

ACKNOWLEDGMENT

REFERENCES

1. Mateos, M., and Davidson, D. T., "Lime and Fly Ash Proportions in Soil-Lime-Fly Ash Mixtures." HRB Bull. 335, pp. 40-64 (1962).

2. Mateos, M., and Davidson, D. T., "Cementitious Properties of Some Iowa Fly Ashes Without Lime Additive." Iowa Acad. of Sci. Proc., 69: 362-369 (1962).

3. Vincent, R. D., Mateos, M., and Davidson, D. T., "Variation in Pozzolanic Behavior of Fly Ashes." ASTM Proc., 61: 1098-1118 (1961).

4. Mateos, M., and Davidson, D. T., "Steam Curing and X-ray Studies of Fly Ashes." ASTM Proc., 62: 1008-1018 (1962).

5. Mateos, M., "Physical and Mineralogical Factors in Stabilization of Iowa Soils With Lime and Fly Ash." Ph. D. thesis, Iowa State Univ. Lib. (1961).

6. "Procedures For Testing Soils." ASTM, Philadelphia (1958).

7. O'Flaherty, C. A., Edgar, C. E., and Davidson, D. T., "Iowa State Compaction Apparatus for Measurement of Small Soil Samples." Highway Res. Record 22, pp. 48-63 (1963).

8. George, K. P., "Base Course Mix Design Criteria for Cement Treated Loess." Ph. D. thesis, Iowa State Univ. Lib. (1963).

9. Mateos, M., and Davidson, D. T., "A Quick Test to Evaluate the Pozzolanic Quality of a Fly Ash." Iowa State Univ. Eng. Exp. Sta., Soil Res. Lab., Mimeo Rept. (1962).

10. Davidson, D. T., Mateos, M., and Katti, R. K., "Activation of the Lime-Fly Ash Reaction by Trace Chemicals." HRB Bull. 231, pp. 67-91 (1959).

11. Mateos, M., and Davidson, D. T., "Further Evaluation of Promising Chemical Additives for Accelerating Hardening of Soil-Lime-Fly Ash Mixtures." HRB Bull. 304, pp. 32-50 (1961).

12. Mateos, M., and Davidson, D. T., "Stabilization of Alaskan Silty Soils with Inorganic Additives." 9th Pan Amer. Highway Cong., OAS, Washington, Doc. 29 (May 1963).

Effect of Heat on Physico-Chemical Properties of Soils

M. C. LI, Associate Professor of Civil Engineering, New York University

This paper is based on a laboratory investigation of 36 soil samples prepared from 9 various clay minerals and their modifications as a result of breakdown of chemical constituents and changes in physico-chemical properties by heat treatment at three different temperatures. The multiple correlation drawn between the independent variables of plasticity index, particle-size less than $2\,\mu$, cation exchange capacity, and sodium and the dependent variable, free-swelling, gives a coefficient of 0.974. If surface area is used instead of clay fractions less than $2\,\mu$, the coefficient of multiple correlation is 0.976. Simple correlations among clay fractions less than $2\,\mu$, surface area, and composite index are also analyzed.

● THE BEHAVIOR and action of soil are affected not only by the inherent physical, chemical, mineralogical, hydraulic, microbiological, and optical properties but also are governed by many environmental factors, such as water, pressure, weather, and geological formation. The interrelationships in this polydisperse and multicharacter soil system are so intricate that many of them are only partially understood and yet to be found by basic researches.

SOIL SAMPLES

To insure uniformity, homogeneity, and purity of clay fractions in soil samples under strict laboratory control, ten clay minerals were collected from various parts of the United States and Canada. A pilot clay mineral (No. 0) was heated to 400 and 800 C for 12 and 36 hr to determine the effect of prolonged heating on physico-chemical properties. There were only insignificant changes. Thirty-six soil samples were prepared by heat treatment of the nine clay minerals (Nos. 1 to 9) at three different temperatures (300, 600, and 900 C) for 24 hr in a laboratory furnace with electronic controller. Table 1 gives the clay minerals, their chief constituents and sources of supply.

EXPERIMENTAL PROCEDURES

Physical tests of soils were performed in accordance with ASTM and AASHO standard methods and procedures (1, 2). Surface areas were determined by the glycerol retention method with pretreatment developed by the Bureau of Public Roads (3, 4). Specimens, 1 in. in diameter and 2 in. in height, were molded by Iowa State University drop-hammer impact compaction machine modified and constructed by New York University. The specimens were cured in a constant humidity room for 1 wk and tested on unconfined compression apparatus for cohesive strength.

Cation exchange capacities and exchangeable cations (calcium, sodium, magnesium, and potassium) were tested on prepared leachates (5) by means of a flame attachment on a Beckman spectrophotometer (6). A Beckman Zeromatic pH meter (5) was used to determine pH values, exchangeable hydrogen, and total exchangeable metallic bases.

A simple free-swelling test procedure in which the soil is allowed to expand freely

TABLE 1

CONSTITUENTS AND SOURCES OF CLAY MINERALS

No.	Type	Source	Chemical Constituents (%)									S.R.[a]	O.M.[b]
			SiO_2	Al_2O_3	Fe_2O_3	TiO_2	CaO	MgO	Na_2O	K_2O	SO_3		
0	Kaolinite	Ga.	---	---	---	---	---	---	---	---	---	---	0
1	Na-Ca bentonite	Manitoba, Can.	57.9	19.9	6.1	---	1.8	4.2	---	---	3.2	4.13	15.2
2	Ca-bentonite	Miss.	58.8	18.4	5.9	0.9	3.3	3.3	0.5	0.6	0.1	4.50	4.9
3	Ca-bentonite	Miss.	56.8	20.3	8.4	0.9	1.4	3.1	0.3	0.7	0.2	3.74	15.2
4	Attapulgite	Ga.	---	---	---	---	---	---	---	---	---	---	3.8
5	Na-bentonite	Wyo.	61.9	21.1	3.9	0.2	1.2	2.4	2.6	0.4	0.6	4.45	15.3
6	Kaolinite	Fla.	46.5	37.9	0.8	0.2	0.1	0.2	0.3	0.2	---	2.05	19.5
7	Illite	Ill.	61.5	17.8	5.0	1.1	0.6	1.5	4.3		1.2	4.97	10.3
8	Kaolinite	Ill.	63.6	19.9	2.4	1.5	0.1	0.2	2.4		---	5.03	5.5
9	Pyrophyllite	---	---	---	---	---	---	---	---	---	---	----	3.2

[a] Silica-sesquioxide ratio.
[b] Organic matter as determined by decrease in liquid limit of oven-dried samples.

TABLE 2

SUMMARY OF TEST RESULTS[a]

No.[b]	Atterberg Limits (%)					Size and Surface Area			Cation Exchange (m.eq./100 gm)			Free Swelling (%)	Cohesion (psi)
	w_{100}	w_L	w_P	I_P	w_S	< 2 μ (%)	C.I.	S.A. (%)	CEC	Ca	Na		
1 A	127.2	134.8	55.5	79.3	11.8	92.8	0.796	36.0	123.5	27.7	31.3	41.2	176
B	130.6	85.5	49.1	36.4	29.7	78.0	0.746	39.8	62.2	30.0	30.9	54.6	161
C	71.2	44.5	47.6	0	43.9	23.0	0.400	7.5	19.6	26.4	13.9	5.1	10
D	61.2	40.9	42.9	0	47.4	18.2	0.303	0.6	1.5	21.6	0.7	4.4	0
2 A	124.2	98.9	53.5	45.4	12.3	84.6	0.633	32.6	82.7	79.8	0.5	45.3	243
B	132.2	78.5	51.9	26.6	15.5	54.0	0.792	32.9	79.0	76.9	0.5	43.4	174
C	78.0	51.7	47.5	4.2	50.8	34.2	0.627	12.1	7.7	47.7	0.3	14.9	81
D	62.5	43.2	---	NP	41.1	25.4	0.600	7.6	5.8	14.3	0	7.1	0
3 A	122.5	155.0	45.0	110.0	4.2	100.0	0.781	31.3	59.0	55.0	0.6	50.2	330
B	118.5	117.0	45.0	72.0	0	100.0	0.879	29.8	47.4	24.6	0.4	62.5	118
C	60.4	45.5	42.4	3.1	40.2	23.0	0.482	7.4	15.5	6.9	0.1	7.2	3
D	---	---	---	NP	44.0	18.0	0.314	0.6	2.1	0.8	0	5.3	0
4 A	239.0	255.0	128.4	126.6	57.8	99.8	0.699	16.4	37.2	23.2	0.5	36.3	248
B	231.0	166.6	139.0	27.6	87.4	58.0	0.424	16.6	31.1	23.2	0.4	31.3	98
C	209.5	134.5	136.0	0	114.6	39.4	0.338	10.2	39.7	6.3	0.4	12.6	6
D	153.0	87.9	---	NP	91.8	34.0	0.331	0.8	8.4	6.1	0.1	12.1	2
5 A	273.0	623.0	45.1	577.9	0	100.0	0.781	35.1	75.8	22.2	63.4	239.0	281
B	310.5	592.0	44.7	547.3	0	100.0	0.482	32.5	73.6	23.6	66.4	271.0	109
C	194.0	146.2	47.1	99.1	10.9	62.0	0.608	26.4	60.3	23.6	57.0	156.4	49
D	---	---	---	NP	30.6	17.2	0.438	0	3.3	14.3	0.7	7.4	1
6 A	83.5	90.0	45.0	45.0	43.4	96.2	0.677	2.7	12.6	1.0	2.2	24.0	138
B	81.7	64.6	41.7	22.9	25.8	89.0	0.645	2.0	2.6	0.9	0.5	20.6	115
C	88.7	59.5	56.4	3.1	55.9	22.8	0.380	1.4	0	0.6	0.1	5.3	5
D	90.1	63.2	---	NP	59.0	21.2	0.364	1.2	0	0.5	0	4.5	0
7 A	56.1	58.1	22.2	35.9	13.8	65.8	0.745	7.9	38.4	13.7	1.8	21.2	83
B	56.0	47.2	27.1	20.1	11.8	53.0	0.563	4.7	16.1	14.9	1.9	25.5	285
C	52.7	34.3	29.2	5.1	26.1	23.2	0.613	6.9	20.5	14.7	2.8	12.9	49
D	52.2	28.1	30.1	0	24.8	15.0	0.546	0	2.4	6.1	0.4	4.2	1
8 A	32.6	27.1	16.6	10.5	9.7	38.5	0.620	3.4	9.9	4.4	0.9	13.3	149
B	33.6	21.4	15.4	6.0	11.3	34.0	0.770	3.4	6.8	4.0	1.0	5.7	97
C	35.5	23.8	19.7	4.1	24.0	18.6	0.714	2.2	6.4	4.3	1.2	7.3	22
D	37.6	24.7	24.5	0.2	26.2	13.5	0.632	0.4	1.9	2.8	0.3	6.9	0
9 A	64.0	47.6	34.3	13.3	41.1	26.0	0.405	0.3	2.3	0.5	0.1	0	8
B	55.3	41.7	36.8	4.9	36.0	25.0	0.379	0	0	0.4	0.1	0.5	2
C	57.5	46.4	42.6	3.8	37.1	24.7	0.370	0	0	0.4	0.1	2.4	2
D	76.9	51.0	47.6	3.4	48.9	22.8	0.360	0	3.8	0.4	0.4	3.9	1

[a] Terms and symbols used are as follows: w_{100} = water content for 100% saturation; w_L = liquid limit; w_P = plastic limit; I_P = plasticity index; w_S = shrinkage limit; <2μ = clay fraction less than 2μ; CEC = cation exchange capacity; C.I. = particle-size composite index = log $(Q_3/Q_1)^{1/2}$ in which Q_3 and Q_1 are the third and first quartile deviations or the particle sizes having 75% and 25% passing on the grain-size distribution curve, respectively; and S.A. = surface area (to obtain surface area in sq m/gm, multiply by 17.65).
[b] A = raw soil; B, C, D = soils heated for 24 hr at 300, 600, and 900 C, respectively.

TABLE 3

CORRELATION EQUATIONS[a]

Equation No.	Independent Variables	Dependent Variable	Estimating Equation	Standard Error of Estimate	Coefficient	
					Determination	Correlation
(a) Simple Correlation: S = Free Swelling						
1	I_P	S	$S = 0.4436 \, I_P + 11.3219$	21.32	0.8823	0.9393
2	w_S	S	$S = 69.6024 - 1.0092 \, w_S$	56.04	0.1869	0.4323
3 a	$< 2 \, \mu$	S	$S = 1.1689 \, (< 2 \, \mu) - 21.6976$	49.57	0.3638	0.6031
3 b	S.A.	S	$S = 3.0182 \, S.A. + 0.5524$	45.35	0.4362	0.6606
3 c	C.I.	S	$S = 100.7489 \, C.I. - 21.4823$	57.98	0.0784	0.2800
4	CEC	S	$S = 1.1845 \, CEC + 3.5958$	49.40	0.3680	0.6067
5	Ca	S	$S = 0.8115 \, Ca + 21.0915$	59.90	0.0710	0.2664
6	Na	S	$S = 3.0594 \, Na + 11.2133$	25.71	0.8288	0.9104
(b) Multiple Correlation: S = Free Swelling						
7	I_P, $< 2 \, \mu$, CEC, & Na	S	$S = 0.2521 \, I_P + 0.1694 \, (< 2 \, \mu) + 0.0040 \, CEC + 1.4535 \, Na + 1.8894$	14.67	0.9492	0.9743
8	I_P, S.A., CEC, & Na	S	$S = 0.2638 \, I_P + 0.4798 \, S.A. + 0.0006 \, CEC + 1.3245 \, Na + 5.1013$	13.09	0.9530	0.9762
(c) Simple Correlation						
9 a	$< 2 \, \mu$	S.A.	$S.A. = 0.3187 \, (< 2 \, \mu) - 4.0343$	8.97	0.5646	0.7514
9 b	S.A.	$< 2 \, \mu$	$< 2 \, \mu = 1.7717 \, S.A. + 28.3253$	20.56	0.5646	0.7514
10 a	$< 2 \, \mu$	C.I.	$C.I. = 0.00338 \, (< 2 \, \mu) + 0.3978$	0.135	0.3935	0.6273
10 b	C.I.	$< 2 \, \mu$	$< 2 \, \mu = 116.4463 \, C.I. - 16.8229$	24.27	0.3935	0.6273
11 a	C.I.	S.A.	$S.A. = 46.9578 \, C.I. - 14.9329$	10.91	0.3557	0.5964
11 b	S.A.	C.I.	$C.I. = 0.00758 \, S.A. + 0.4753$	0.135	0.3557	0.5964
12 a	w_L	I_P	$I_P = 0.9463 \, w_L - 44.1404$	28.76	0.9517	0.9755
12 b	I_P	w_L	$w_L = 1.0057 \, I_P + 49.5460$	29.65	0.9517	0.9755
13 a	w_L	w_{100}	$w_{100} = 0.4534 \, w_L + 59.0300$	38.34	0.7301	0.8545
13 b	w_{100}	w_L	$w_L = 1.6104 \, w_{100} - 66.2519$	70.10	0.7301	0.8545
14	C	S	$S = 0.2590 \, C + 13.2330$	56.54	0.1722	0.4150

[a]For notations (definitions) see Table 2 footnotes.

in a vertical direction without any load and restraint was developed to measure the relative values of volumetric changes of clay minerals tested under identical conditions. After being placed in an air-tight cabinet with saturated humidity for at least two weeks, a 5-gm sample is molded in a 1.12-in. transparent lucite cylinder with a porous stone base under a static load of 50 psi for 1 min. The load is applied and released at a constant rate of 33-psi/min. A porous stone is placed on the top of the compacted specimen and 25 ml of distilled water at room temperature is introduced from the top. Increases in thickness are measured to 0.001 in. until no further swelling occurs. Free swelling is defined as the increase in thickness divided by the original thickness and multiplied by 100. Initial and final water contents are determined. The mass specific gravity, void ratio, porosity, degree of saturation before and after the test, and water content to reach full saturation are computed.

The test results significant in subsequent correlation analyses are summarized in Table 2.

CORRELATION ANALYSIS

Simple and multiple correlation analyses (8) of various combinations were made on the 36 soil samples by using free swelling as the dependent variable and physico-chemical properties as the independent variables after elimination of some of the test results which were either too insignificant, erratic, or confusing to show any apparent relations. Simple correlation analyses show the predominance of linear relationships between the dependent and independent variables.

The most rational combination (9, 10, 11, 12) seems to be the multiple correlation between free swelling as the dependent variable and the four independent variables

(plasticity index, clay fraction in terms of particle size less than $2\,\mu$ or surface area, cation exchange capacity, exchangeable sodium) as shown by Eqs. 7 and 8 in Table 3. Both equations give a coefficient of multiple correlation of about 0.975.

Because the relationships between free swelling and shrinkage limit (13) and between free swelling and calcium are weak, as shown by their coefficients of correlation of 0.432 and 0.266, respectively, they are not included in the equations.

Equations 9, 10 and 11 (Table 3) show the simple relationships among surface area, clay fraction less than $2\,\mu$, and composite index. The coefficient of correlation of 0.751 between surface area and clay fraction less than $2\,\mu$ is highest. The relationship between liquid limit and plasticity index (14, 15) in Eq. 12 is excellent, as indicated by a coefficient of correlation of 0.976.

DISCUSSION

Free swelling tested under conditions in this study is a measure of relative volume changes of soils and may be used as an indication of swelling tested under other conditions (16, 17). Free swelling developed in this study can be estimated by either of two equations:

$$S\ (\%) = 0.252\ I_p + 0.169 < 2\,\mu + 0.004\ CEC + 1.454\ Na + 1.889 \qquad (15)$$

$$S\ (\%) = 0.264\ I_p + 0.480\ S.A. + 0.001\ CEC + 1.325\ Na + 5.101 \qquad (16)$$

By using surface area instead of clay fraction less than $2\,\mu$, Eq. 16 gives a slightly higher coefficient of multiple correlation. Surface area may be a better indication of the true activity of the clay fraction than a single 2-μ size (18). A coefficient of determination of about 0.95 indicates that 95 percent of the variations in free swelling is associated with variations in the four factors included in the equations.

The effect of heat treatment on physico-chemical properties of soils can be readily seen from the test results in Table 1. With heating at 900 C for 24 hr, practically all soils become nonplastic (19). Plasticity index decreases with increase in temperature.

ACKNOWLEDGMENTS

REFERENCES

1. "Procedures for Testing Soils." ASTM (1958).
2. "Standard Specifications for Highway Materials and Methods of Sampling and Testing." AASHO (1961).
3. Kinter and Diamond, "Pretreatment of Soils and Clays for Measuring External Surface Area by Glycerol Retention." Public Roads, pp. 187-190 (June 1959).
4. Kinter and Diamond, "Surface Areas of Clay Minerals as Derived from Measurements of Glycerol Retention." Proc. 5th Nat. Conf. on Clay and Clay Minerals, pp. 334-347 (1958).
5. Jackson, M. L., "Soil Chemical Analysis." Prentice-Hall (1958).
6. Willard, Merritt and Dean, "Instrumental Methods and Analysis." D. Van Nostrand Co. (1958).
7. Krumbein, W. C., "The Use of Quartile Measure in Describing and Comparing Sediments." Amer. Jour. of Sci., 37:98-111 (1936).
8. Ezekiel and Fox, "Methods of Correlation and Regression Analysis." John Wiley (1959).

9. Winterkorn, H. F., "Physico-Chemical Properties of Soils." Proc. 2nd Internat. Conf. on Soil Mechanics and Foundation Eng., 1:23-29 (1948).

10. Gill and Reaves, "Relationships of Atterberg Limits and Cation Exchange Capacity to Some Physical Properties of Soil." Proc. Soil Sci. Soc. of Amer., 21:491-494 (1957).

11. Odell, Thornburn and McKenzie, "Relationships of Atterberg Limits to Some Other Properties of Illinois Soils." Proc. Soil Sci. Soc. of Amer., 24(4):297-300 (1960).

12. Brooks, Bower and Reeves, "The Effect of Various Exchangeable Cations upon the Physical Conditions of Soils." Proc. Soil Sci. Soc. of Amer., 20(3):325-327 (1956).

13. Seed, Woodward and Lundgren, "Closure on Prediction of Swelling Potential for Compacted Clays." ASCE Proc. Sep. 3528 (May 1963).

14. Casagrande, A., "Classification and Identification of Soils." ASCE Proc., 73:783-810 (1947).

15. Matsuo, S., "Character of Consistency of Soils as Shown in the Plasticity Chart." Rept. on Res. and Invest., Japanese Comm. on Soil Mechanics and Foundation Eng., pp. 9-11 (1952).

16. Seed, Woodward and Lundgren, "Prediction of Swelling Potential for Compacted Clays." ASCE Proc. Sep. 3169 (June 1962).

17. Lambe, T. W., "The Character and Identification of Expansive Soils." FHA Tech. Studies Rept. (Dec. 1960).

18. Li, M. C., "Discussion on Prediction of Swelling Potential for Compacted Clays." ASCE Proc. Sep. 3378 (Dec. 1962).

19. Rao and Wadhawan, "Plasticity of Heated Soils." Irrigation and Power Jour., India, 12(2) (April 1955).

Physical Properties of Aggregates Stabilized With Papermill Wastes

HYOUNGKEY HONG and LLOYD F. RADER
Respectively, Assistant Professor of Civil Engineering, Marquette University,
Milwaukee, Wisconsin, and Professor of Civil Engineering, University of Wisconsin,
Madison

This investigation covers the determination of physical properties
of road aggregates stabilized with lignosulfonic acids and ligno-
sulfonic acid polymers, including the effects of heat treatment and
the incorporation of hydrated lime. In addition, a limited amount
of information on aggregate stabilization by spent sulfite liquor is
presented for comparison.

The purpose of this study was to investigate the possibilities of
better utilization of sulfite liquor wastes from papermills in stabi-
lizing road aggregates. Because sulfite liquor is water soluble,
attempts have been made to produce materials of higher molecular
weight from this liquor, thereby decreasing solubility. As a result,
lignosulfonic acids and their polymers have been experimentally
developed.

The physical properties investigated comprised compressive
strength, density, insolubility, and immersion moisture content.
Insolubility was determined by the optical density and the Folin-
Denis methods.

The lignosulfonic acid polymers investigated were less soluble
in water than the lignosulfonic acids. With respect to the com-
pressive strength, relatively good results were obtained with: (a)
the heat-treated mixture containing 1 percent lignosulfonic acid
polymers without any hydrated lime, and (b) the non-heat-treated
mixture containing 1 percent lignosulfonic acids with 3 percent
hydrated lime.

For the aggregates investigated, mixtures containing 3 percent
hydrated lime without other additives, heat-treated or non-heat-
treated, showed relatively high values of compressive strength and
practically no solubility.

•THE PROPER disposal of spent sulfite liquor (SSL), an industrial waste of papermills,
has been a great problem to the paper manufacturers for many years. The great amount
of pollution produced by these wastes has caused objections to their disposal into streams
and rivers.

As a result of studies made of the proper utilization of SSL, it has been employed ex-
tensively as a binder on gravel roads. One of the biggest disadvantages of such utiliza-
tion is its water solubility. There are three possible ways of alleviating this problem:
(a) addition of chemicals such as hydrated lime to form insoluble materials, (b) laying a
bituminous mat over SSL-treated bases so that little rainwater will flow through the base
courses to dissolve SSL solids, and (c) increasing the molecular weight of SSL by form-
ing lignosulfonic acid polymers, which are relatively insoluble in water.

In recent years, the Sulphite Pulp Manufacturers' Research League at Appleton, Wis.,
developed lignosulfonic acids (LSA) and lignosulfonic acid polymers (LSAP) from SSL by

an ion exchange method. The most important property of these new materials is their high molecular weight as compared to SSL. It is believed that as the molecular weight of these materials increases, the compressive strength and the insolubility increases. Furthermore, the addition of proper amount of hydrated lime (with or without heat treatment) to LSA or LSAP may produce much improved water insolubility and higher strength, as it has with SSL (1, 2, 4). The application of heat to the stabilized soil samples was suggested by previous research (3).

PURPOSES AND SCORE

The purposes of this study were:

1. To determine the effects on the compressive strength when aggregates were stabilized with various amounts of LSA or LSAP and hydrated lime;

2. To determine the effects on the compressive strength when specimens were heat-treated and then immersed in water;

3. To determine the optical density of solution and solids content produced by the partial dissolution of LSA or LSAP solids from treated specimens immersed in constant volume of water bath for 4 days;

4. To determine the moisture content of specimens at the end of the 4-day immersion in water;

5. To determine the effects on the density and optimum moisture content (or molding moisture content) of stabilized specimens; and

6. To compare these physical properties of LSA and LSAP with the corresponding properties obtained for SSL and hydrated lime.

PROPERTIES OF MATERIALS

Aggregates

The quarry from which all aggregates were obtained is located in the Platteville formation. The lower beds are of the Pecatonica member and the upper thinner beds of the McGregor member. The aggregates are primarily dolomitic limestones. This type of aggregate was selected as typical of aggregates used for base and wearing courses in eastern and southern parts of Wisconsin where LSA and LSAP materials would be available if manufactured in quantity by papermills.

The aggregate properties are given in Table 1, and the design gradation which meets the gradation specification for crushed stone base course of the State Highway Commission of Wisconsin is shown in Figure 1.
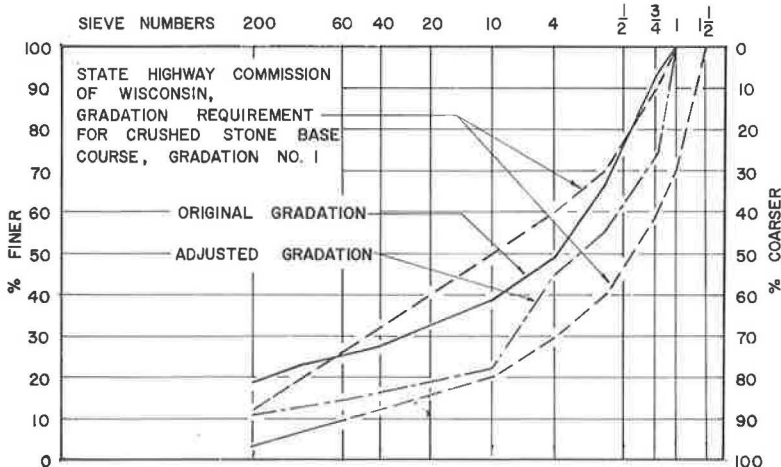

Figure 1. Design gradation.

TABLE 1

PROPERTIES OF AGGREGATES

Property	Value
Coarse aggregates, >2.0 mm (% by wt)	76
Coarse sand, 2.0-0.42 mm (% by wt)	8
Fine sand, 0.42-0.074 mm (% by wt)	5
Silt and clay, 0.074-<0.005 mm (% by wt)	11
Eng. classif.	A-2-4
Liquid limit[a]	17.4
Plastic limit[a]	NP
Bulk spec. grav.[b]	2.570
Bulk spec. grav., saturated surface dry base[b]	2,660
Apparent spec. grav.[b]	2.830
Bulk spec. grav.[c]	2.860
Adsorption, R-4 material (%)	3.27
pH	8.0
Organic content	Negative

[a]Atterberg limits.
[b]Material retained on No. 4 sieve.
[c]Material passing No. 10 sieve.

TABLE 2

COMPOSITION OF LIME

Material	Percent
Silica and other insolubles	1.2
Fe_2O_3	0.5
Free H_2O	0.7
$CaCO_3$	1.6
$Ca(OH)_2$	54.0
$Mg(OH)_2$	41.9
MgO	0.5

Hydrated Lime

The hydrated lime is designated as special finishing hydrated lime of ASTM Designation C 207-49 and meets Federal Specification SS-L-351 Type M (Masonry). It is dolomitic hydrated lime with a specific gravity of 2.358 and a plasticity of 0.300. Its composition is given in Table 2.

LSA and LSAP

The properties of LSA and LSAP are as follows:

1. Strong organic acid;
2. High dispersion properties;
3. Adhesive properties increase with increasing molecular weight;
4. Cationic ion exchange activity;
5. Strong reducing agent;
6. LSA at high molecular weight form gels;
7. LSA react with trivalent metals (Cr^{+++});
8. LSA act as sequestering and chelating agents for many metals, especially iron and copper;
9. Viscosity of clay mixtures decreases with increasing molecular weight of LSA up to a certain limit (relative molecular weight of about 20,000), and then increases with further increase in molecular weight (Fig. 2); and
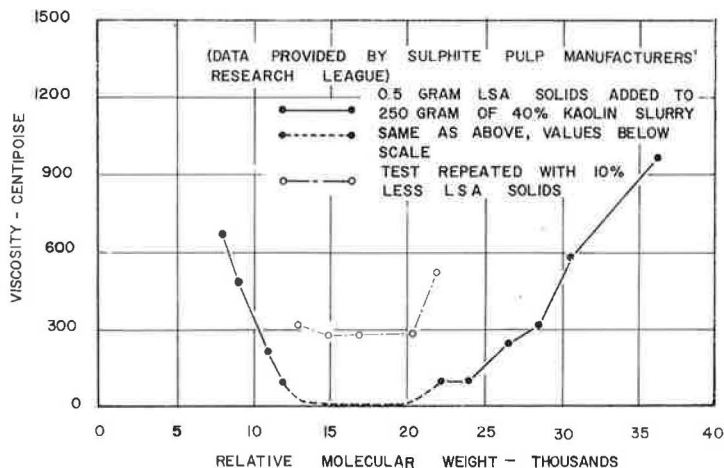

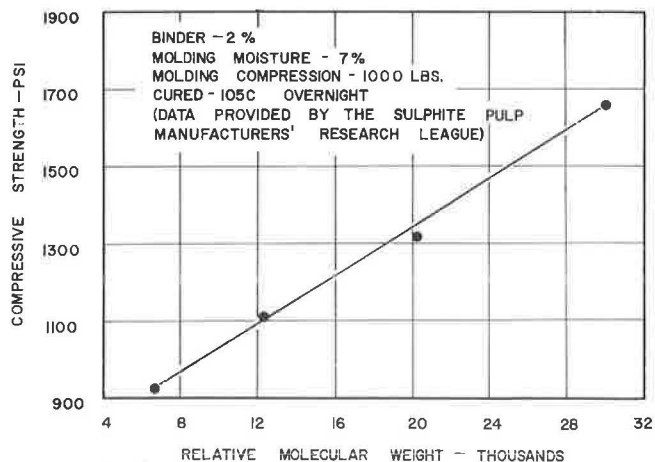Figure 2. Change of dispersing properties with increasing relative molecular weight.

Figure 3. Relative molecular weight: compressive strength relationship of iron ore briquettes.

TABLE 3

PROPERTIES OF LSA AND LSAP

Acid	pH	Solids (%)	Reducing Sugars (%)[a]	Mol Wt
LSA	0.12	51.5	8.50	10,700
LSAP	0.69	45.0	5.84	22,800

[a]By wt of solids.

TABLE 4

COMPOSITION OF SSL SOLIDS

Material	Percent
Lignosulfonates	55
Hexose sugars	14
Pentose sugars	6
Sugar acids and residues	12
Resins and extractives	3
Ash	10

TABLE 5

ANALYSIS OF SSL

Material	Percent
Lignin	54.5
Total sugar	19.3
Iron	0.024
Magnesium oxide	0.27
Calcium oxide	6.5
Sodium oxide	0.033
Sulfated ash	16.3
Sulfone SO_2	3.6
Sulfur trioxide	0.7
Free sulfur dioxide	0.17
Total sulfur	6.1
Volatile acids	1.2
Calcium lignosulfonate	65.0
Fe and Al as oxides	0.1

10. Compressive strength of iron ore briquettes stabilized with LSA increases with increasing relative molecular weight (Fig. 3).

Additional data are given in Table 3.

SSL

SSL used in this investigation is of softwood origin and produced by calcium base process. Its solids content is 11.0 percent. The composition of the SSL solids is given in Table 4.

An analysis of the dried lignin powder used in this study is given in Table 5. The compound has a specific gravity of 0.31 and a pH in 10% solution of 4.3.

MOLDING AND CURING OF SPECIMENS

All specimens were molded in CBR molds. Each specimen was compacted in five equal layers with 25 blows for each layer and 18 in. of free fall by a 10-lb rammer. The specimens were cured for 7 days in 50 percent RH at 75 ± 3 F. Three specimens were made and tested for each category and the average of each three values are used.

After air curing, specimens, which were not to be heat-treated, were immersed in water for 4 days, then tested wet for unconfined compressive strength.

Specimens, which were to be heat-treated, were cured at 210 F for 24 hr and then cured again at 340 F for another 24 hr. They were then cooled to room temperature for 24 hr, immersed in water for 4 days, and tested while moist for unconfined compressive strength.

During immersion of the specimens, some of the uncombined SSL and LSA or LSAP solids were dissolved by water. As the amount of dissolved solids increased, the intensity of color of the solution increased to dark brown. Approximately 1 pint of this solution was taken for optical density, solids content, and pH determinations. Some specimens completely disintegrated during immersion and others were flaked on the surfaces. Some specimens maintained their original shapes quite successfully throughout the immersion period.

TABLE 6

MOLDING MOISTURE CONTENTS AND DRY DENSITIES OF MIXTURES

Stabi-lizer (%)	Molding Moisture (%)				Dry Density (pcf)			
	0% Lime	3% Lime	6% Lime	9% Lime	0% Lime	3% Lime	6% Lime	9% Lime
(a) LSA Stabilizer								
0	6.0	6.8	7.7	8.6	143.0	140.4	138.0	135.0
1	5.4	7.9	8.6	8.8	139.5	137.0	134.0	131.0
2	5.4	8.5	9.5	10.7	138.0	134.0	132.0	128.0
3	—[a]	9.4	10.6	11.6	—[a]	130.0	128.0	125.0
4	—[a]	10.5	11.5	12.5	—[a]	126.0	124.0	122.0
(b) LSAP Stabilizer								
0	6.0	6.8	7.7	8.6	143.0	140.4	138.0	135.0
1	6.4	9.4	10.1	11.0	137.0	134.0	132.0	129.0
2	7.0	10.3	11.0	11.9	135.0	130.0	128.0	126.0
3	7.8	11.0	11.7	12.7	131.5	126.5	125.0	122.0
4	—[a]	11.9	12.6	13.3	—[a]	123.5	122.0	120.0

[a]Semiliquid mixture.
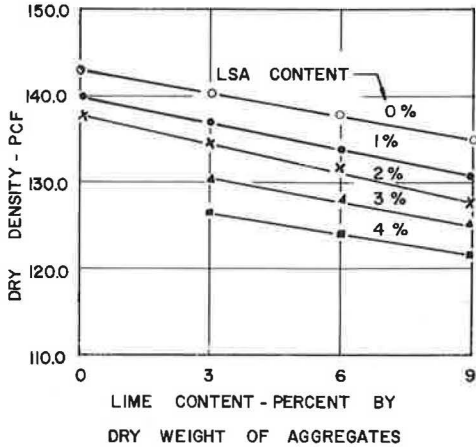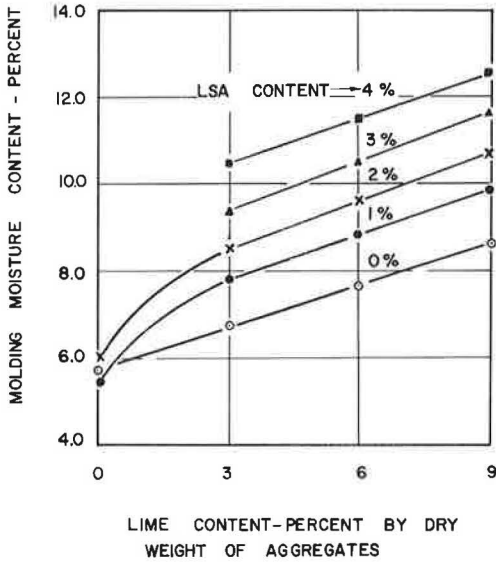
Figure 4. Molding moisture content of aggregate-LSA-lime mixture (Groups 1 and 2).

Figure 5. Dry density of aggregate-LSA-lime mixture (Groups 1 and 2).
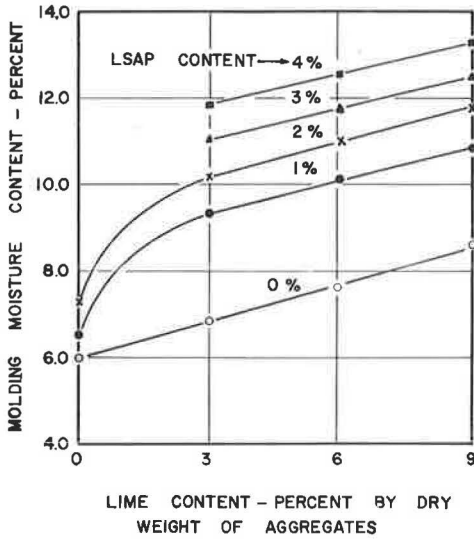
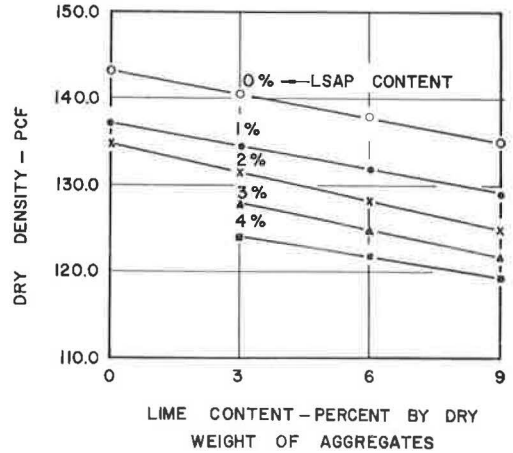Figure 6. Molding moisture content of aggregate-LSAP-lime mixture (Groups 3 and 4).

Figure 7. Dry density of aggregate-LSAP-lime mixture (Groups 3 and 4).

All immersed specimens were capped with plaster of paris for the compressive strength test. The rate of compression was 0.05 ipm.

The molding moisture content for each composition was determined by trial, beginning at the optimum moisture content and reducing the moisture content until a desirable solidity of soil specimen was obtained. This reduction was necessitated by the slight slumping of specimen at the optimum moisture content. These molding moisture contents were generally from 0.5 to 1 percent less than the optimum moisture content for each composition.

The molding moisture content and the corresponding dry densities for the various combinations of lime and aggregates with LSA and LSAP are given in Table 6. These values are also shown in Figures 4 to 7.

In both LSA and LSAP mixtures, molding moisture contents increased with increasing amount of additives, whereas the dry densities decreased with the increasing amount of additives.

DATA AND DISCUSSION OF RESULTS

Results of the various tests are given in Table 7.

Group 1

Specimens were made with aggregates, LSA, and lime and were heat-treated. The compressive strength is shown in Figure 8. Aggregates stabilized with 3 percent hydrated lime and no other additives indicated the highest compressive strength in this group. However, when aggregates were stabilized with both LSA and lime, relatively high compressive strengths occurred where the ratio of LSA to lime content was about 1 to 3 by weight. At this ratio the compressive strengths were nearly the same.

The immersion moisture content in percent by dry weight of specimen is shown in Figure 9. Aggregates stabilized with LSA alone or with relatively large amounts of LSA as compared to the lime present were quite susceptible to water penetration. Therefore, a certain proportion between LSA and lime contents must be observed to reduce or prevent the water susceptibility, consistent with the desired compressive strength.

This susceptibility to moisture was also reflected in the compressive strength. It is recalled that the compressive strengths of specimens with LSA alone or with a

TABLE 7
PHYSICAL PROPERTIES OF STABILIZED MIXTURES[a]

Stabi-lizer (%)	Compressive Strength (psi)				Immersion Moisture (%)				Optical Density				Stabilizer Solids (gm/l)[b]			
	0% Lime	3% Lime	6% Lime	9% Lime	0% Lime	3% Lime	6% Lime	9% Lime	0% Lime	3% Lime	6% Lime	9% Lime	0% Lime	3% Lime	6% Lime	9% Lime
(a) Group 1: LSA Stabilizer[c]																
0	D	242	218	193	D	6.9	7.4	8.2	0	0	0	0	0	0	0	0
1	41	146	134	100	10.0	7.2	7.7	8.3	30.7	6.3	3.0	2.6	3.6	0.8	0.4	0.7
2	40	114	148	126	10.0	7.2	7.6	8.2	53.6	20.7	8.3	5.2	6.6	2.6	1.0	1.6
3	PD	18	109	142	PD	11.0	8.8	7.9	49.2	53.5	19.3	10.0	6.1	6.6	2.4	1.2
4	—	13	80	96	—	11.5	9.0	8.6	—	45.7	21.1	17.6	—	5.7	2.6	2.2
(b) Group 2: LSA Stabilizer[d]																
0	D	280	212	114	D	7.8	8.5	9.1	0	0	0	0	0	0	0	0
1	D	163	156	112	D	7.9	8.5	8.7	26.6	12.9	2.7	2.4	3.3	1.6	0.3	0.3
2	D	125	110	81	D	8.4	8.8	9.5	49.8	11.9	6.7	5.1	6.2	1.5	0.8	1.6
3	—	107	96	73	—	9.2	9.2	10.5	—	25.0	10.4	11.4	—	3.1	1.3	1.4
4	—	57	98	80	—	9.7	9.5	9.9	—	34.1	13.6	12.6	—	4.4	1.7	1.6
(c) Group 3: LSAP Stabilizer[c]																
0	D	242	218	193	D	6.9	7.4	8.2	0	0	0	0	0	0	0	0
1	180	122	125	90	6.8	8.0	8.4	8.9	12.4	2.8	1.4	2.0	1.5	0.4	0.2	0.3
2	122	85	96	84	6.8	8.5	9.0	9.8	22.1	7.6	3.6	2.1	2.7	0.9	0.5	0.3
3	92	52	80	74	—	10.5	9.6	10.2	19.8	23.7	4.0	3.9	2.5	2.9	0.5	0.5
4	—	28	50	57	—	11.5	10.2	10.4	—	26.2	8.9	5.0	—	3.3	1.1	0.6
(d) Group 4: LSAP Stabilizer[d]																
0	D	280	212	114	D	7.8	8.5	9.1	0	0	0	0	0	0	0	0
1	45	113	109	80	9.7	8.7	9.0	8.9	7.9	2.2	0.9	1.0	1.0	0.3	0.1	0.1
2	22	95	94	64	9.7	9.0	9.0	9.7	24.6	5.4	5.4	2.5	3.1	0.7	0.3	0.3
3	—	62	71	58	—	10.4	10.4	10.5	—	8.5	5.9	4.1	—	1.1	0.7	0.5
4	—	44	62	51	—	11.5	11.4	11.2	—	16.5	7.5	2.9	—	2.0	0.9	0.4
(e) Group 5: SSL Stabilizer																
0.9d	D	140	88	77	D	7.6	8.3	9.0	10.0	3.1	2.7	2.7	1.3	0.4	0.3	0.3
2de	D	140	133	120	D	7.4	7.7	8.3	36.4	8.7	4.4	4.0	4.5	1.1	0.6	0.5
2ce	D	118	141	94	D	6.8	7.5	8.3	9.4	6.5	4.9	5.0	5.0	1.2	0.8	0.6

[a] D denotes disintegration of specimen in water; PD denotes partial disintegration in water.
[b] Estimated by Folin-Denis method. [c] Heat-treated. [d] Non-heat-treated. [e] Dried lignin.
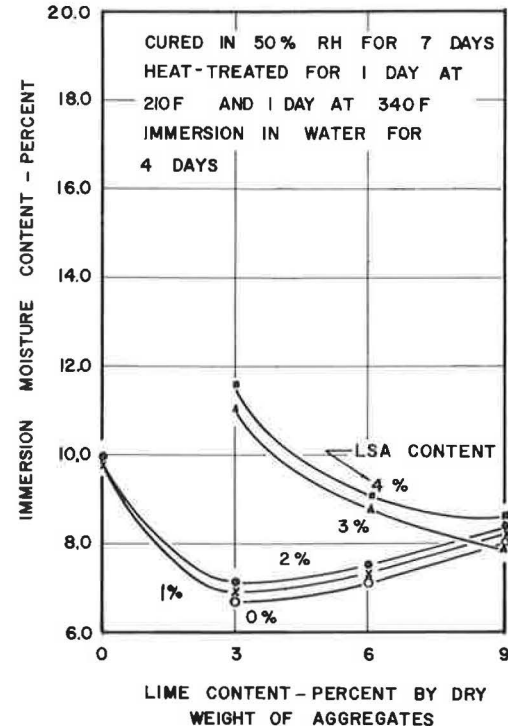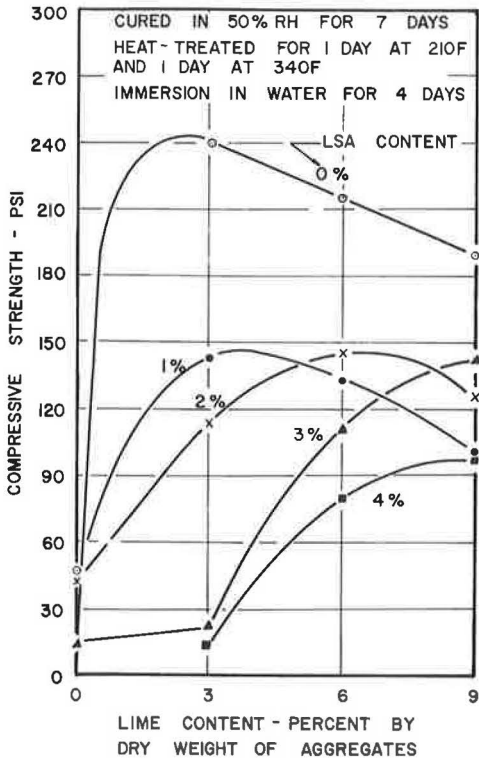

Figure 8. Compressive strength of aggregate-LSA-lime mixture (Group 1).

Figure 9. Immersion moisture content of aggregate-LSA-lime mixture (Group 1).
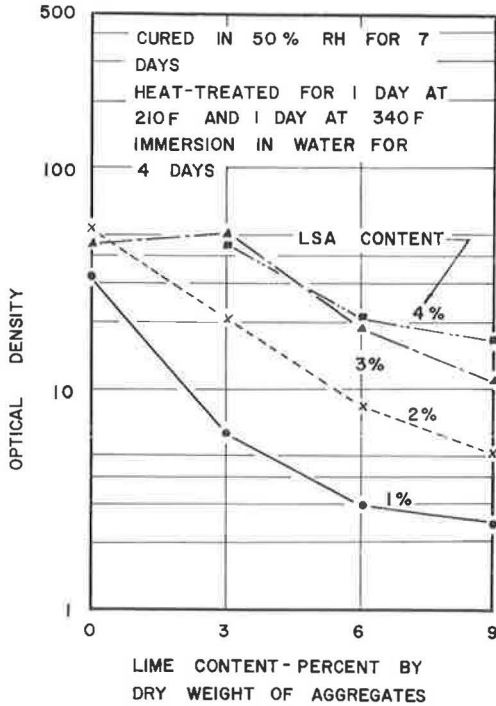
Figure 10. Optical density value of solution of aggregate-LSA-lime mixture (Group 1).

large amount of LSA were very low due to the high immersion moisture contents and subsequent surface flaking.

Estimates of LSA solids were made by means of the optical density at 282 mμ wavelength. Lignin content cannot be measured accurately because the exact structure of lignin is not known. For this reason, the results obtained by both the optical density and Folin-Denis methods should be considered very rough approximations, based on experience with similar products. The results of optical density and solids content determinations are shown in Figure 10. The amount of LSA solids dissolved in water, as measured by optical density and Folin-Denis methods, increased with increasing amounts of LSA (with one exception), but decreased considerably with increase in lime content for each LSA content. With zero percent LSA, the solution showed zero value of optical density for the lime contents between 3 and 9 percent.

Group 2

Specimens were made with aggregates, LSA, and lime and were not heat-treated.

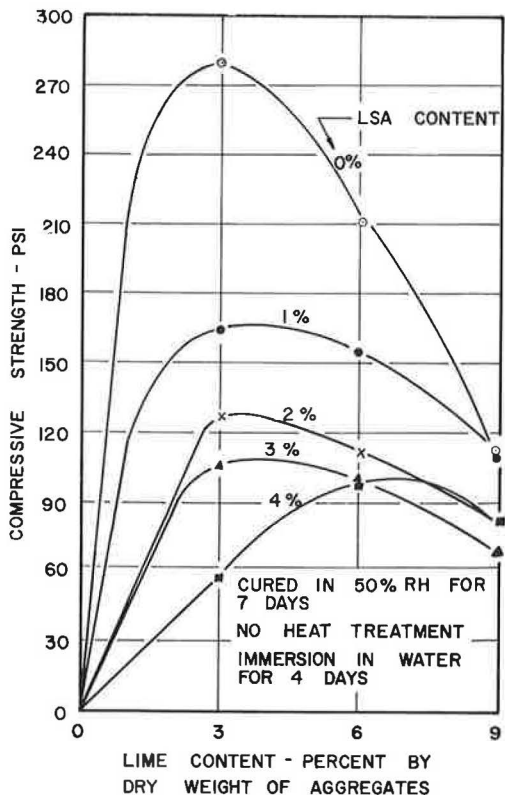Aggregates stabilized with 3 percent lime and no other additives indicated the highest compressive strength. When aggregates were stabilized with both LSA and lime, the combination of 1 percent LSA and 3 percent lime indicated higher compressive strength than other combinations of LSA and lime (Fig. 11).

The immersion moisture content is shown in Figure 12. Without the addition of lime, the specimens disintegrated in water, but the addition of only 3 percent lime prevented disintegration. With further increase of lime, the immersion moisture content remained fairly constant for each LSA content.

The optical density increased considerably with the increasing amount of LSA, and decreased with the increasing lime content. For all LSA contents, this reduction in optical density was considerable when 0 to 6 percent lime was added, but beyond 6 percent lime content, the reduction was almost negligible.

Group 3

Specimens were made with aggregates, LSAP, and lime and were heat-treated. Aggregates stabilized with 3 percent hydrated lime and no other additives indicated the highest compressive strength in this group (Fig. 14). On the other hand, when aggregates were stabilized with both lime and LSAP, the combination of 1 percent LSAP and zero percent lime indicated higher compressive strength than other combinations of LSAP and lime. Addition of lime definitely decreased the compressive strengths of all LSAP contents.

The immersion moisture content in percent by dry weight of specimen is shown in Figure 15. Lime was effective in reducing the moisture absorption for 3 and 4 percent LSAP contents. For low LSAP contents (1 and 2 percent), moisture absorption increased slightly with increasing lime content. The highest compressive strength occurred where the immersion moisture content was the lowest.
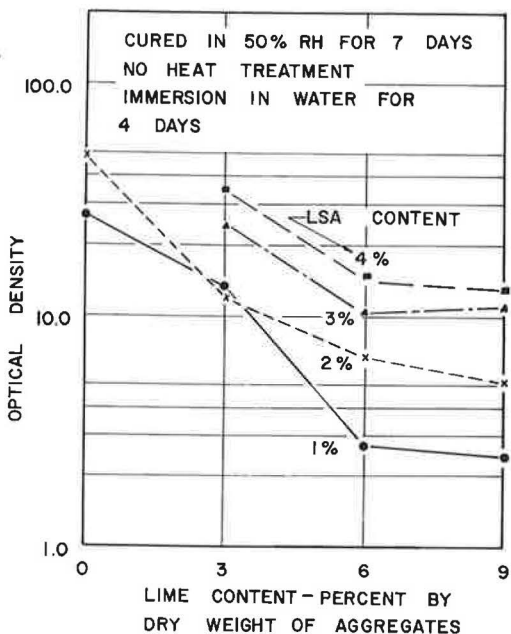
Figure 11. Compressive strength of aggregate-LSA-lime mixture (Group 2).

Figure 12. Immersion moisture content of aggregate-LSA-lime mixture (Group 2).

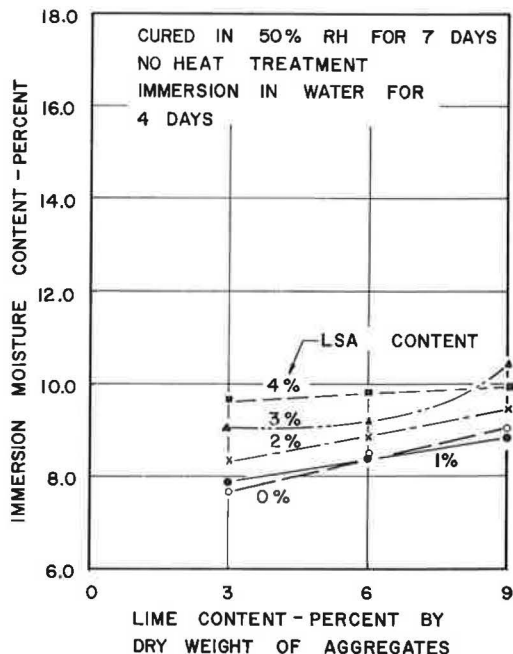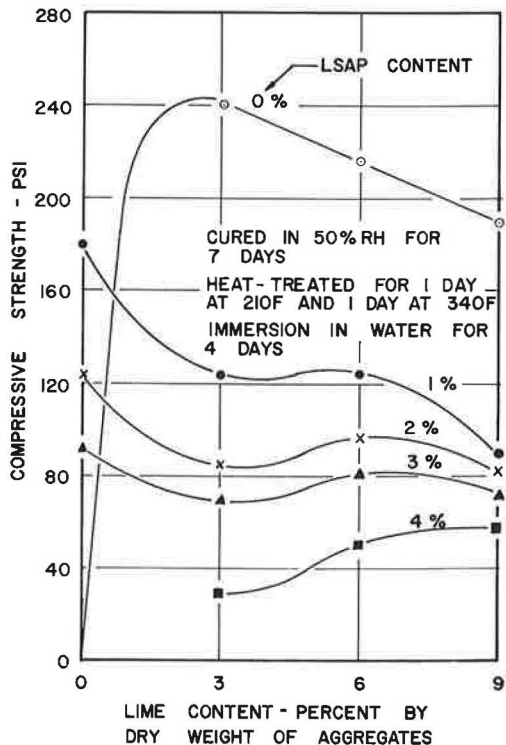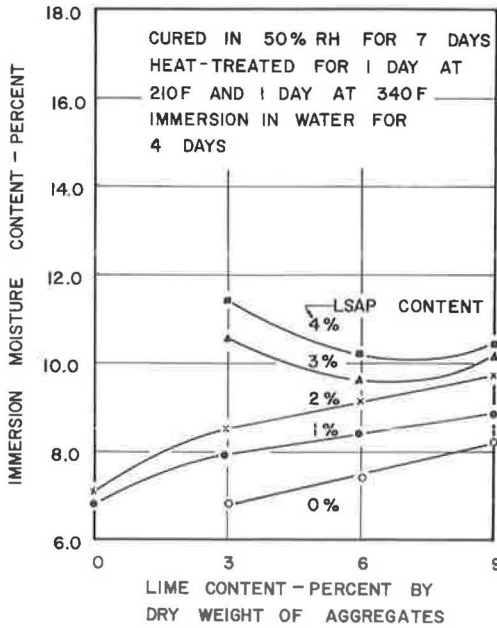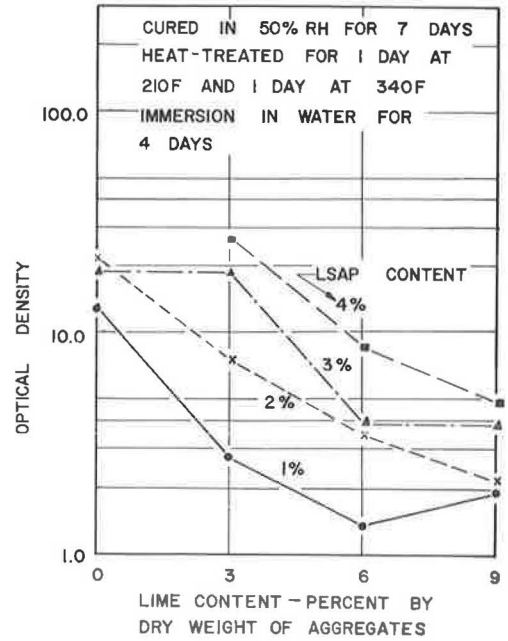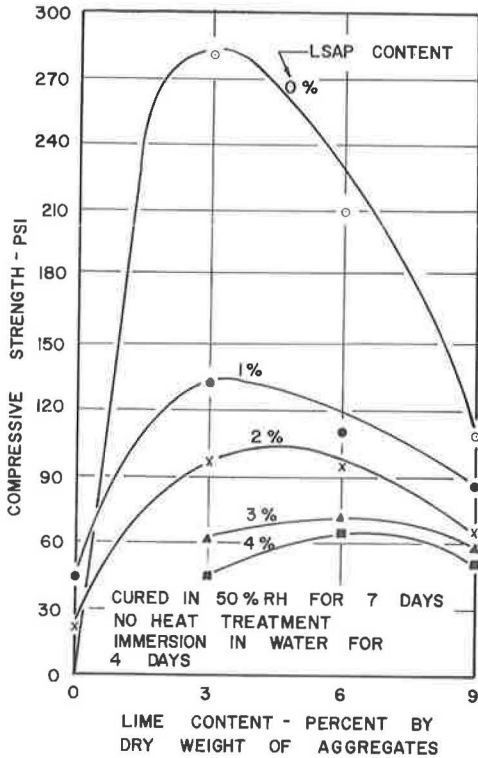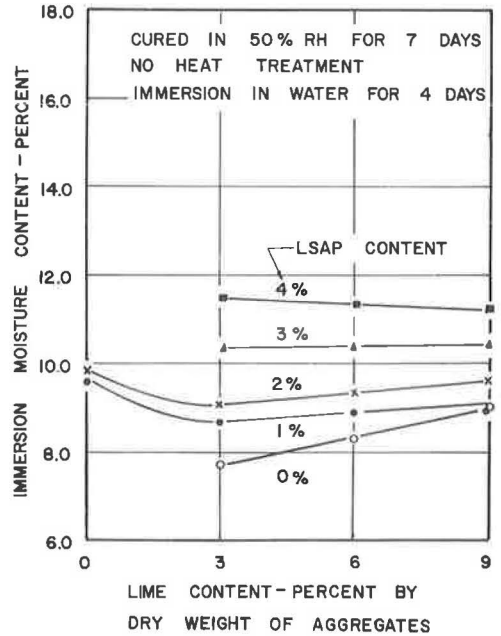Figure 13. Optical density value of aggregate-LSA-lime mixture (Group 2).

Figure 14. Compressive strength of aggregate-LSAP-lime mixture (Group 3).

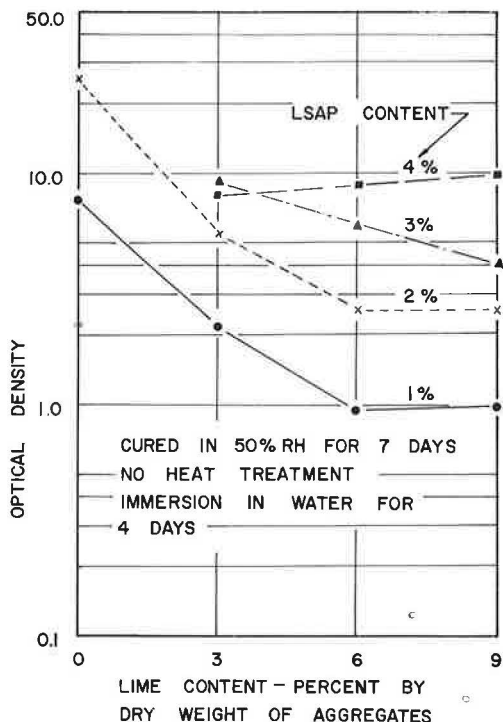Figure 15.   Immersion moisture content of aggregate-LSAP-lime mixture (Group 3).

Figure 16.   Optical density value of aggregate-LSAP-lime mixture (Group 3).

Figure 17.   Compressive strength of aggregate-LSAP-lime mixture (Group 4).

Figure 18.   Immersion moisture content of aggregate-LSAP-lime mixture (Group 4).

The optical density or dissolved solids decreased considerably with the increasing lime content and decreasing LSAP content. In general, beyond 6 percent lime, no significant reduction in optical density was observed (Fig. 16).

Group 4

Specimens were made with aggregates, LSAP, and lime and were not heat-treated. Aggregates stabilized with 3 percent lime and no other additives indicated the highest compressive strength in this group (Fig. 17). When aggregates were stabilized with both LSAP and lime, the combination of 1 percent LSAP and 3 percent lime indicated higher compressive strength than any other combinations of LSAP and lime. Further increase in lime or LSAP content was detrimental to obtaining high compressive strength.

The immersion moisture content in percent by dry weight of specimen is shown in Figure 18. Lime was effective in increasing resistance to water penetration. However, lime content greater than 3 percent may not be necessary, because the reduction in immersion moisture content was almost negligible.

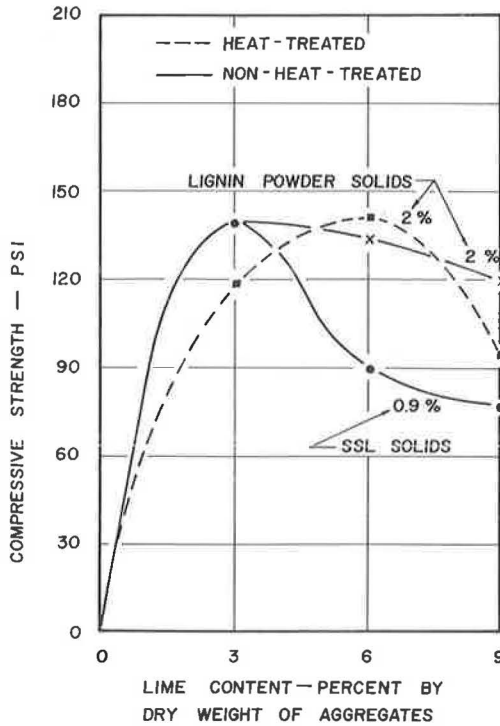The results of optical density and solids content determinations are shown in Figure 19. Lime was effective in reducing the amount of LSAP solids dissolved in water. Lime content greater than 6 percent may not be necessary.

Figure 19.   Optical density value of aggregate-LSAP-lime mixture (Group 4).

Comparison of Groups 1, 2, 3, and 4

In all cases investigated in this study, aggregates stabilized with lime and no other additives indicated higher compressive strength than others stabilized with both LSA (or LSAP) and lime for corresponding lime content. Aggregates stabilized with 3 percent lime without any other additives indicated the highest compressive strength.

Comparing the compressive strengths of heat-treated specimens of LSA and LSAP, the strength of LSAP without lime was higher than other combinations of additives. If any lime was to be added at all, the compressive strengths of LSA with lime were higher than those of LSAP with lime. With non-heat-treated specimens, the strength of 1 percent LSA at 3 percent lime was higher than other combinations of additives.

The addition of lime to the specimen prevented the disintegration of specimen in the water. Addition of 3 percent lime considerably decreased the immersion moisture content, except in one case. Lime content of greater than 3 percent did not improve the moisture resistance of specimens. The optical density and solids content values of LSA specimens were higher than those of LSAP specimens at all lime contents, regardless of heat treatment. In other words, LSA solids were more soluble in water than the LSAP solids at all lime contents, regardless of heat treatment.

These observations confirm the earlier statement that as the relative molecular weight of LSA increases up to about 20,000, the insolubility of LSA solids increases. As indicated earlier, the relative molecular weight of LSA is 10,700 and that of LSAP is 22,800.

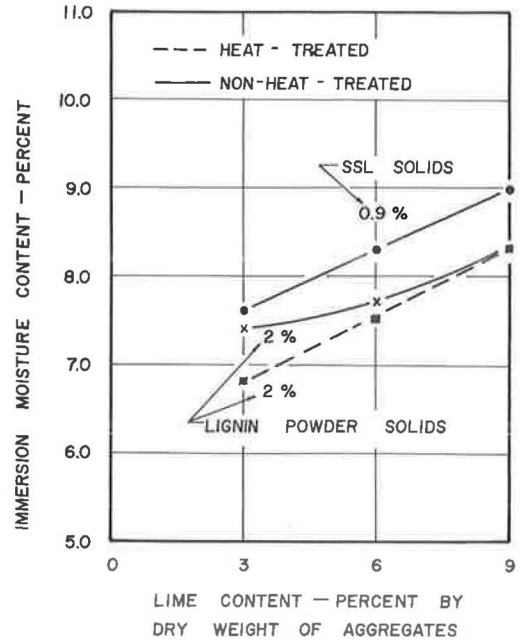Figure 20. Compressive strength of aggregate-SSL-lime mixture (Group 5).

Figure 21. Immersion moisture content of aggregate-SSL-lime mixture (Group 5).
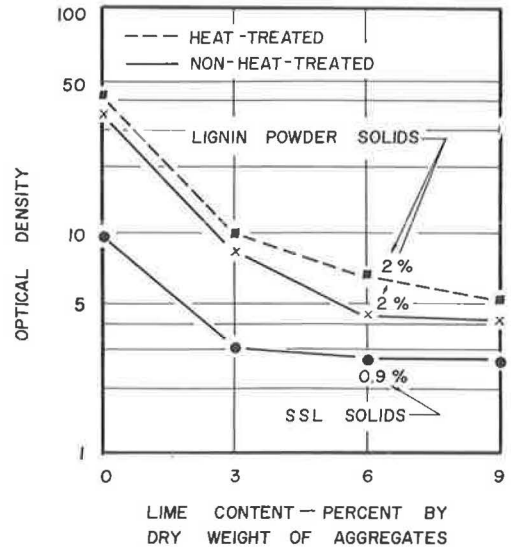
Figure 22. Optical density value of solution of aggregate-SSL-lime mixture (Group 5).

Comparison of Aggregate Stabilization by SSL, LSA, and LSAP

A limited amount of pertinent data on the compressive strength, immersion moisture content, and optical density of aggregate-SSL-lime mixture are shown in Figures 20, 21, and 22, respectively, for comparison with the results of LSA and LSAP aggregate stabilization.

Figures 8 and 20 (heat-treated) indicate that the maximum compressive strength attained for 2 percent solids of SSL and LSA was nearly the same at 6 percent lime content. It is noted, however, that at zero percent lime content, LSA specimens had some strength and maintained their shape fairly well in water, whereas SSL specimens disintegrated completely in water.

In Figures 14 and 20 (heat-treated), the maximum compressive strength for 2 percent solids of LSAP was lower than that of SSL for the lime contents of 3, 6, and 9 percent. However, at zero percent lime, LSAP showed considerable compressive strength in contrast to the disintegration of SSL specimens in water.

Comparison of Figures 11 and 20 (non-heat-treated) indicates that the compressive strength of 1 percent LSA was higher than that of 0.9 percent SSL solids at all lime

contents. However, for 2 percent solids, the compressive strength of SSL was higher than that of LSA at all lime contents. Without lime, all specimens of both SSL and LSA disintegrated in water.

Figures 17 and 20 (non-heat-treated) indicate that the maximum compressive strength of SSL for 2 percent solids was higher than that of corresponding LSAP solids at all lime contents. For 0.9 percent of SSL solids and 1 percent of LSAP solids the maximum compressive strengths of SSL samples were slightly higher than that of LSAP at 3 percent lime, but at 6 and 9 percent lime, lower strength was observed for SSL samples.

Comparison of the optical density values of all five groups indicates that for the corresponding solids content of SSL, LSA, and LSAP, LSAP samples showed lower optical density values than those of SSL and LSA. SSL specimens, however, indicated lower values of optical density than those of LSA (Figs. 10, 13, 16, 19 and 22).

CONCLUSIONS

Based on the materials and methods employed in this investigation, the following conclusions may be stated:

1. Mixtures containing hydrated lime and no other additives, both heat-treated and non-heat-treated, showed relatively high values of compressive strength and practically no solubility. The optimum lime content for high compressive strength was 3 percent.

2. The non-heat-treated mixture containing 1 percent LSA with 3 percent hydrated lime gave higher compressive strength than any other combination of LSA and hydrated lime, both heat-treated and non-heat-treated; this mixture also gave higher compressive strength than any combination of SSL and hydrated lime investigated.

3. The heat-treated mixture containing 1 percent LSAP and no other additives indicated higher compressive strength values than for higher percentages of LSAP, heat-treated and non-heat-treated, and for any combination of LSAP and hydrated lime, both heat-treated and non-heat-treated; this 1 percent LSAP with no additive also had higher compressive strength than any combination of SSL and hydrated lime investigated.

4. The insolubility values of LSAP stabilized specimens were generally higher than those of LSA and SSL specimens for corresponding hydrated lime contents, whether heat-treated or non-heat-treated.

5. Hydrated lime was effective in reducing the penetration of water into the specimens of aggregates stabilized with LSA or LSAP. The optimum lime content from the standpoint of resistance to water penetration was 3 percent.

REFERENCES

1. Hong, H., "Investigation of Physical Properties of Road Aggregates Stabilized with Sulphite Liquor and Hydrated Lime." Ph. D. Diss., Univ. of Wisconsin, Madison (1962)
2. Kubita, Z., "The Use of Spent Sulphite Liquor for Road Maintenance." Znojomo, Jour.: Papir a Celulosa, 10:221-223 (1954).
3. Sulphite Pulp Manufacturers' Research League, Unpubl. Rept. on Compressive Strength of Soil Briquettes Stabilized with Modified Spent Sulphite Liquor Solids, Appleton, Wis. (Oct. 1961).
4. Wolf, J., "The Utilization of Pulping Wastes in Dust Abatement." Jour. Silnice, 4 (10):235-263 (1955).